NEURONAL AND MICROGLIAL INTERACTIONS WITH OLIGODENDROCYTES REGULATE MYELIN SHEATH FORMATION AND ELIMINATION

by

ALEXANDRIA NICOLE HUGHES

B.S. Boise State University, 2014

A thesis submitted to the

Faculty of the Graduate School of the

University of Colorado in partial fulfillment

of the requirements for the degree of

Doctor of Philosophy

Neuroscience Program

2020

This thesis for the Doctor of Philosophy degree by

Alexandria Nicole Hughes

has been approved for the

Neuroscience Program

by

Linda A. Barlow, Chair

Ethan G. Hughes

Chandra L. Tucker

Matthew J. Kennedy

Jason Aoto

Bruce Appel, Advisor

Date: 14 December 2020

Hughes, Alexandria Nicole (Ph.D., Neuroscience)

Neuronal and microglial interactions with oligodendrocytes regulate myelin sheath formation and elimination

Thesis directed by Professor Bruce Appel

ABSTRACT

During development, oligodendrocytes contact and ensheathe numerous axons with myelin, a proteolipid-rich membrane that increases conduction velocity and provides trophic support. After myelin sheath formation, some wraps stabilize and mature, but other nascent sheaths are spontaneously lost. What determines sheath outcome? This dichotomy is reminiscent of synaptogenesis, wherein some nascent synapses stabilize but others are pruned. In this dissertation, I investigated mechanisms underlying myelin sheath formation and elimination using zebrafish to combine pharmacological and genetic manipulations paired with live-imaging of interactions between microglia, oligodendrocytes, and neurons. First, to investigate the likeness of myelin sheath formation to synaptogenesis, I labeled synaptic machinery and visualized axon-myelin interfaces in live larvae. I found that molecules canonically associated with synapse formation are present at the axon-myelin interface. I then disrupted transsynaptic adhesion molecules in oligodendrocytes, which revealed that a subset of these regulate sheath growth. Next, I investigated mechanisms that drive sheath elimination. I found that myelin sheaths can be eliminated both by microglia and also independently of microglial contact, similar to autonomous and non-cell autonomous elimination of synapses by microglia. By generating transgenic lines to label and ablate

microglia in tandem with oligodendrocyte reporters and transient manipulations of neuronal activity, I found that microglia phagocytose nascent myelin sheaths in a neuronal activity-regulated manner, and suppression of this program results in myelin overgrowth and ectopic wrapping of neuronal cell bodies. Together, my thesis work has identified neuronal and microglial mechanisms that regulate myelin sheath formation and elimination during development.

The form and content of this abstract are approved. I recommend its publication.

Approved: Bruce Appel

ACKNOWLEDGMENTS

I am grateful to past and current members of the Appel laboratory. Three alumni, Andy Ravanelli, Maria Cattell, and Mellissa Delcont taught me a lot of what I know about molecular cloning. Andy, Bruce, and Christina Kearns taught me how to live-image zebrafish on a confocal microscope. Bruce taught me how to perform 1-cell stage injections. I used these three techniques multiple times a week for the past several years and my graduate work simply would not have been possible without the time and energy these folks spent to teach me. Countless discussions with Caleb Doll have both sharpened my questions and emboldened me as a researcher. Katie Yergert joined the lab at the same time that I did, and I have always been inspired by her organization and professional approach to science. I want to thank the lab as a whole for always making time to provide feedback on practice talks and to celebrate the good stuff. I want to additionally thank Bruce for more than I can concisely write here. Thanks for cultivating a lab that explores in several different directions. This outlook has made boundaries between fields feel permeable and has instilled in me the confidence to take risks. Thanks also for teaching me to pair my off-grid explorations with reasonable 3- or 6-month expiration dates should experiments not be interesting or fruitful. This is a practice that I know will serve me well for years to come.

I want to thank the Neuroscience Program for taking a chance on me, a student without any background or research experience in neuroscience. Thanks for trusting that I would catch up. I hope that you all will continue to take risks on others who are similarly motivated but may have unconventional evidence of that motivation. I want to

thank my thesis committee, and especially my fearless chair, Linda Barlow, for supporting me in both the science and human realms of this endeavor.

I am thankful for my undergraduate research mentor, Julie Oxford, for letting me into her lab and introducing me to the possibility of an academic science career. Julie's lab studies the extracellular matrix of cartilage and bones, which gave me an appreciation for the lesser-studied components of biological systems and got me interested in glia, a similarly lesser-studied part of the CNS. I also want to thank Jonathon Reeck and Neda Shefa, graduate students in the lab who taught me how to pipette and helped my thinking make the jump from textbook-biology to designing experiments in the lab. Jon told me in my first week that no techniques in biology are hard to learn, you just have to learn how to do them. I am starting to disagree with this, but I still let it reassure me nearly every time I need to power through learning something new.

I want to thank my partner, Nick, for a lot. For consoling me during my early "aims meltdowns" leading up to comps and for eating dinner with me in the microscope room when experiments ran too late. We dip in and out of science talk at all hours of the day and it is wonderful. I love imagining with you all the ways science could be better, fairer, more rigorous. There's not a figure in this thesis you haven't seen or (more likely) listened to me present 10+ times to our confused cat.

TABLE OF CONTENTS

ABBREVIATIONS

AMPA	A-amino-3-hydroxy-5-methyl-4-isoxazolepropionic acid
AMPAR	AMPA receptor
AQuA	Astrocyte Quantification and Analysis
ATP	Adenosine triphosphate
BDNF	Brain-derived neurotrophic factor
BFP	Blue fluorescent protein
BoNT/B	Botulinum toxin type B
C1q	Complement component 1q
C3	Complement component 3; cleaved form abbreviated iC3b
Cadm	Cell adhesion molecule family
CADM1B	Cell adhesion molecule 1b
CADM4	Cell adhesion molecule 4
CARS	Coherent anti-Stokes Raman scattering/spectroscopy
CASK	Calcium/calmodulin-dependent serine protein kinase
CD11c	Cluster of differentiation 11c; integrin alpha X
CD47	Cluster of differentiation 47; integrin associated protein
Clec7a	C-type lectin domain containing 7A
CNS	Central nervous system
CoPA	Commissural primary ascending
COX8A	Cytochrome C oxidase subunit 8a
cpAMPAR	Calcium-permeable AMPA receptor
CR3	Complement receptor 3
CRISPR	Clustered regularly interspaced short palindromic repeats
CSF1R	Colony stimulating factor 1 receptor
CSPG4	Chondroitin sulfate proteoglycan-4; NG2 (neuron-glial antigen-2)
DLF	Dorsal longitudinal fasciculus
DLG4	Discs large homolog-4
DMSO	Dimethyl sulfoxide

DoLA	Dorsal longitudinal ascending
dpf	Days post-fertilization
EAE	Experimental autoimmune encephalitis
ECM	Extracellular matrix
EGFP	Enhanced green fluorescent protein
EM	Electron microscopy
EPSP	Excitatory post-synaptic potential
FASN	Fatty acid synthase
FGF2	Fibroblast growth factor-2
Fiji	Fiji is just Imagej
FingR	Fibronectin intrabodies generated by mRNA display
GPHN	Gephyrin
Gpr56	G protein-coupled receptor 56
hpf	Hours post-fertilization
IFN-γ	Interferon gamma
Ig	Immunoglobulin
Igf1	Insulin-like growth factor 1
IgSF	Immunoglobulin superfamily
IL-1β	Interleukin 1-beta
IL-6	Interleukin 6
IRF8	Interferon regulatory factor-8
Kv1.2	Potassium voltage-gated channel subfamily A member 2
LRRTM	Leucine rich repeat transmembrane protein
MAG	Myelin-associated glycoprotein
MAGUK	Membrane-associated guanylate kinase
MBP	Myelin basic protein
MLF	Medial longitudinal fasciculus
MNI-glutamate	4-methoxy-7-nitroindolinyl-caged glutamate
MOG	Myelin oligodendrocyte glycoprotein
Mpeg1.1	Macrophage-expressed 1, tandem duplicate 1
mRNA	Messenger RNA

MS	Multiple sclerosis
NeuroD	Neurogenic differentiation 1
NF155	Neurofascin 155 kDa
NGF	Nerve growth factor
NGL	Netrin-G ligand
NLGN	Neuroligin
NMDA	N-methyl-D-aspartate
NMDAR	NMDA receptor
NPE-caged ATP	P(3)-[1-(2-nitrophenyl)]ethyl ester of ATP
NTR	Nitroreductase (*E. coli Nfsb*)
OPC	Oligodendrocyte precursor cell; NG2 cell
P2RY12	Purinergic receptor P2Y12
p75-NTR	P75 neurotrophin receptor
PBS	Phosphate-buffered saline
PDZ	Initialism for domain contained in PSD95, Dlg1, ZO-1
Phox2b	Paired-like homeobox 2b
PLP	Proteolipid protein
pMN	Progenitor of motor neurons domain
PN-1	Protease nexin-1 (encoded by *Serpine2*)
PNS	Peripheral nervous system
PSD95	Postsynaptic density protein 95 kda
RB	Rohon-Beard
RFP	Red fluorescent protein
ROI	Region of interest
SCAP	SREBP cleavage activating protein
scRNA-seq	Single cell RNA-sequencing
SIRPα	Signal regulatory protein α
SOX10	SRY-box transcription factor-10
SREBP	Sterol regulatory-element binding protein
SRRF	Super resolution radial fluctuations

SypHy	Synaptophysin-pHluorin
TeNT	Tetanus neurotoxin light chain
Tgm2	Transglutaminase-2
TMEM119	Transmembrane protein 119
TNF-α	Tumor necrosis factor alpha
TRPV1	Transient receptor potential cation channel subfamily V member 1
TTX	Tetrodotoxin
VAMP2	Vesicle-associated membrane protein-2

CHAPTER I

INTRODUCTION

A centennial history of oligodendrocytes and microglia

1. Ramón y Cajal & Pío del Río-Hortega

Methods for visualizing cells in tissue enables research, but the limitations of these methods can alter the conclusions we form. This is as true today as it was when Ramón y Cajal (1852-1934), often referred to as the father of modern neuroscience, used and developed metallic staining techniques that labeled neurons and astrocytes, but poorly labeled other cells in brain tissue. Cajal labeled and studied neurons with Camillo Golgi's method of silver staining and later developed a gold chloride sublimate-based method that unveiled both protoplasmic and fibrous astrocytes. Such strategies enabled the first investigations and characterizations of these important cell types. Less appreciated is that the poor labeling of other cell types led Cajal to conclude that brain cells other than neurons and astrocytes were devoid of cellular processes. Cajal referred to these undistinguished cells as the "tercer elemento", or "third element", behind neurons and astrocytes, the "first" and "second elements" of the brain, respectively (Ramón y Cajal, 1913). In this dissertation, I examine the Cajal's elusive third element, cells we now know as oligodendrocytes and microglia, and investigate how these cells interact both with each other and with neurons during development of the nervous system.

Pío del Río-Hortega (1882-1945) started his scientific training, following medical training, with Nicholás Achúcarro (1880-1918), whose lab was located in the same building as Cajal's (Sierra et al., 2019). In Achúcarro's lab, del Río-Hortega developed a

new staining technique, ammoniacal silver carbonate-based labeling, which unveiled a different set of brain cell types than the previously established methods that were in use by Cajal. In particular, del Río-Hortega's method clearly delineated the boundaries and processes of microglia and oligodendrocytes, which he called mesoglia and interfascicular glia, named for his correct hypothesis that microglia were mesoderm-derived and observation that oligodendrocytes aligned with axons. After training with Achúcarro, del Río-Hortega continued to investigate microglia and oligodendrocytes in Cajal's laboratory and published a set of papers in 1919 in a scientific journal edited by Cajal, *Boletin de la Sociedad Espanola de Biologia*, titled "Third Element of the Neural Centers" (an English translation of the collection is available in (Sierra et al., 2016)). In these papers, del Río-Hortega challenged Cajal's dismissal of the third element as a group of apolar cells and provided evidence that these cells comprise two populations of cells that both have processes. Cajal and others doubted del Río-Hortega's findings, including the essential premise that oligodendrocytes existed. This led to a feud between the two and ultimately Cajal removed del Río-Hortega from his laboratory in 1920 (Pérez-Cerdá et al., 2015).

Del Río-Hortega started his own lab soon after and continued to work on microglia and oligodendrocytes. He made a number of claims about these cells that later turned out to be correct. Del Río-Hortega predicted that microglia are mesoderm-derived and phagocytic, and even speculated that phagocytosis serves to remove dead neurons and clear fragmented processes to support brain development (del Rio-Hortega, 1921). He noted morphological similarities of oligodendrocytes to Schwann cells, the myelinating cell type of the peripheral nervous system, prior to determining

that these cells formed myelin (myelin had been earlier discovered and named in 1854 by Rudolf Ludwig Virchow, but the cellular source of the substance was unknown (Boullerne, 2016)) (del Rio-Hortega, 1921). After determining that oligodendrocytes form myelin and performing a comprehensive characterization of oligodendrocytes in different brain regions, del Río-Hortega described four types of myelinating oligodendrocytes in the CNS (del Rio-Hortega, 1928). Within the last few years, single cell RNA-seq approaches have provided evidence for oligodendrocyte heterogeneity in a number of model organisms and brain regions (Marisca et al., 2020; Marques et al., 2016), well in alignment with del Río-Hortega's predictions about diversity within the lineage from nearly a century ago (del Rio-Hortega, 1928).

2. Developments in glial neurobiology after del Río-Hortega

Investigations of neurons and glia became markedly separate mid-century, a schism driven by a major advance: the advent of electrophysiology, and in particular the adaptation of voltage clamp for neuronal intracellular recordings (Hodgkin and Huxley, 1952). Neurons are electrically excitable, but glia largely are not (Somjen, 1975; Watson, 1974). Therefore, the right technique emerged at the right time for the field of neuronal physiology to blossom, but glia research continued at the pace of labeling individual cells and studying morphology. Myelin became relevant as it applied to neuronal conduction velocity and microglia research stalled for nearly forty years.

2.1 Oligodendrocyte milestones after del Río-Hortega

Oligodendrocyte history is somewhat muddled by the independent discovery of myelin long before del Río-Hortega found that oligodendrocytes form myelin. I will focus on those oligodendrocyte-specific milestones that followed del Río-Hortega's discovery,

but prior to del Río-Hortega there was rampant speculation about myelin's source and composition. For example, Cajal (who never accepted del Río-Hortega's work on oligodendrocytes) believed that axons produced their own myelin, a view that some in the field held into the 1970's, and Virchow, who named myelin, thought myelin was formed of the same material as egg yolks (reviewed in (Boullerne, 2016)). The use of electron microscopy and culturing methods to study myelin and oligodendrocytes began to overturn some of these previous speculations about myelin's form and function.

In 1960 and 1961, Mary Bartlett Bunge and Richard Bunge developed the first demyelination model, using the cat spinal cord, and observed remyelination by cells that invaded the lesion and contacted axons (Bunge et al., 1961, 1960). The Bunges noted that the cells that invaded the lesion to participate in remyelination did not fit the ultrastructural descriptions of either oligodendrocytes or astrocytes, so they instead called these remyelinating cells "reactive macroglia" (Bunge et al., 1961, 1960). At the time, oligodendrocyte maturation had not been studied and almost all investigations had focused on mature, myelinating cells. A few years later, James Vaughn studied oligodendrocytes in developing and adult rat optic nerve and first characterized differences between mature myelinating oligodendrocytes, newer oligodendrocytes, and cell types he called small and large glioblasts that he speculated may be precursors for both oligodendrocytes and astrocytes (Vaughn, 1969). Vaughn noted that younger oligodendrocytes were bigger and had more prominent endoplasmic reticulum and Golgi apparatus than mature oligodendrocytes and he called these cells "active", potentially similar to the newly myelinating "reactive macroglia" observed by the Bunges. Following Vaughn, Mori and Leblond (1970) visualized oligodendrocytes in rat

corpus callosum by electron microscopy and observed three distinct groups of cells, each having cytoplasmic matrix that appeared light, medium, or dark in micrographs. At early ages, the light oligodendrocytes were more common than the other categories, but tissue from older animals contained more dark oligodendrocytes, raising the possibility that these variants corresponded to maturational states (Mori and Leblond, 1970). This hypothesis was confirmed later by ^{3}H-thymidine labeling that found light oligodendrocytes frequently divided, corresponding to a precursor, medium oligodendrocytes seldom divided, and dark oligodendrocytes never divided (Paterson et al., 1973). Up to this point, most work on oligodendrocytes took place *in situ*, but the advent of culturing methods accelerated research on oligodendrocyte cell biology. For example, Martin Raff and Mark Noble discovered that a common progenitor, called the O-2A progenitor cell, could give rise to both oligodendrocytes and astrocytes in the absence or presence of serum, respectively (Raff et al., 1983).

In the 1990's, attention turned toward the potential roles of axons in tuning myelination. Ben Barres had used patch-clamp during his graduate studies with David Corey to discover that oligodendrocyte lineage cells express numerous neurotransmitter receptors and ion channels, raising the possibility that oligodendrocytes listen and adapt to neuronal activity (Barres, 1991; Barres et al., 1988, 1990). He then pursued a postdoctoral position with Martin Raff in which he investigated neuron-glial interactions directly, by manipulating neuronal activity and investigating effects on the oligodendrocyte lineage. Using the rat optic nerve as a model system, Barres found that nerve transection or intraocular administration of tetrodotoxin (TTX) to block neuronal action potentials severely depleted oligodendrocyte lineage cells (Barres and Raff,

1993), indicating that intact neuronal activity regulates oligodendrocyte number in this system. A few years later, Catherine Lubetzki's group performed a similar investigation in mice and investigated myelination both in vivo and in culture (Demerens et al., 1996). Lubetzki's group performed intraocular injections of TTX and measured myelin segments formed on axons. They performed these injections after oligodendrocytes were formed and thus found that although cell number was unchanged, oligodendrocytes formed fewer myelin segments on axons. Conversely, increasing activity in cultures treated with α-scorpion toxin increased myelination of the axons over 2-fold. Taken together, these studies indicated that the oligodendrocyte lineage is responsive to neuronal activity and set the foundation for later work on activity-dependent myelination and axon-myelin interactions.

2.2 Microglia milestones after del Río-Hortega

After del Río-Hortega, there was a relative paucity of work on microglia until the mid-1960's, at which time several individuals, including David Maxwell, Lawrence Kruger, and David Caley began to express doubt that microglia constituted a CNS cell type at all (Caley and Maxwell, 1968; Ibrahim et al., 1974; Maxwell and Kruger, 1965). Labeling methods for microglia were poor: there were no methods other than del Río-Hortega's silver labeling technique and microglia were hardly identifiable by electron microscopy (Caley and Maxwell, 1968). Furthermore, the observation that pericytes are phagocytic convinced Maxwell and Kruger that del Río-Hortega's phagocytic microglia were merely misidentified pericytes (Maxwell and Kruger, 1965). A few years later, Georg Kreutzberg's lab developed a new model of microglial activation that, in retrospect, was the first of many microglia investigations performed by an investigator

other than del Río-Hortega that was not centered on debunking the existence of these cells (Blinzinger and Kreutzberg, 1968). In Kreutzberg's model, the group lesioned the peripheral right facial nerve in rats and investigated microglial interactions with the central origin of the nerve, located in the facial nucleus in the brainstem (Blinzinger and Kreutzberg, 1968; Moran and Graeber, 2004). They visualized microglia by electron microscopy and found that microglia proliferated and surrounded the facial nucleus, and that motor neurons had fewer synapses on the somas and proximal dendrites. This led the group to conclude that microglia participate in synapse elimination, or "synaptic stripping" in response to neuronal injury. It is still unclear if the motor neuron synapses in this model are actively phagocytosed by microglia or eliminated by the neurons themselves, but the group did not detect any evidence of phagocytosis.

A few years after synaptic stripping was discovered, Mohammed Ibrahim and others developed the first selective chemical labels for microglia, which detected high levels of ATPase and UDPase in microglia relative to other CNS cell types (Ibrahim et al., 1974). This was the first new method since del Río-Hortega's metallic staining protocol and helped push back against the ongoing doubt about whether microglia existed. Further advances in labeling, taking advantage of selective expression of microglia-specific expression of the calcium binding protein Iba1, took another two decades to develop and Iba1 continues to be widely used to detect microglia (Ito et al., 1998). In that time, Helmut Kettenmann, a trainee of Georg Kreutzberg, founded his own lab and developed protocols for culturing microglia and studying microglial physiology by both patch-clamp and fura-2 ratiometric calcium imaging (Kettenmann et al., 1990; Walz et al., 1993). Kettenmann's group found that cultured microglia respond

to ATP with large inward currents and calcium transients, and postulated based on limited responses to adenosine and AMP that this was likely mediated by a P2 class ATP receptor (Walz et al., 1993). When microglia were first imaged *in vivo* in upper layers of mouse cortex, Dimitrios Davalos and Axel Nimmerjahn confirmed that ATP is the predominant chemoattract for microglia in injury and also discovered that microglia are quite active (surveillant) even in the absence of injury (Davalos et al., 2005; Nimmerjahn et al., 2005).

An ongoing technical barrier has been identifying transcriptional differences between microglia and peripheral macrophages to enable cell type-specific manipulation of each of these cell types. Kettenmann noted in 1990 that membrane properties differ between these cell types (Kettenmann et al., 1990) but identifying differences in gene expression amenable to microglia-specific labeling and manipulation has taken much longer. In mouse and human, a transmembrane protein of unknown function, TMEM119, appears to be expressed in microglia but not macrophages (Bennett et al., 2016; Satoh et al., 2016). However, TMEM119 is not expressed by microglia in all model organisms (Geirsdottir et al., 2019), its expression decreases in inflammatory conditions (Bennett et al., 2016), and, contrary to original reports, it is expressed by a subset of peripheral macrophages during development (Grassivaro et al., 2020). P2RY12 (sometimes called P2Y12) is another promising marker that appears to label microglia and dural and choroid plexus macrophages, but not other macrophages (McKinsey et al., 2020). Single cell RNA-seq-based approaches have uncovered a great deal of microglial cell-state heterogeneity (Hammond et al., 2019; Li et al., 2019) and have determined markers that define macrophage-fated microglia (Utz

et al., 2020), raising the possibility that such approaches will allow for the discovery of more restricted and constitutive microglia-specific markers.

Oligodendrocyte biology

1. Overview of myelin development and plasticity

Oligodendrocytes wrap neuronal axons with myelin to increase conduction velocity (Ford et al., 2015) and provide trophic support (Fünfschilling et al., 2012; Lee et al., 2012). Oligodendrocytes develop from oligodendrocyte precursor cells (OPCs), which are specified in ventricular zones, including the pMN progenitor domain of the ventral spinal cord. OPCs migrate toward target axons and a subset differentiate into myelinating oligodendrocytes. Whether OPCs that do not differentiate represent an equipotent reserve pool or are a distinct subset with yet unknown functions is not clear (reviewed by (Bergles and Richardson, 2016; Mangin and Gallo, 2011)). Those cells that are myelin-fated elaborate processes that wrap axons and begin to synthesize proteins and lipids that comprise myelin. This process requires the initiation of myelin gene expression, which is largely under the control of the transcription factor, myelin gene regulatory factor (Myrf) (Emery et al., 2009). Myrf initiates transcription of several major myelin genes, including *Mbp*, *Plp*, *Mag*, and *Mog*. Wrapping requires the generation and localization of these adhesive myelin proteins in concert with robust lipid synthesis (each of these is covered in more detail below). Following initial wrapping, layers of myelin sheaths undergo compaction, which extrudes most cytoplasm from the sheaths. Far from a static product, myelin sheaths undergo protein and lipid turnover

and new oligodendrocytes and myelin are generated into adulthood in humans (Yeung et al., 2014).

After formation, myelin sheaths remain mutable, tunable structures that can change in an activity- or experience-dependent manner. The responsiveness of the oligodendrocyte lineage to neuronal activity was first documented in the visual system by Barres and Lubetzki and has since been investigated in numerous systems and contexts (Barres and Raff, 1993; Demerens et al., 1996). Learning how to juggle and play the piano, activities that engage populations of neurons, are associated with white matter additions in relevant brain areas (Scholz et al., 2009). This activity-dependent myelin growth, or “myelin plasticity”, can be recapitulated at the cellular level by optogenetic or chemogenetic stimulation of neurons (Gibson et al., 2014; Mitew et al., 2018) or expression of clostridial neurotoxins to suppress vesicular release from neurons (Hines et al., 2015; Koudelka et al., 2016; Mensch et al., 2015; Wake et al., 2015). Do activity-dependent changes in myelin impact CNS function? Recent work is consistent with this possibility. New oligodendrocytes and new myelin are required for motor learning and memory preservation (McKenzie et al., 2014; Pan et al., 2020; Steadman et al., 2020; Wang et al., 2020). These systems-level adaptations are presumably driven by activity-dependent oligodendrocyte proliferation and differentiation (Barres and Raff, 1993; Gibson et al., 2014; Hughes et al., 2018) and myelin growth and remodeling on behaviorally relevant neurons. However, all glial cells are responsive to neuronal activity, raising the possibility that other glial cells may promote or solidify adaptive changes by regulating properties of myelin. Getting the whole picture will

require determining not only how cell types interact with one another in isolation, but also as a complex, functioning unit.

2. Myelin wrapping and adhesion

Myelin is a specialized membrane that differs from the plasma membrane, particularly enriched in lipids, comprising 75% of the dry weight of myelin (Nave and Werner, 2014) and proteins that organize myelin structure and adhesion to the axon. In the current model of myelin wrapping, actin polymerization drives the advancement of the innermost wrap (the “inner tongue”) around the axon and trailing depolymerized (G-) actin permits lateral membrane spreading behind the F-actin rich leading edge (Nawaz et al., 2015; Snaidero et al., 2014; Zuchero et al., 2015). After the first wrap around the axon, the inner tongue maintains proximity to the axon by subverting the previous layer and continuing to wrap. To maintain multiple layers of myelin membrane, two adhesive events must occur: 1) the adhesion of myelin layers together to form a compact sheath, and 2) the adhesion of myelin to the axon. The major proteins myelin basic protein (MBP) and proteolipid protein (PLP), which together account for 68% of total myelin protein (Jahn et al., 2009, 2020) regulate myelin sheath compaction by adhering internal and external membrane leaflets, respectively. MBP is also required for actin disassembly during wrapping to promote membrane spreading (Zuchero et al., 2015), potentially explaining the earlier and more significant phenotype of MBP mutant mice relative to the milder PLP null phenotype (Dupouey et al., 1979; Gould et al., 2018; Imagawa et al., 2014; Klugmann et al., 1997).

To promote adhesion to the axon, adhesion proteins must be corralled into the lateral edges that will form the paranodal loops that adhere to the axon (reviewed by

(Rasband and Peles, 2016)). The most well-studied adhesion protein at this interface is neurofascin-155 (NF155), which binds axonal contactin-1 (Cntn1) (Gollan et al., 2003). Additional adhesion molecules from the immunoglobulin superfamily also coordinate axon-myelin adhesion along the juxtaparanode and internode, including Tag-1, Cadm1, and Cadm4 (Elazar et al., 2018; Hughes and Appel, 2019; Poliak et al., 2003; Traka et al., 2003). Manipulation of these adhesion molecules disrupts myelin sheath number, length, targeting to axons, and lamellar organization (Djannatian et al.; Elazar et al., 2019; Hughes and Appel, 2019; Klingseisen et al., 2019), raising the possibility that endogenous mechanisms that modify adhesion may enable myelin plasticity.

Modification of adhesion complexes, either autonomously by the axon or myelin, or by other glial cells, represents one way that myelination can be adjusted. High frequency firing (100 Hz) can induce reversible myelin lifting at the paranodes that is visualizable with CARS imaging (Huff et al., 2011), but the mechanism underlying this adhesive flexibility has not been identified. Over 95% of nodes of Ranvier in the rat brain are contacted by astrocytes and 30-50% are contacted by OPCs, a position that grants these cell types proximity to neighboring paranodal adhesion complexes. Recent work found that astrocytes exocytose a thrombin inhibitor, protease nexin-1 (PN-1, encoded by *Serpine2*), that prevents thrombin-mediated cleavage of NF155 (Dutta et al., 2018), the glial adhesion protein that anchors myelin paranodal loops to the axon. At steady state, about 20% of nodes exhibited lifted paranodes, which was further increased when astrocytic exocytosis was blocked. This model suggests that astrocytic secretion of PN-1 can promote sheath stability by preventing thrombin-mediated NF155 cleavage. Although the regulation of astrocyte exocytosis of PN-1 has not been

elucidated, such a mechanism could in principle permit the lifting and adjustment of myelin sheaths on axons. In mouse cortex, OPCs express *Serpine2* at levels comparable to astrocytes (Zhang et al., 2014), raising the possibility that OPCs may also regulate modify paranodal adhesion through this mechanism.

3. Myelin lipid synthesis is supported by astrocytes and microglia

Although proteins are essential for myelin form and function, myelin is comparatively protein-poor and lipid-rich, containing 25% protein and 75% lipid by dry mass (vs 50/50%, typical of most cell membranes (Park, 2001)). However, because there are far fewer methods available to study lipids compared to proteins (Muro et al., 2014), lipid localization and trafficking in myelin remains a technical blind spot in myelin biology. One strategy that has been used to overcome this barrier is to study the genes and proteins that regulate lipid synthesis, with the caveat that synthesized lipids may localize differently than the enzymes that synthesize them. This approach revealed that cholesterol is required for the earliest stages of axon wrapping: wrapping is almost entirely blocked by global loss of function mutation of *hmgcs1*, which encodes the rate-limiting enzyme for cholesterol synthesis (Mathews et al., 2014). Do oligodendrocytes synthesize cholesterol and other lipids autonomously? Mice with oligodendrocyte-specific deletion of fatty acid synthase (*Fasn*) had hypomyelination in various CNS regions, but this could be partially rescued by increasing dietary lipids (Penelope Dimas et al, 2019). Indeed, lipid analysis of purified myelin revealed that oligodendrocytes incorporate circulating lipids to build myelin (Camargo et al., 2017; Nave and Werner, 2014), consistent with the possibility that proximal neurons and glia may also provide and influence the lipids available for myelin construction.

Both microglia and astrocytes support lipid synthesis by oligodendrocytes, but in distinct ways. The presence of microglia supports the autonomous generation of myelin lipids by oligodendrocytes (Hamilton and Rome, 1994). Oligodendrocytes cultured with microglia or in microglia-conditioned medium formed 2- to 7-fold more sulfatide, a major myelin lipid, than oligodendrocytes that were cultured alone. These data raise the possibility that microglia secrete a soluble factor that acts on oligodendrocytes to stimulate myelin synthesis. Such a factor may be secreted more robustly in the presence of inflammation, because inflammatory stimulation of microglia further increased myelin production by oligodendrocytes (Setzu et al., 2006). In addition to microglial stimulation of myelin lipid synthesis, astrocytes provide lipids to oligodendrocytes directly. It was recently revealed that astrocytes provide the majority of required lipids to oligodendrocytes (Camargo et al., 2017). Astrocyte-specific deletion of the major lipid biosynthesis regulator SREBP cleavage activating protein (SCAP) caused more severe and persistent hypomyelination than oligodendrocyte-specific loss of SCAP, which resolved after a brief developmental delay (Camargo et al., 2017). This is consistent with previous findings from a mouse model of oligodendrocyte-specific deletion of *Fdft1*, the gene encoding squalene synthase, also required for cholesterol synthesis, which exhibited early hypomyelination that also caught up by adulthood (Saher et al., 2005). Therefore, in addition to uptake of lipids and cholesterol from the extracellular environment (Nave and Werner, 2014), oligodendrocytes build myelin primarily from astrocyte-derived lipids. Intriguingly, this may depend on regional astrocyte heterogeneity. Grey matter astrocytes were found to secrete more cholesterol than white matter astrocytes, and inhibiting cholesterol synthesis from white matter-

derived astrocytes improved in vitro myelination (Werkman et al., 2020), raising the possibility that astrocyte provisions may differ regionally with consequences for myelination. Together, these data extend the known role of astrocytes in providing cholesterol to neurons to promote synapse formation (Mauch et al., 2001) to include oligodendrocytes to enable myelin formation.

4. Synapses in the oligodendrocyte lineage

Dwight Bergles discovered during his postdoc with Craig Jahr that OPCs form *bona fide* structural and functional synapses with neurons (Bergles et al., 2000). Since then, these neuron-to-OPC synapses have been found to be formed by pyramidal neurons and interneurons in hippocampus (Bergles et al., 2000; Lin and Bergles, 2004), axons in corpus callosum (Etxeberria et al., 2010; Ziskin et al., 2007), and climbing fiber neurons in cerebellum (Lin et al., 2005). The function of these synapses is not entirely clear, beyond their noted success at “upsetting the old order established by neuronal physiology” (Mangin and Gallo, 2011). One possibility is that these synapses precede myelination and can turn into myelin sheaths (Almeida and Lyons, 2014). This idea is intuitively appealing, but evidence largely runs counter to this possibility. Ziskin et al. (2007) found that OPCs received glutamatergic inputs from only the unmyelinated axons in the corpus callosum (Ziskin et al., 2007), and OPCs receive synaptic input from other unmyelinated neurons, including climbing fibers of the cerebellum (Lin et al., 2005). In OPC and dorsal root ganglion cell myelin-forming cocultures, no synaptic input could be recorded from OPCs prior to myelination (Wake et al., 2015). Furthermore, glutamatergic signaling to OPCs impeded differentiation but promoted proliferation in organotypic slices (Fannon et al., 2015), which is inconsistent with a role for excitatory

synaptic signaling in promoting myelination. However, if neuron-OPC synapses do function to support OPC proliferation, perhaps these synapses increase the number of oligodendrocyte lineage cells that are available to differentiate and myelinate. Indeed, an investigation using a mouse lacking functional OPC synapses (*Gria3* null; *Gria2* and *Gria4* oligodendrocyte lineage-specific conditional knockout mouse to ablate nearly all AMPA receptor-mediated input to OPCs) found a reduced number of oligodendrocytes and an increase in oligodendrocyte-lineage apoptotic cells (Kougioumtzidou et al., 2017), suggesting these synapses maintain OPC number and survival. Dye-filled individual oligodendrocytes had myelin sheaths of normal length and number, indicating that AMPA receptor mediated signaling may function to maintain OPC numbers but does not appear to modify myelination in ways that were measured by the authors (Kougioumtzidou et al., 2017).

Among OPCs that receive synapses but later differentiate into myelinating cells, it has been observed that neurotransmitter ceases to evoke somatic currents in oligodendrocytes (Etxeberria et al., 2010; Kukley et al., 2010), which has been interpreted to indicate that synapses are disassembled upon myelination. Disassembly is also supported by downregulation of neurotransmitter receptor expression by myelinating oligodendrocytes (Zhang et al., 2014). A limitation of the disassembly hypothesis is that synapses have not been imaged to detect disassembly[1]. Potentially, a loss of somatic currents could be explained by recording distant from the synapse (space clamp) in a cell recognized for generating vast amounts of insulating lipids. This explanation is further supported by modeling work that found EPSPs decay especially

[1] In Chapter II, I label and image synaptic proteins at the axon-myelin interface.

fast in OPC distal processes (Chan et al., 2013) and are less likely to reach the soma than dendritic EPSPs in neurons. Altogether, whether OPC synapses are disassembled or are merely difficult to detect is unclear. Furthermore, it is also unclear if these synapses or neurotransmitter-mediated signaling support oligodendrocyte function in any discernable way. NMDARs present on myelinating oligodendrocytes render them vulnerable to excitotoxic injury in ischemia (Káradóttir et al., 2005), and OPCs appear to acquire more AMPARs and NMDARs in aging (Spitzer et al., 2019), but a clear tie to oligodendrocyte function has remained elusive. Kougioumtzidou et al. (2017) found that oligodendrocyte lineage cells lacking AMPARs differentiated normally into myelinating oligodendrocytes with typical myelin sheath lengths and numbers (Kougioumtzidou et al., 2017). Additionally, a mouse model with oligodendrocyte lineage-specific deletion of the obligate NMDA receptor subunit NR1 had OPCs that formed normally functioning synapses and differentiated into oligodendrocytes with no apparent myelination defects (De Biase et al., 2011). However, De Biase et al. (2011) did observe that OPCs substantially increased cell surface localization of calcium permeable AMPARs (cpAMPARs). Potentially, the upregulation of cpAMPARs reflects compensation and indicates that NMDARs do perform a function in oligodendrocytes that was not assessed by the authors. Indeed, later work showed that oligodendrocyte NMDARs regulate glucose supply to axons (Saab et al., 2016), a function that De Biase et al. (2011) likely would not have assessed because oligodendrocyte provision of trophic support to axons was not an established function of oligodendrocytes until the following year (Fünfschilling et al., 2012; Lee et al., 2012).

Potentially, conflicting views on whether synaptic proteins and receptors are required for oligodendrocyte function arises from our incomplete knowledge of the full repertoire of oligodendrocyte functions. Currently, oligodendrocytes are thought to insulate axons and provide trophic support, but even these functions are less resolved than is typically assumed. For example, the field has known that oligodendrocytes provide trophic support to axons for less than a decade (Fünfschilling et al., 2012; Lee et al., 2012). Additionally, earlier this year it was revealed that the insulation provided by myelin is incomplete and the submyelin space is conductive (Cohen et al., 2020). Depolarization of the inner tongue of myelin sheaths is supported by this new model (Cohen et al., 2020), which may allow oligodendrocytes to detect neuronal activity at the resolution of single action potentials and provide commensurate trophic support. These oligodendrocyte functions, and functions yet to be discovered, will likely be further compounded by oligodendrocyte heterogeneity. Marques et al. (2016) reported thirteen transcriptionally distinguishable subtypes of oligodendrocyte lineage cells, including six types of myelinating oligodendrocytes (Marques et al., 2016). Later work attributed some of the OPC diversity to different developmental states (Marques et al., 2018), but oligodendrocyte heterogeneity has already been shown to have consequences for the provision of trophic support: oligodendrocytes provide lactate to axons in the optic nerve, but glucose to axons in the corpus callosum (Meyer et al., 2018). Without a complete understanding of oligodendrocyte functions, it is difficult to determine whether synaptic proteins, or any other proteins, are required or not for the function of the lineage.

Microglia biology

1. Microglia develop from macrophages and share macrophage functions

Microglia are the tissue-resident macrophages of the CNS. They share common cellular features and functions with other types of tissue-resident macrophages, such as osteoclasts in bone and Kupffer cells of the liver. Every tissue type has a resident macrophage, which serve alongside neutrophils in the innate immune system, the first line of defense against pathogens. Macrophages phagocytose pathogens and debris (from Greek, macrophage = makròs phagein = “large eater”), present antigens to T-cells to trigger the adaptive immune response, and secrete both pro- and anti-inflammatory cytokines and chemokines to signal to other immune cell types. Microglia in the CNS perform these functions, but are also quite active, or “surveillant”, even in the absence of disease or injury (Davalos et al., 2005; Nimmerjahn et al., 2005). How do microglia influence CNS form and function during normal development?

Studying the contributions of microglia to CNS development and function requires tools to manipulate or ablate microglia. A number of existing tools target vulnerabilities of microglial development. Although microglia development is more thoroughly reviewed elsewhere (Nayak et al., 2014), I will introduce milestones relevant to perturbation. Erythromyeloid progenitors in the yolk sac, and specifically the rostral blood island in teleost, are specified to become either macrophages or neutrophils in an interferon regulatory factor 8 (Irf8) -dependent manner (Holtschke et al., 1996; Scheller et al., 1999; Shiau et al., 2015). Deletion or loss of function mutations in *Irf8* cause excessive neutrophils and absence of most types of macrophages, including microglia. A subset of yolk sac macrophages will migrate to invade the CNS and differentiate into

microglia. It was recently revealed that this microglia-fated subset is transcriptionally distinguishable within the yolk sac, suggesting that these cells are hardwired for microglia fate (Utz et al., 2020). The distribution and survival of microglia within the CNS depends on colony stimulating factor-1 receptor (CSF1R) function, a receptor that binds ligands IL-34 and CSF-1 (Erblich et al., 2011; Ginhoux et al., 2010). Whereas both Irf8 and CSF1R disruption have allowed investigators to study how the CNS develops without microglia (Figure 1.1), CSF1R inhibition is increasingly favored due to the development of drugs targeting this receptor (Elmore et al., 2014). Newly identified markers for yolk sac microglia-fated macrophages may enable the discovery of new targets for earlier or more specific perturbation of microglia (Utz et al., 2020).

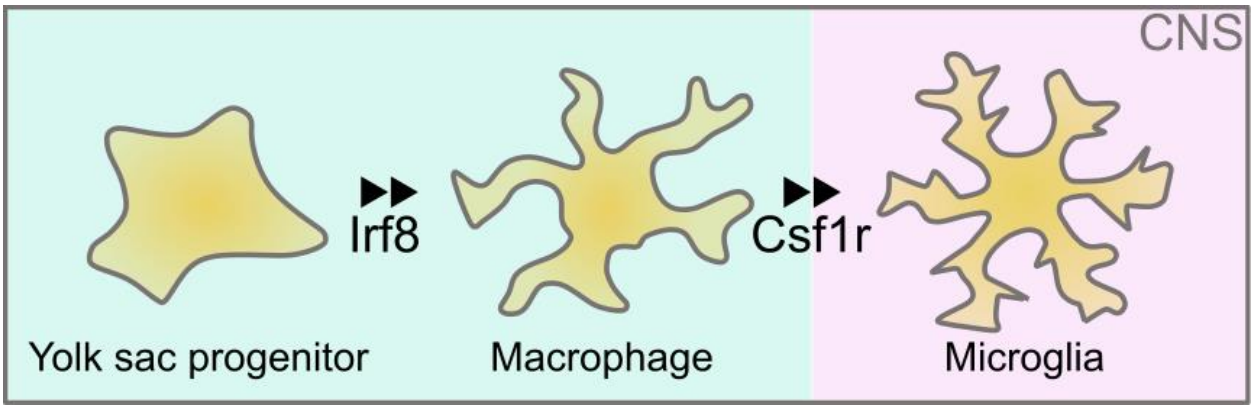

Figure 1.1. Microglia development. Yolk sac progenitor cells (rostral blood island in teleosts) are specified to become macrophages by interferon regulatory factor 8 (Irf8). Macrophages that invade the CNS require colony stimulating factor receptor 1 (Csf1r) function to distribute and survive as microglia.

2. Microglial contributions to CNS development

In addition to their roles in the innate immune response, microglia are also phagocytic and secretory during normal brain development. Microglia eliminate excess neurons and synapses. They also secrete factors that promote programmed cell death, the survival, proliferation, and differentiation of neural progenitors, vascularization and vascular branching, and OPC proliferation and differentiation (reviewed by (Frost and Schafer, 2016)).[2]

2.1 Microglial interactions with neurons

Microglia can both initiate neuronal apoptosis and clear cell corpses following programmed cell death. A large number of neurons are overproduced during development and then cleared by microglia. The earliest published example that implicated microglia in clearance explored cell death in upper layers of cortex in developing rat (Ferrer et al., 1990). Ferrer et al. used del Río-Hortega's silver labeling protocol to identify microglia and found that ameboid, phagocytic microglia appeared at the time of peak cell death and phagocytosed neuronal cell bodies and axons. The group speculated that such engulfment might serve to eliminate redundant connections or remove neurons that had not been innervated, because the arrival of microglia temporally correlated with the establishment of thalamocortical and corticothalamic projections. It was unclear at the time if microglia were responding to dying neurons or if microglia actively determined neurons for removal. Later work in the chick retina favored the latter possibility. Frade and Barde (1998) found that microglia in the retina actively

[2] In Chapter III, I provide evidence that microglia additionally refine myelination by phagocytosing myelin sheaths.

promote neuronal cell death by producing nerve growth factor (NGF), which signals to p75-NTR located on neurons to induce death (Frade and Barde, 1998). Cell death was reduced in retinas lacking microglia (retinas that had been separated prior to microglial colonization) and was also reduced in microglia-containing retinas that were treated with an NGF function-blocking antibody. NGF expression was largely limited to the retinal microglial population, suggesting that microglial NGF actively signals to neurons to promote death. The induction of neuronal death by microglia has also been observed in other systems; surprisingly, microglia appear to utilize a variety of secreted cues to induce the death of different types of neurons. Spinal cord microglia / macrophages secrete TNF-α to promote the death of spinal motor neurons in rat embryos (Sedel et al., 2004). Additionally, Purkinje cells in early postnatal mouse cerebellum are induced to undergo programmed cell death in response to superoxide ions produced by microglia (Marín-Teva et al., 2004). The group tested additional candidate signaling molecules and found that NGF signaling does not contribute to Purkinje cell death or clearance, in contrast to the mechanism of cell death induction by microglia in the retina (Frade and Barde, 1998). Together, these studies demonstrate that microglia utilize an array of signaling molecules to induce neuronal cell death, raising the possibility that a ligand-receptor code exists in different brain regions to mediate microglial refinement of circuitry in a specific and targeted manner.

In addition to modulating neuronal viability, microglia can acutely suppress activity by contacting neuronal cell bodies (Cserép et al., 2020; Eyo et al., 2014; Li et al., 2012; Peng et al., 2019). These flexible and reversible contacts occur at specialized somatic junctions on neurons and persist on a timescale of minutes to hours, with over

80% of neurons in human and mouse brain receiving microglial contact (Cserép et al., 2020). Several studies have converged on the following activity-dependent model of contact initiation: Upon vesicular- or hemichannel-mediated ATP release from active neurons (Cserép et al., 2020; Li et al., 2012), the microglia-specific ATP receptor P2ry12 mediates microglial detection and process extension toward active neurons (Cserép et al., 2020; Eyo et al., 2014; Peng et al., 2019). Following contact, the intrinsic excitability and firing rate of neurons decreases (Li et al., 2012; Peng et al., 2019), but the mechanism of activity suppression is not yet resolved. Notably, Cserép et al. (2020) found that microglia contact neuronal somas specifically near clusters of Kv1.2 channels, raising the possibility that microglia interactions with Kv1.2 channels underlies activity suppression. In line with the vast number of microglia-neuron contacts, microglial depletion caused aberrant neuronal activity in mouse (Szalay et al., 2016) and seizures in human patients with microglia-depleting mutations in *CSF1R* (Oosterhof et al., 2019). Taken together, these data provide evidence that microglia can suppress neuronal activity and may contribute to activity homeostasis, but future work is needed to identify the mechanism of activity suppression.

2.2 Microglial interactions with synapses

Microglia also contact synapses, and somewhat surprisingly the activity-suppressing effects of microglia contact on neuronal cells bodies have not yet been explored at synapses. Instead, most work on microglia-synapse interactions has investigated synapse elimination or structural modification. The earliest example of microglia-synapse interactions was performed in the later 1960's in which Georg Kreutzberg's lab identified microglia-mediated synapse elimination (not necessarily

phagocytosis) in response to neuronal injury (Blinzinger and Kreutzberg, 1968). Beth Stevens, while a postdoc with Ben Barres, found that mice lacking components of the classical complement cascade had more retinogeniculate synapses (Stevens et al., 2007), suggesting that a CNS cell type responsive to complement deposition (probably microglia) may regulate synapse elimination. Later work by Dorothy Schafer, a postdoc in the Stevens's lab, revealed that microglia engulf synapses in a complement- and activity-regulated manner to drive eye-specific segregation of retinal ganglion cells inputs to lateral geniculate nucleus of the thalamus (Schafer et al., 2012). Schafer found that microglia engulfed more synapses when retinal ganglion cell activity was suppressed by intraocular administration of TTX. By contrast, an earlier study found that intraocular TTX caused microglia in visual cortex to contact synapses less frequently, raising the interesting question of how microglia both contact fewer and engulf more synapses. A possible explanation for these seemingly disparate findings is that microglia-synapse interactions may be multimodal and vary regionally or among synapse types, similar to the numerous parallel mechanisms used by microglia for induction of neuronal apoptosis and clearance. There are many other examples of microglia-synapse interactions that seem to vary among and within brain regions and model systems. In vivo timelapse imaging in mouse visual cortex by Marie-Ève Tremblay et al. (2010) found that visual deprivation (dark rearing) altered microglial interactions with dendritic spines and increased the phagocytosis of synaptic elements by microglia (Tremblay et al., 2010). Following microglial contact, some spines grew while others shrunk, and a greater proportion of spines that were contacted were later eliminated than uncontacted spines. Additionally, some of the signaling molecules that

cue synapses for microglia-mediated elimination vary between brain regions (Gunner et al., 2019), with fractalkine signaling regulating synapse elimination in mouse barrel cortex and complement receptor 3 regulating elimination in lateral geniculate nucleus (Gunner et al., 2019; Schafer et al., 2012). It is also unclear what parts of synapses are engulfed by microglia and this may contribute to variable findings. Reports of engulfment frequently report presynaptic element engulfment (Schafer et al., 2012; Tremblay et al., 2010; Weinhard et al., 2018), and less frequently postsynaptic engulfment (Paolicelli et al., 2011), but a recent timelapse imaging analysis of ~9000 spines in hippocampus found that microglia never engulfed any spines (Weinhard et al., 2018). These disparate findings point to substantial variability in the underlying rules governing microglia-synapse interactions, potentially resulting from regional, synaptic, or microglial heterogeneity.

2.3 Microglia interactions with the oligodendrocyte lineage

Microglia secrete cues that promote OPC proliferation, differentiation, and myelination. By ablating microglia during early postnatal development (P2-P7) with the CSF1R inhibitor BLZ945, Hagemeyer et al. (2017) found that microglia maintain OPC numbers and myelination in corpus callosum and cerebellum (Hagemeyer et al., 2017). Mice without microglia had fewer OPCs during development and by early adulthood had reduced myelin. Some of the phenotypes varied between brain regions, which could reflect regional heterogeneity in oligodendrocytes (Marques et al., 2016) or microglia (De Biase et al., 2017; Hammond et al., 2019; Li et al., 2019). Indeed, a specific subset of microglia that express *Cd11c* are present in developing white matter and specific ablation or conditional knockout of Igf1 in these cells impaired myelination (Wlodarczyk

et al., 2017). Together, these data suggest that a subset of microglia promote myelination through Igf1 production. Other signaling pathways between microglia and OPCs may also modify myelin development. Giera et al. (2018) found that an adhesion G-protein coupled receptor, Gpr56, located on OPCs, interacts with Transglutaminase-2 (Tgm-2) secreted by microglia to promote OPC proliferation in the presence of the extracellular matrix (ECM) protein laminin-111 (Giera et al., 2018). Importantly, remyelination following a demyelinating lesion was impaired in knockout mice lacking Tgm2 – Gpr56 signaling, suggesting that this microglia-OPC-ECM signaling axis is essential not only for OPC numbers but functional remyelination (Giera et al., 2018). Tgm2 can also be expressed by astrocytes, raising the possibility that regions with differential densities of astrocytes and microglia may maintain signaling via this signaling axis (Espitia Pinzon et al., 2019). Furthermore, microglial deposition of the ECM molecule CSPG4 in aging shifts the microenvironment to favor the differentiation of NG2 cells into astrocytes at the expense of oligodendrocytes (Baror et al., 2019). Taken together, microglia-ECM interactions may promote OPC proliferation and differentiation in development but appear to increasingly inhibit OPC differentiation in later life.

In addition to Igf1 production, microglia are secretory cells that generate a variety of molecules and cytokines that have been studied in regulation of neuronal and synaptic activity (reviewed by (York et al., 2018)). However, some of these secreted molecules have been independently implicated in regulating myelination. For example, microglia secrete brain derived neurotrophic factor (BDNF) (Coull et al., 2005; Gomes et al., 2013; Nakajima et al., 2002; Parkhurst et al., 2013) which has been found to

promote myelination in numerous contexts (Geraghty et al., 2019; Lundgaard et al., 2013; Mctigue et al., 1998), but the contribution of microglia-derived BDNF to myelination has not been investigated. By contrast, astrocyte-derived BDNF has been shown to support remyelination after cuprizone-mediated demyelination (Fulmer et al., 2014), consistent with the possibility that microglial-derived BDNF may also promote myelination. Microglia also secrete factors including TNF-α, IL-6, FGF2, IL-1β, IFN-γ and others that stimulate OPC proliferation and differentiation (Miron, 2017; Shigemoto-Mogami et al., 2014), but the precise roles for these secreted cues in myelination have yet to be investigated.

Recent investigations of microglial heterogeneity have identified a population of white matter-associated microglia present during early postnatal development in mouse (Hammond et al., 2019; Li et al., 2019; McNamara and Miron, 2020). The role of this microglia subset is not yet known, but microglia in this subset (*Clec7a*+) were found to contain *Mbp* transcripts (Li et al, 2019), which is specifically expressed by oligodendrocytes and is particularly enriched in myelin sheaths (Herbert et al., 2017; Thakurela et al., 2016). The presence of *Mbp* mRNA in microglia raises the possibility that white matter microglia phagocytose myelin or oligodendrocytes during normal development. Microglia do phagocytose myelin and myelin debris in disease, wherein the clearance of myelin debris allows for remyelination to occur (Lampron et al., 2015). Earlier work used microglia / macrophage cultures provided with purified myelin to study myelin phagocytosis in disease and found that phagocytosis was potentiated by the presence of serum complement (van der Laan et al., 1996) or astrocytes (Smith and Hoerner, 2000). Notably, while these experiments were intended to model disease, the

cultures contained purified cells interacting with purified myelin and found that myelin phagocytosis by microglia occurs quite readily (even without the supplementation of complement or astrocytes), raising the possibility that microglia phagocytose myelin under normal physiological conditions.

Zebrafish as a model system for investigating nervous system development

Zebrafish provide an excellent vertebrate model system for investigating cell-cell interactions *in vivo*. Zebrafish embryos develop *ex utero*, making single-cell embryos accessible for the microinjection of DNA, RNA, dyes, or other materials. A single clutch may contain >100 embryos; therefore, 500-1000 embryos can be collected or injected in a 2-3 hour window and the majority will survive and develop for experiments. All major organ systems form in the first 24 hours post-fertilization (hpf) and stereotyped swimming, hunting, and navigation behaviors emerge by 5 days post-fertilization (dpf) (Kimmel et al., 1995). Larvae remain transparent into early juvenile stages and can be immobilized with low-percentage agarose for live imaging or physiology experiments. George Streisinger, who developed the zebrafish as a model system, chose zebrafish over several other fish species to cultivate this set of advantages (Grunwald and Eisen, 2002; Streisinger et al., 1981). Since then, it has been found that 71% of human genes have at least one clear ortholog in zebrafish (Howe et al., 2013), enabling *in vivo* investigations in both basic and translational neuroscience.

An ideal region for investigating nervous system development in the zebrafish is the spinal cord: a simple architecture and a manageable number of neurons and glia

make this an especially tractable model for investigating CNS myelination. Two myelinated tracts, the dorsal and medial longitudinal fasciculi (DLF, MLF) run parallel along the length of the spinal cord. The DLF, positioned dorsally, contains the morphologically distinguishable Rohon-Beard, dorsal longitudinal ascending (DoLA), commissural primary ascending (CoPA), and other ascending commissural axons, whereas the MLF, positioned in the ventral cord, contains the large Mauthner axon and 21 other bilaterally symmetric pairs of reticulospinal myelinated axons (Hildebrand et al., 2017; Kuwada, 1986; Kuwada et al., 1990; Lewis and Eisen, 2003), among some other unmyelinated axons. Many of the ventral axons execute motor commands from the brain, and project to motor neurons either directly or via interneurons, whereas many of the dorsal axons have somatosensory relay functions and transmit sensory information to the brain (Lu et al., 2015). Notably, the Mauthner axon in the MLF innervates motor neurons and a single action potential can initiate the C-bend escape response, a stereotyped movement that allows the fish to turn quickly away from a stimulus (Eaton et al., 1977).[3]

Zebrafish have CNS glia similar to mammals, including oligodendrocyte lineage cells, microglia, and astroglia-like radial glia. In the spinal cord, oligodendrocyte lineage cells are specified in the ventrally-located pMN domain, migrate toward target axons, and differentiate into myelinating oligodendrocytes (Kirby et al., 2006). The Mauthner axon is the first axon to be myelinated, occurring at ~60 hpf, and widespread myelination of both tracts proceeds thereafter until ~96 hpf, at which point the addition

[3] In Chapter IV, I investigate the role of myelin patterning on the Mauthner axon on the function of this circuit.

of new sheaths slows but formed sheaths elongate and begin compaction (Figure 1.2) (Almeida et al., 2011; Buckley et al., 2010). Microglia invade the CNS as macrophages at ~30 hpf and colonize the CNS before undergoing a phenotypic transition into microglia by 60 hpf (Herbomel et al., 2001). Microglia are phagocytic and ameboid until 5 dpf, at which point they begin to cycle morphologically between appearing ramified ("resting") and ameboid (Svahn et al., 2012). Radial glia, or radial astrocytes, are morphologically heterogeneous and appear as early as 15 hpf (Bernardos and Raymond, 2006; Marcus and Easter, 1995). Unlike mammalian radial glia, these cells persist into adulthood in zebrafish (Tomizawa et al., 2000), and in addition to this persistence these cells are, by most functional measures, similar to mammalian astrocytes (Diaz Verdugo et al., 2019; Lyons and Talbot, 2015; Mu et al., 2019).

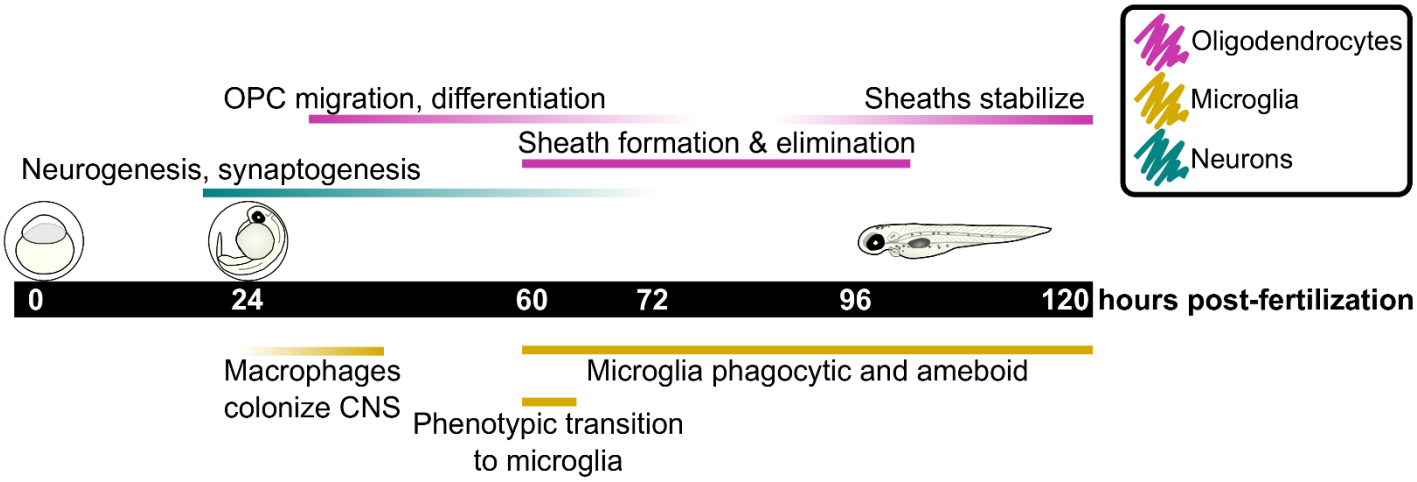

Figure 1.2. Timeline of oligodendrocyte and microglia development in zebrafish.

CHAPTER II

OLIGODENDROCYTES EXPRESS SYNAPTIC PROTEINS THAT MODULATE MYELIN SHEATH FORMATION[4]

Abstract

Vesicular release from neurons promotes myelin sheath growth on axons. Oligodendrocytes express proteins that allow dendrites to respond to vesicular release at synapses, suggesting that axon-myelin contacts use similar communication mechanisms as synapses to form myelin sheaths. To test this, we used fusion proteins to track synaptic vesicle localization and membrane fusion in zebrafish during developmental myelination and investigated expression and localization of PSD95, a dendritic post-synaptic protein, within oligodendrocytes. Synaptic vesicles accumulate and exocytose at ensheathment sites with variable patterning and most sheaths localize PSD95 with patterning similar to exocytosis site location. Disruption of candidate PDZ-binding transsynaptic adhesion proteins in oligodendrocytes cause variable effects on sheath length and number. One candidate, Cadm1b, localizes to myelin sheaths where both PDZ binding and extracellular adhesion to axons mediate sheath growth. Our work raises the possibility that axon-glial communication contributes to myelin plasticity, providing new targets for mechanistic unraveling of developmental myelination.

[4] This work is adapted from Hughes, A.N., Appel, B. Oligodendrocytes express synaptic proteins that modulate myelin sheath formation. *Nat Commun* 10, 4125 (2019). DOI: 10.1038/s41467-019-12059-y

Introduction

Cellular communication in the central nervous system (CNS) depends on billions of connections. Synapses, the connections between neurons, are plastic structures that grow and change with experience-evoked neuronal activity. Additionally, connections form between neurons and oligodendrocytes, the myelinating cell type of the CNS. Myelin sheaths also are plastic structures, mutable in length, number, and thickness (Auer et al., 2018; Etxeberria et al., 2016; Gibson et al., 2014). Some of this plasticity may be triggered by experience, because motor learning paradigms increase myelination (McKenzie et al., 2014; Sampaio-Baptista et al., 2013) and social and sensory deprivation paradigms reduce myelination of relevant brain regions (Barrera et al., 2013; Etxeberria et al., 2016; Makinodan et al., 2012). What accounts for myelin sheath plasticity? One possibility is that neuronal activity tunes ensheathment, similar to activity-dependent plasticity at synapses (Bliss and Lømo, 1973). Consistent with this possibility, Demerens and colleagues demonstrated more than 20 years ago that inhibiting action potential propagation with tetrodotoxin (TTX) reduced myelination of cultured neurons (Demerens et al., 1996). Activity-mediated communication from axons to myelin sheaths could ensure that active neurons receive enough myelin to faithfully propagate impulses toward termini, facilitating circuit function and higher-order cognitive processes (Pajevic et al., 2014). However, almost nothing is known about communication between axons and myelin sheaths.

Neuronal vesicular release promotes sheath growth and stability (Hines et al., 2015; Mensch et al., 2015; Wake et al., 2015). Upon cleavage of neuronal vesicular release machinery by clostridial neurotoxins, oligodendrocytes formed shorter sheaths

on impaired axons and selected unimpaired axons when presented with a choice (Wake et al., 2015). Importantly, timelapse imaging revealed that oligodendrocytes retracted nascent sheaths from impaired axons more quickly than from controls (Hines et al., 2015). These studies indicate that oligodendrocyte processes can detect and respond to axonal vesicular secretion. How might oligodendrocytes detect vesicular release? Oligodendrocytes express numerous genes encoding neurotransmitter receptors, synaptic scaffolds, transsynaptic adhesion molecules, and Rho-GTPases (Hrvatin et al., 2017; Marques et al., 2016; Zhang et al., 2014) that, when expressed by neurons, endow dendrites with the ability to detect and respond to release at synapses. Similar to their function in dendrites, these proteins may allow oligodendrocytes to sense, adhere, and respond to axonal secretion (Almeida and Lyons, 2014). Do oligodendrocytes utilize these proteins similarly to neurons to stabilize nascent myelin sheaths on axons?

Determining how neurons communicate to oligodendrocytes to shape developmental myelination requires an experimental model where both axons and oligodendrocytes can be monitored and manipulated during normal myelination. Here, we used zebrafish to examine features of synapse formation between axons and their myelinating oligodendrocytes, including the accumulation of presynaptic machinery, exocytosis at the junction, and postsynaptic assembly. These synaptic features manifest at the axon-glial junction from the onset of myelination at 3 days post-fertilization (dpf) through 5 dpf, when sheaths are stabilized. Surprisingly, we uncovered unforeseen diversity in the synaptic features present at these contacts: exocytosis sites vary in shape and position under sheaths, and the major postsynaptic scaffold PSD95 also localizes with variable position within some, but not all sheaths. To test whether the

synaptic features of the axon-myelin interface are important for normal myelination, we manipulated synaptogenic adhesion proteins in oligodendrocytes. When these same proteins are disrupted in neurons, synaptogenesis falters and synapses are abnormal in size and number. Taking a similar approach, we found that oligodendrocytes expressing dominant-negative adhesion proteins form myelin sheaths with abnormal length and number. We focused on one candidate, Cadm1b (SynCAM1), and found that it localizes to myelin sheaths, where its PDZ binding motif is required for myelin sheath growth. Furthermore, by manipulating the extracellular domain of Cadm1b we found that transsynaptic signaling to axons promotes myelin sheath length. Our work suggests shared mechanisms of synaptic and myelin plasticity and raises the possibility that synaptogenic factors have previously unrecognized roles in developmental myelination.

Results

1. Axons accumulate synaptic vesicle machinery under myelin sheaths

Vesicular secretion from axons promotes myelin sheath growth and stability (Hines et al., 2015; Mensch et al., 2015; Wake et al., 2015). However, we know nothing about the temporal or spatial qualities of vesicular communication to oligodendrocytes. To determine where vesicular release occurs to support sheath growth, we investigated the localization of vesicular release machinery in axons that are myelinated in an activity-regulated manner (Hines et al., 2015). By imaging live larvae expressing Syp-eGFP or Vamp2-eGFP we tracked the synaptic vesicle proteins Synaptophysin (Syp) and Synaptobrevin (Vamp2) in individual *phox2b*+ reticulospinal axons (Fig. 2.1a, b, b'). At early larval stages, *phox2b*+ axons were sparsely covered by myelin sheaths (~15%

of length) (Hines et al., 2015), permitting us to visualize synaptic vesicle machinery in both ensheathed and bare stretches of axons. Syp-eGFP is distributed in axons in a punctate pattern (Fig. 2.1b), whereas Vamp2-eGFP diffusely labels membrane (Fig. 2.1b'), similar to previous observations (Pennuto, 2003). We quantified Syp-eGFP puncta over the course of developmental myelination in both bare and ensheathed regions (Fig. 2.1c). By 4 days post-fertilization (dpf), and continuing through 5 dpf, axons accumulate more Syp-eGFP puncta at ensheathment sites relative to bare regions of axon (Fig. 2.1d). These data indicate that axons cluster synaptic release machinery at ensheathment sites over time, consistent with the possibility that vesicular secretion mediates axon-oligodendrocyte communication.

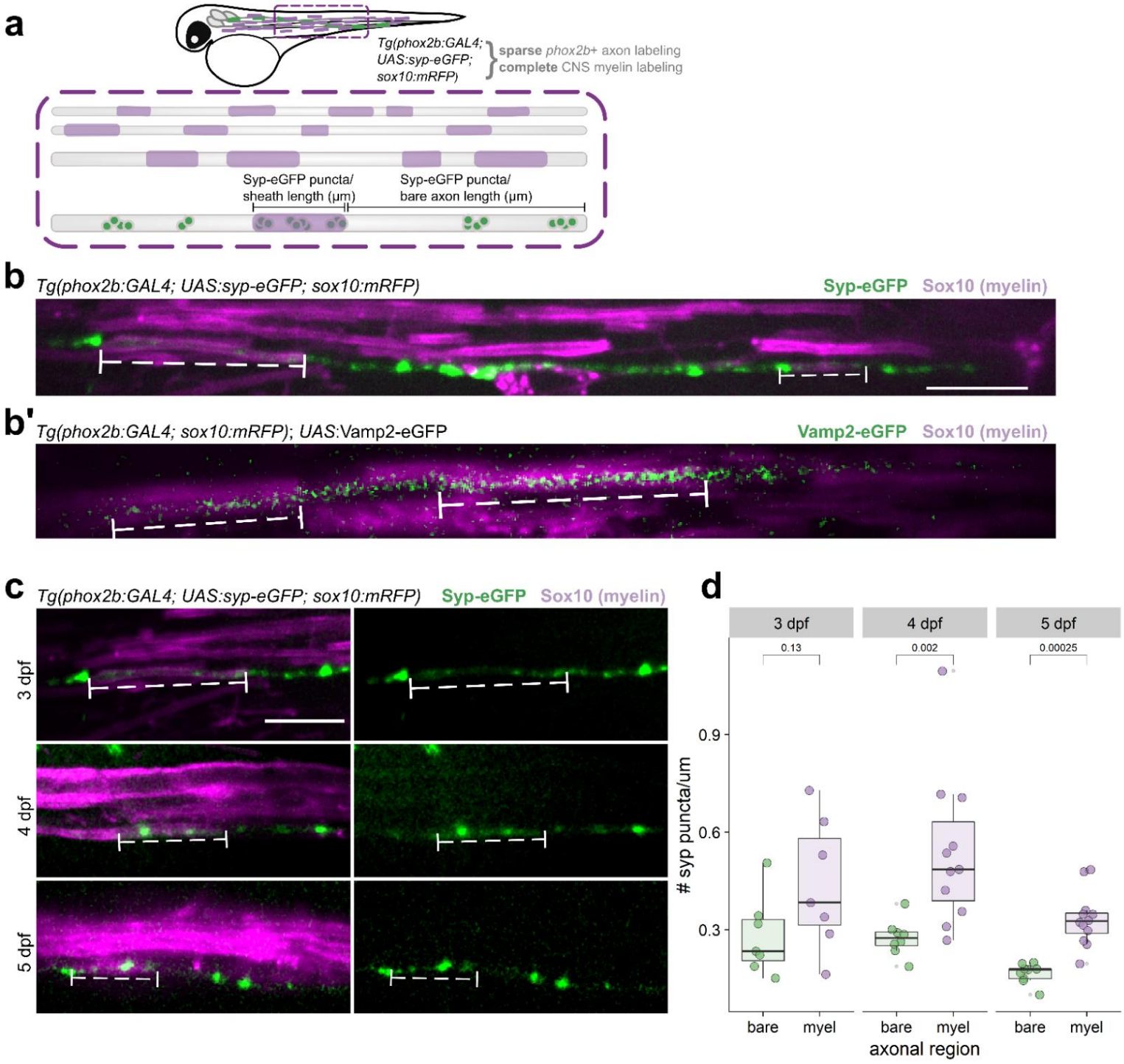

Figure 2.1. Axons accumulate synaptic vesicle release machinery under myelin sheaths. (a) Schematic of transgenes used to assess synaptic puncta density along myelinated and bare regions of axons. (b) Representative image of Syp-eGFP in a myelinated *phox2b*+ axon in a living 3 dpf *Tg(phox2b:GAL4; UAS:syp-eGFP; sox10:mRFP)* larva. Bracketed dashed lines indicate two myelin sheaths (rectangles) on the axon. (b') Same as (b) for Vamp2-eGFP; animal genotype is *Tg(phox2b:GAL4; sox10:mRFP)* with transient expression of *UAS*:Vamp2-eGFP. (c) Representative images of Syp-eGFP distribution in myelinated *phox2b*+ axons at 3, 4, and 5 dpf. (d) Comparisons of Syp-eGFP puncta density within bare vs myelinated regions of axons at each timepoint. n=7 bare

regions/98 puncta and 7 sheaths/18 puncta (3 dpf); 8 bare/119 puncta and 11 sheaths/43 puncta (4 dpf); 9 bare/75 puncta and 12 sheaths/38 puncta (5 dpf). Wilcox rank-sum test, p=0.13, p=0.002, p=0.00025 for 3, 4, and 5 dpf, respectively. Scale bars, 10 μm.

To test whether synaptic vesicle machinery is functional at ensheathment sites, we expressed an exocytosis reporter, Syp-pHluorin (SypHy) (Granseth et al., 2006), in reticulospinal axons. SypHy is pH-sensitive and quenched within vesicles but fluoresces upon exocytosis into neutral extracellular space. When extracellular SypHy is endocytosed and reacidified, SypHy is again quenched. By acutely blocking reacidification with the v-ATPase inhibitor bafilomycin A1, endocytosed SypHy remains fluorescent and axonal exocytosis “hotspots” accumulate signal (Alabi and Tsien, 2012) (Fig. 2.2a). We raised embryos microinjected with *Tol2.neuroD:sypHy* DNA and mRNA encoding Tol2 transposase at the 1-cell stage until 4 dpf, the timepoint at which we first detected enhanced Syp-eGFP clustering under sheaths (Fig. 2.1d). At 4 dpf, we treated larvae with 1 µM bafilomycin or DMSO vehicle and allowed them to behave freely for 1 hour before mounting for imaging. SypHy fluorescence is minimal when larvae are exposed to DMSO vehicle, reflecting the net balance of exo- and endocytosis along axons (Fig. 2.2a). By contrast, bafilomycin treatment reveals numerous exocytic hotspots along reticulospinal neurons, reflecting net exocytic activity over the hour (Fig. 2.2a). We confirmed that bafilomycin-induced hotspots resulted from exocytosis by performing the same experiment while blocking vesicular release by cleaving vesicular release machinery with botulinum toxin light chain (BoNT/B) (Liu et al., 2019a) or by suppressing exocytosis with dominant-negative Vamp2 (dnVamp2), a truncation that lacks the transmembrane domain (Dutta et al., 2018; Pascual et al., 2005; Wang et al., 2012) (Fig. 2.2b). Both suppress bafilomycin-induced fluorescent hotspots (Fig. 2.2b, right), indicating that the hotspots reflect exocytosis sites.

To determine if myelin sheaths are sites of exocytosis hotspots, we performed microinjections into *Tg(sox10:mRFP)* embryos at the 1-cell stage and imaged bafilomycin-treated larvae at 4 dpf. SypHy hotspots are abundant underneath myelin sheaths (Fig. 2.2c) but variable in morphology. Frequently, SypHy hotspots are punctate, resembling the size and shape of the Syp-eGFP fusion protein (Fig. 2.1b) and puncta are almost exclusively located near perinodal ends of sheaths. In addition, some hotspots are restricted to the ensheathed region but diffusely bright underneath the sheath (“filled”), and occasionally axons are entirely illuminated with no visually discernable differences under myelin sheaths (“uniform”) (Fig. 2.2c, d, d’). These categories may reflect different axonal release mechanisms, including synaptic and volume transmission. However, no category is associated with longer sheaths than other categories (Fig. 2.2e), suggesting that the diversity of release site shape or position does not account for differences in sheath length. These data are consistent with the possibility that axon vesicle fusion promotes sheath length.

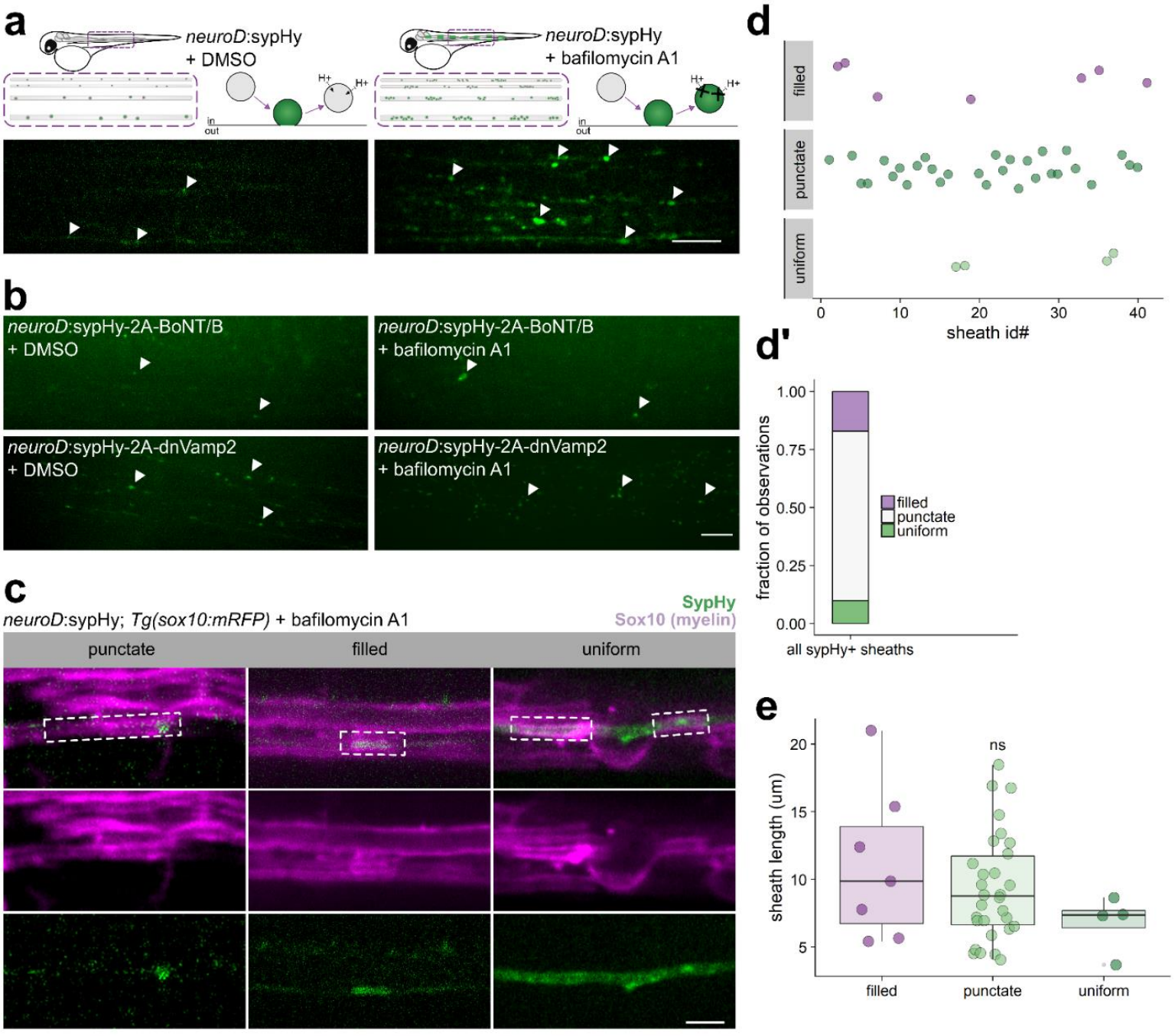

Figure 2.2. Variable synaptic vesicle exocytosis sites under myelin sheaths. (a) Left, schematic of Syp-pHluorin (SypHy) function and transient expression in spinal cord neurons and representative max-projection image of a live 4 dpf larva expressing *neuroD*:sypHy. Arrowheads indicate dim spots of SypHy signal. Right, similar but in the presence of bafilomycin A1 to inhibit vesicle reacidification. Note appearance of several large SypHy+ "hotspots" along axons. Scale bar, 10 µm. (b) Similar to (a) except larvae are co-expressing inhibitors of exocytosis, botulinum toxin (BoNT/B) or dominant-negative Vamp2 (dnVamp2). Both BoNT/B and dnVamp2 suppress bafilomycin induction of SypHy hotspots. Arrowheads indicate a few visible SypHy spots. Scale bar, 10 µm. (c) Expression of *neuroD*:sypHy in *Tg(sox10:mRFP)* larvae treated with bafilomycin reveals three types of SypHy-reported exocytosis sites

under myelin sheaths: punctate, filled, and uniform. Boxes outline individual myelin sheaths. Scale bar, 5 µm. (d) Classification plot of SypHy signal under 41 sheaths (from n=20 larvae) by category. Presented as a bar in (d') for visible contribution of each category to the total. (e) No association between category and sheath length, Kruskal-Wallis test.

2. The postsynaptic scaffold protein PSD95 localizes to myelin sheaths

We investigated oligodendrocyte expression and localization of the membrane-associated guanylate kinase (MAGUK) postsynaptic density protein 95 (PSD95), a scaffold known for anchoring neurotransmitter receptors at excitatory postsynaptic terminals, to learn if myelin sheaths have characteristics of postsynaptic terminals. To detect endogenous PSD95 expression, we used a CRISPR/Cas9-mediated GAL4 enhancer trap strategy (Kimura et al., 2014) to generate knock-in transgenic larvae that reports cells expressing *dlg4b*, the gene encoding PSD95. Nearly all *mbpa:*tagRFP+ oligodendrocytes also express *dlg4b*, indicating that myelinating oligodendrocytes of the spinal cord express PSD95 (Fig. 2.3a). As expected, many *dlg4b*+ cells do not express *mbpa:*tagRFP, likely reflecting expression of PSD95 in neurons.

We took multiple approaches to label PSD95 to determine its subcellular localization (Fig. 2.3b, b', b''). First, expressing a PSD95-GFP fusion protein that has been previously used to track PSD95 in zebrafish (Niell et al., 2004) reveals punctate enrichment at the terminal ends of myelin sheaths and a few sites of enrichment within the lengths of sheaths (Fig. 2.3b). We additionally labeled endogenous PSD95 by expressing a genetically-encoded intrabody, PSD95.FingR-GFP, that binds zebrafish PSD95 (Gross et al., 2013; Son et al., 2016). The intrabody contains a transcriptional regulation system that allows unbound FingR to repress further transcription by binding a zinc finger binding site upstream of the regulatory DNA. We first expressed the FingR in oligodendrocytes directly with *myrf* regulatory DNA but without a zinc finger binding site ("unregulated"). The unregulated PSD95.FingR-GFP broadly labels the cytoplasm of oligodendrocytes, with some puncta evident at the ends of sheaths (Fig. 3b'). We

then implemented the transcriptionally-regulated system by providing a zf binding site upstream of *UAS* sequence (Son et al., 2016) that drives PSD95.FingR expression via co-expression of *myrf*:GAL4 (Fig. 2.3b’’). In contrast to the unregulated system, transcriptional regulation of the intrabody unveils several PSD95 puncta within most, but not all sheaths (Fig. 2.3b’’).

We next assessed the intrabody localization within sheaths using the regulated form of PSD95.FingR in a *Tg(sox10:mRFP)* line at 3, 4, and 5 dpf. We identified three unique patterns of sheath labeling: puncta restricted to ends of sheaths (“end”), periodic puncta along the length of sheaths (“periodic”), and faint, diffuse labeling with no obvious localization (“diffuse”) (Fig. 2.3c). Most oligodendrocytes have sheaths with variable labeling: some sheaths contain “periodic” puncta, while other sheaths made by the same cell exhibit only “end” puncta. Our raw observations of puncta locations are plotted in Fig. 2.3d. The most frequent labeling pattern is “end” puncta at every age examined. However, the distribution of localization patterns changes during developmental myelination (Fig. 2.3e), notably via a reduction in diffusely-labeled sheaths and an increase in end-enriched sheaths. At a later stage in development (8 dpf), there are fewer puncta overall but with continued enrichment at sheath ends and along sheath membrane (Fig. 2.3f).

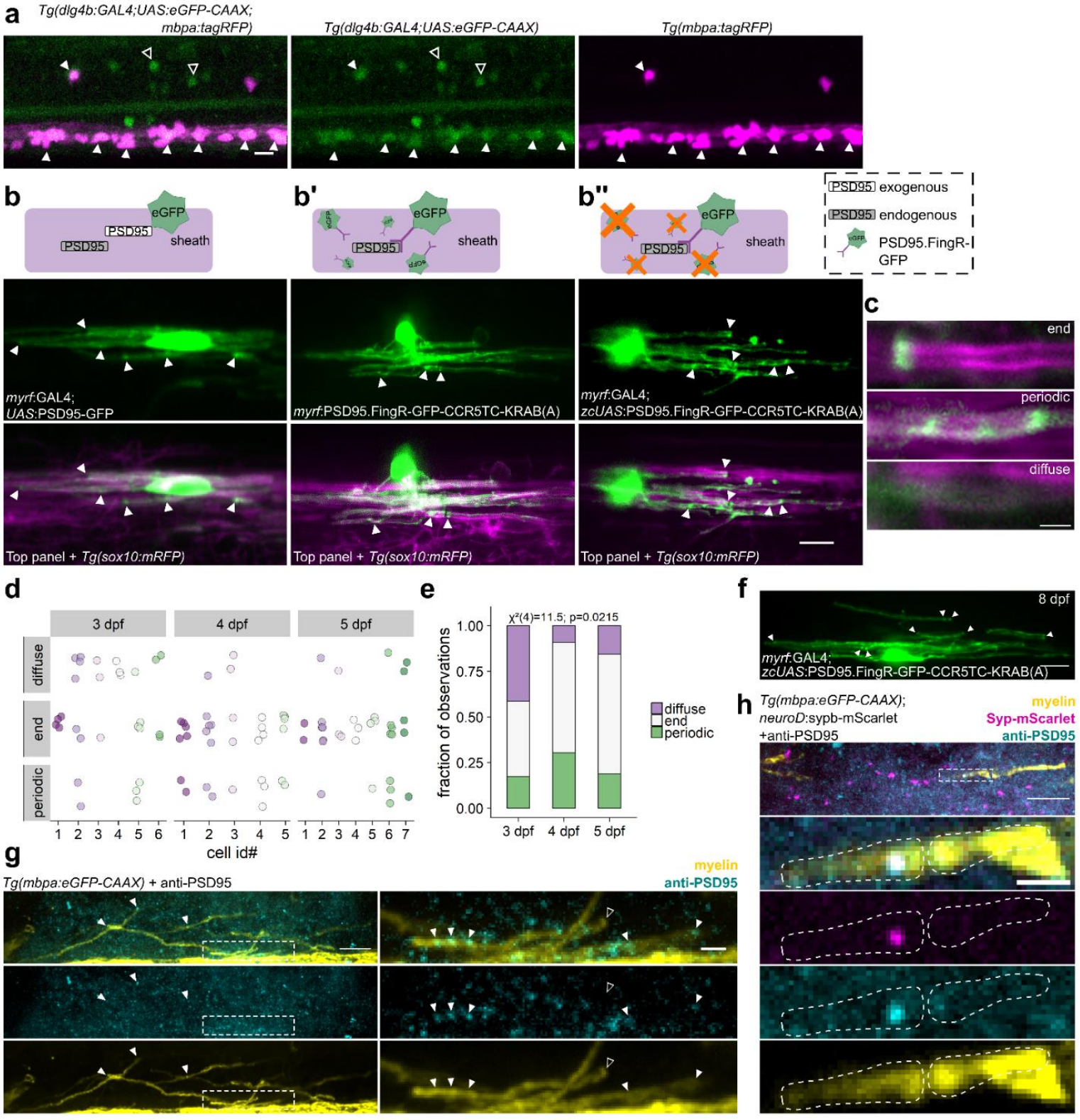

Figure 2.3. PSD95 is expressed by myelinating oligodendrocytes and is variably localized within myelin sheaths. (a) CRISPR/Cas9-mediated GAL4 enhancer trap of *dlg4b* reports spinal cord cells that

express *dlg4b* via *UAS*:eGFP-CAAX expression. Larvae additionally carrying the *mbpa:tagRFP* transgene reveal *mbp*+ myelinating oligodendrocytes. Closed arrowheads indicate *mbp+, dlg4b*+ oligodendrocytes and open arrowheads indicate *mbp-, dlg4b*+ cells. Scale bar, 10 μm. (b, b', b'') PSD95 localization within oligodendrocytes detected by expression of exogenous PSD95-GFP fusion protein (b), expression of PSD95.FingR to detect endogenous PSD95 localization (b'), and expression of PSD95.FingR to detect endogenous PSD95 localization with a transcriptional repression system to limit unbound PSD95.FingR-GFP (b''). Arrowheads indicate puncta, scale bar 10 μm. (c) Expression of the transcriptionally-regulated system (b'') with *Tg(sox10:mRFP)* to label myelin shows that not all sheaths display localized PSD95 puncta ("diffuse"), and among those that do, labeling is either restricted to the sheath end ("end"), or periodic along the length of the sheath ("periodic"). Scale bar, 2 μm. (d) Classification plot of sheath labeling patterns (y-axis) for individual cells (x-axis) at 3, 4, and 5 dpf. n=6 cells/29 sheaths (3 dpf); 5 cells/33 sheaths (4 dpf); 7 cells/32 sheaths (5 dpf). For each age group, dots of the same color denote sheaths belonging to the same cell. Note that most cells formed sheaths with different labeling patterns. Over developmental time, the distribution of labeling patterns changes as assessed by Chi square test (e), notably with a reduction of diffuse labeled sheaths, but all three categories persist at 5 dpf. (f) Later in development (8 dpf), PSD95.FingR-GFP is less punctate overall but remains enriched at the ends of sheaths (arrowheads). (g) Sagittal section of a 5 dpf *Tg(mbpa:eGFP-CAAX)* larva spinal cord fixed and immunolabeled with anti-PSD95. Right panels show higher magnification of the boxed region. Arrowheads indicate PSD95 signal colocalized with sheaths; open arrowhead marks a sheath without PSD95 at the terminal end. (h) Similar to (g) but with transient expression of *neuroD*:sypb-mScarlet to sparsely label synaptic vesicle puncta. Inset shows colocalized PSD95 and Syp-mScarlet within a sheath. Scale bars are 10 μm and 2 μm (insets).

To further validate these findings, we labeled fixed tissue sections using an antibody that detects synaptic PSD95 in zebrafish (Latefi et al., 2009). At 5 dpf PSD95 localizes within myelin sheaths similarly to the end, periodic and diffuse patterns detected by the intrabody (Fig. 2.3g). To assess anti-PSD95 labeling colocalization with myelin, we performed Costes randomization of the anti-PSD95 signal (Bolte and Cordelières, 2006) and found that colocalization does not occur by chance (Supplementary Fig. 2.1). Thus, three independent methods reveal patterns of PSD95 localization in myelin sheaths, consistent with the possibility that nascent myelin sheaths assemble components of postsynaptic complexes.

Do myelin sheath PSD95 puncta align with axonal synaptic vesicles? To answer this question, we sparsely labeled synaptic vesicles with Syp-mScarlet, sectioned larvae in sagittal plane at 5 dpf and labeled sections with anti-PSD95 antibody. This reveals axonal synaptic vesicle puncta in close proximity to myelin sheath PSD95 puncta (Fig. 2.3h). We note, however, that these coincident labeling patterns are not obligatory because not all myelin sheaths localize PSD95 near axon vesicles. Nevertheless, these data indicate that a subset of oligodendrocyte sheaths accumulate PSD95 close to neuronal synaptic vesicles, raising the possibility that sites of coincident localization are sites of axon-myelin sheath communication.

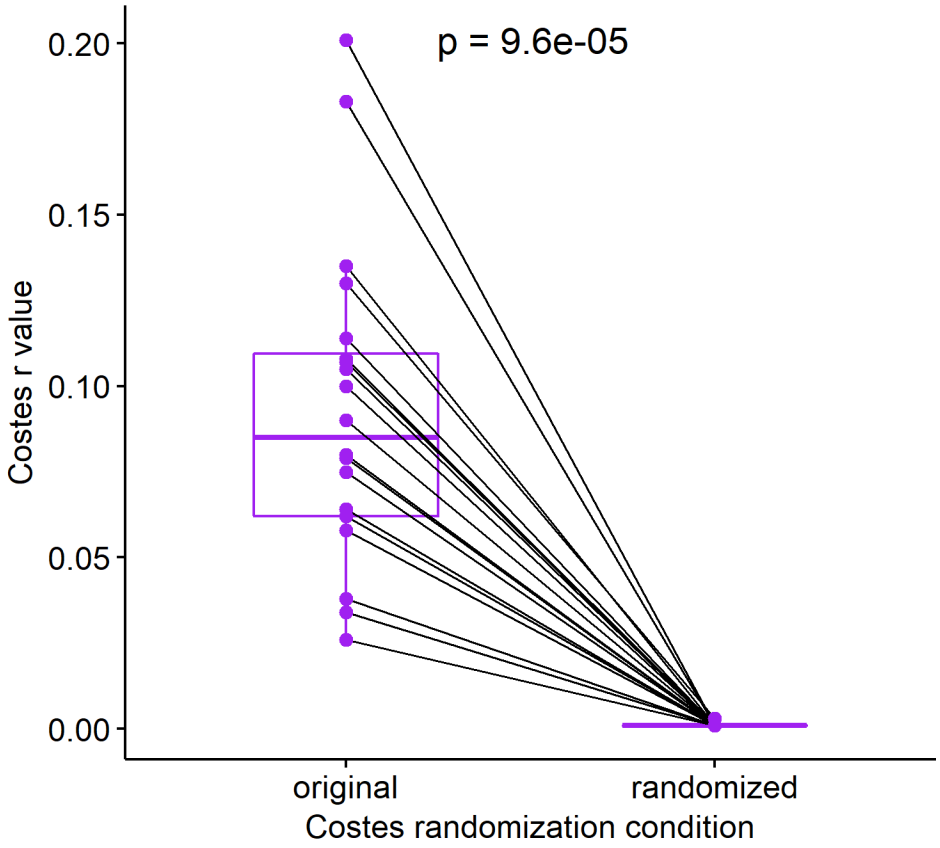

Supplementary Figure 2.1. Costes randomization analysis of PSD95 immunofluorescence colocalization with *Tg(mbpa:eGFP-CAAX)* fluorescence. Costes colocalization analysis of fluorescent signal between anti-PSD95 labeled with AF647 and transgenic reporter *Tg(mbpa:eGFP-CAAX)* before (original) or after (randomized) performing 1000 rounds of randomization per image for n=20 images containing both channels. Analysis was performed with the Fiji plugin JACoP with specific parameters: confocal image, bin width=0.001, pixel size=0.174 µm, randomizing in both the xy and z directions. Data are presented pairwise, analyzed by paired Wilcoxon, and the value plotted for the randomized condition is the maximum value from the output range (e.g., 0 +/- 0.003 is plotted as +0.003).

3. Synaptogenic adhesion molecules tune sheath length and number

In neurons, PSD95 anchors receptors, ion channels, and synaptic signaling molecules at the postsynaptic membrane via its PDZ domains. These domains are found in PSD95 and other synaptic scaffolding proteins, where they bind short, C-terminal PDZ binding motifs located on target proteins destined for synapse localization. PDZ binding motifs direct the localization and function of many synaptogenic, transsynaptic adhesion proteins. This family includes members of the neuroligins, synCAMs, netrin-G ligands, and the leucine rich repeat transmembrane proteins (Missler et al., 2012). In addition to adhering pre- and postsynaptic terminals, these proteins are potent signaling molecules. The signaling they induce across the nascent cleft is sufficient to induce synaptogenesis even when ectopically expressed in non-neuronal HEK293 cells (Biederer et al., 2002; Kim et al., 2006; Linhoff et al., 2009; Scheiffele et al., 2000). Intriguingly, mRNAs encoding many of these synaptogenic adhesion molecules are expressed by oligodendrocytes at levels comparable to neurons (Zhang et al., 2014). If these molecules are sufficient to confer axonal synapses onto HEK293 cells, could a similar mechanism operate at the axon-oligodendrocyte interface to promote sheath growth and stability?

We identified genes that express synaptogenic proteins in oligodendrocytes by querying published transcriptome databases (Hrvatin et al., 2017; Marques et al., 2016; Zhang et al., 2014) and in-house RNA-seq data (Ravanelli et al., 2018). We selected six candidates based on oligodendrocyte expression (Fig. 2.4a, b) and the existence of published dominant negatives that disrupt synapse formation when expressed in neurons: Cadm1b (SynCAM1), Nlgn1 and Nlgn2b (Neuroligin1 and -2), Lrrc4ba (NGL-

3), and Lrrtm1 and Lrrtm2 (Leucine rich repeat transmembrane proteins 1 and -2). We generated dominant-negative alleles of zebrafish proteins predicted to disrupt PDZ binding (Linhoff et al., 2009; Nam and Chen, 2005; Sandau et al., 2011) by omitting conserved C-terminal PDZ binding motifs.

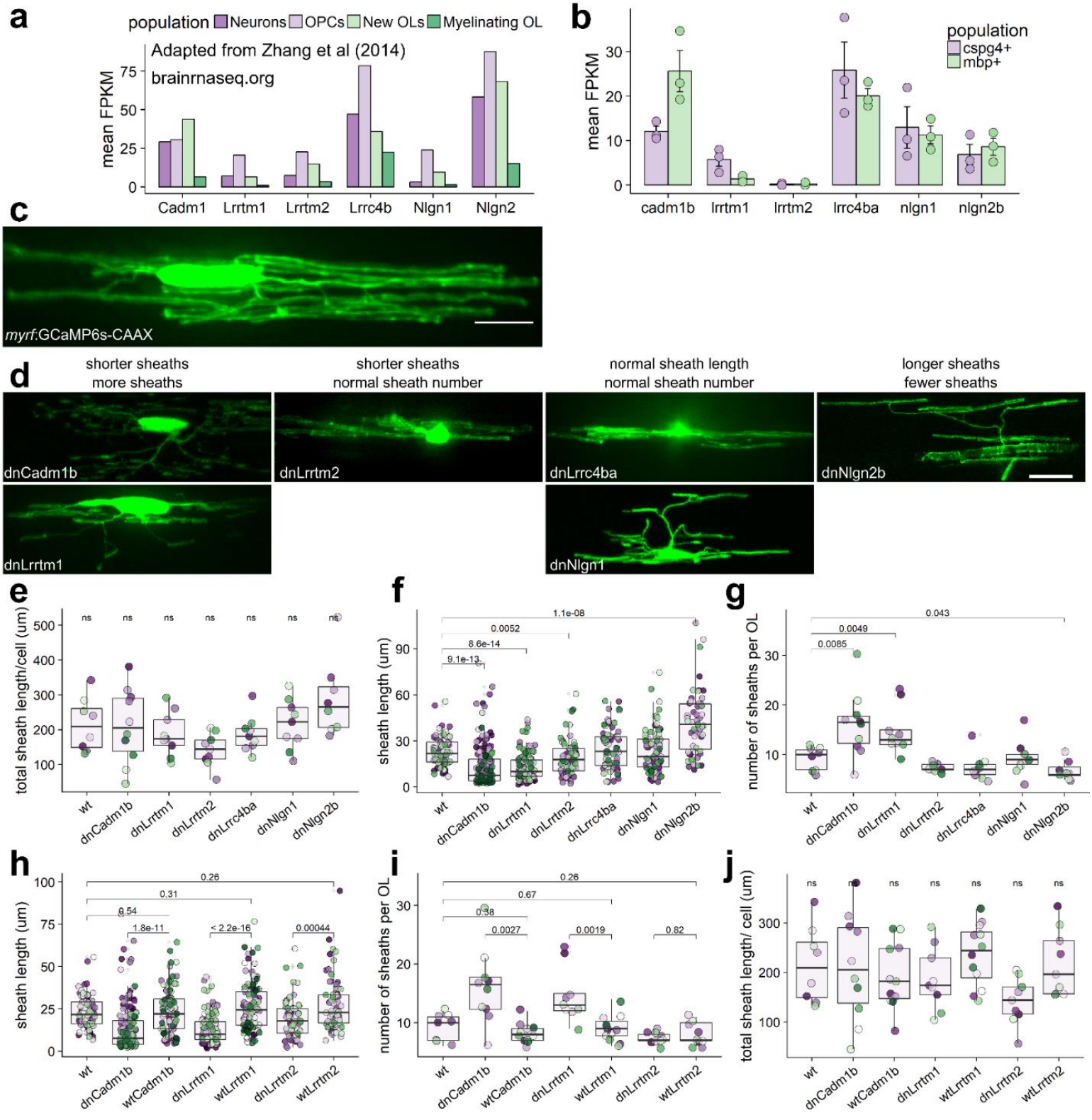

Figure 2.4. Candidate synaptogenic adhesion molecules have variable effects on myelin sheath length and number. (a) RNA-seq FPKM values for mouse cortical neurons, OPCs, new

oligodendrocytes, and myelinating oligodendrocytes for candidates Cadm1, Lrrtm1, Lrrtm2, Lrrc4b, Nlgn1, and Nlgn2. Plot generated using publicly available values from brainrnaseq.org(Zhang et al., 2014). (b) RNA-seq FPKM values for FAC-sorted zebrafish *olig2*+/*cspg4*+ (cspg4+) and *mbpa*+/*olig2*+ (mbp+) cells for zebrafish homologs of the same candidates (Ravanelli et al., 2018). (c) Oligodendrocyte transiently expressing *myrf*:GCaMP6s-CAAX. Scale bar 10 µm. (d) Candidate dominant-negative (dn) alleles expressed transiently as *myrf*:dnX-2A-GCaMP6s-CAAX and grouped by effect on sheath length and number. Scale bar 10 µm. (e) Total sheath length per cell expressing each dominant-negative candidate was unchanged by all candidates, Kruskal-Wallis test. Dot color marks individual cells and matches colored dots in corresponding sheath length and number plots. (f) Sheath length values for each dominant-negative candidate. n (cells/sheaths) = 8/74 wt, 10/159 dnCadm1b, 9/132 dnLrrtm1, 9/67 dnLrrtm2, 9/68 dnLrrc4ba, 9/83 dnNlgn1, 8/55 dnNlgn2b. Data in plots (f)-(i) were tested by Wilcox rank-sum with Bonferroni-Holm correction for multiple comparisons. dnLrrc4ba/wt and dnNlgn1/wt comparisons were ns. (g) Sheath number values for each dominant-negative candidate (n listed in (f)). (H) Decreased sheath length in dnCadm1b, dnLrrtm1, and dnLrrtm2 cells is specific to the DN disruption, because expression of the full-length (wt) protein does not reduce sheath length. n(cells/sheaths) = 11/91 wtCadm1b, 12/108 wtLrrtm1, 9/72 wtLrrtm2. i) Expression of WT forms of the three candidates that reduced sheath length resulted in normal sheath number. (j) Total sheath length per cell expressing each WT candidate was not significantly different for any group, Kruskal-Wallis test.

We expressed each of these dominant-negative constructs with *myrf* regulatory DNA to disrupt transsynaptic adhesion specifically in oligodendrocytes. To label sheaths, we bicistronically expressed membrane-tethered GCaMP6s-CAAX. We imaged living larvae expressing each of the constructs, or a control *myrf*:GCaMP6s-CAAX (wt) construct (Fig. 2.4c, d), at 4 dpf to measure sheath number and length. The total sheath length generated per cell, a general measure of myelinating capacity, does not differ between any of the groups (Fig. 2.4e). However, oligodendrocytes expressing dnCadm1b, dnLrrtm1, and dnLrrtm2 form significantly shorter sheaths, whereas oligodendrocytes expressing dnNlgn2b make longer sheaths (Fig. 2.4f). Intriguingly, dnCadm1b and dnLrrtm1 oligodendrocytes also elaborate several more sheaths than wildtype (wt), whereas dnNlgn2b oligodendrocytes generate slightly fewer sheaths (Fig. 2.4g). Because total sheath length per cell is unchanged, this suggests that these adhesion proteins do not influence the ability of oligodendrocytes to generate myelin but rather tune how oligodendrocytes allocate myelin among sheaths. Importantly, for all three dominant-negative constructs that reduce sheath length (dnCadm1b, dnLrrtm1, dnLrrtm2), expression of the full-length (wt) protein does not reduce sheath length relative to wt control (Fig. 2.4h), indicating that length reduction is specific to disruption of PDZ binding for each of these proteins. Oligodendrocytes expressing full-length proteins also have normal number of sheaths (Fig. 2.4i) and normal total membrane (Fig. 2.4j). These data illustrate that transsynaptic adhesion molecules, typically studied only in the context of synapses, also determine the length and number of myelin sheaths formed by oligodendrocytes.

4. Cadm1b functions at the axon-myelin junction to promote ensheathment

Our dominant-negative approach tested the requirement for each candidate's PDZ binding motif in modulating myelination. PDZ binding is essential for downstream signaling through postsynaptic scaffolds, including PSD95 and CASK, in the recipient cell (or sheath). To determine where in the oligodendrocytes these candidates act to modulate ensheathment, we focused on one candidate, Cadm1b. We first confirmed expression of *cadm1b* in oligodendrocytes by generating a knock-in transgenic, using the same CRISPR/Cas9-mediated enhancer trap strategy as for *dlg4b* (Fig. 2.3a). Nearly all *mbpa:*tagRFP+ oligodendrocytes are also *cadm1b*+ but not all *cadm1b*+ cells are *mbpa:*tagRFP+, likely indicating neuronal expression (Fig. 2.5a).

To track Cadm1b localization we generated a fusion protein, eGFP-Cadm1b, and drove expression with *myrf* regulatory DNA. eGFP-Cadm1b is distributed in both the somatic and sheath compartments (Fig. 2.5b, 5b'). In sheaths, eGFP-Cadm1b signal resembles two parallel lines demarcating the sheath perimeter, raising the possibility that eGFP-Cadm1b is transmembrane in sheaths. To estimate the fraction of our fusion protein associated with sheath membrane vs cytosol, we expressed eGFP-Cadm1b in oligodendrocytes that were transgenically co-labeled with either *Tg(sox10:tagRFP)*, which expresses a cytosolic RFP (Fig. 2.5b), or *Tg(sox10:mRFP)*, which expresses a membrane-tethered RFP (Fig. 2.5b'). We calculated Mander's colocalization coefficient (Bolte and Cordelières, 2006) and found that eGFP-Cadm1b signal robustly colocalizes with membrane RFP but only minimally with cytosolic RFP (Fig. 2.5b''), suggesting that eGFP-Cadm1b is membrane-localized in sheaths.

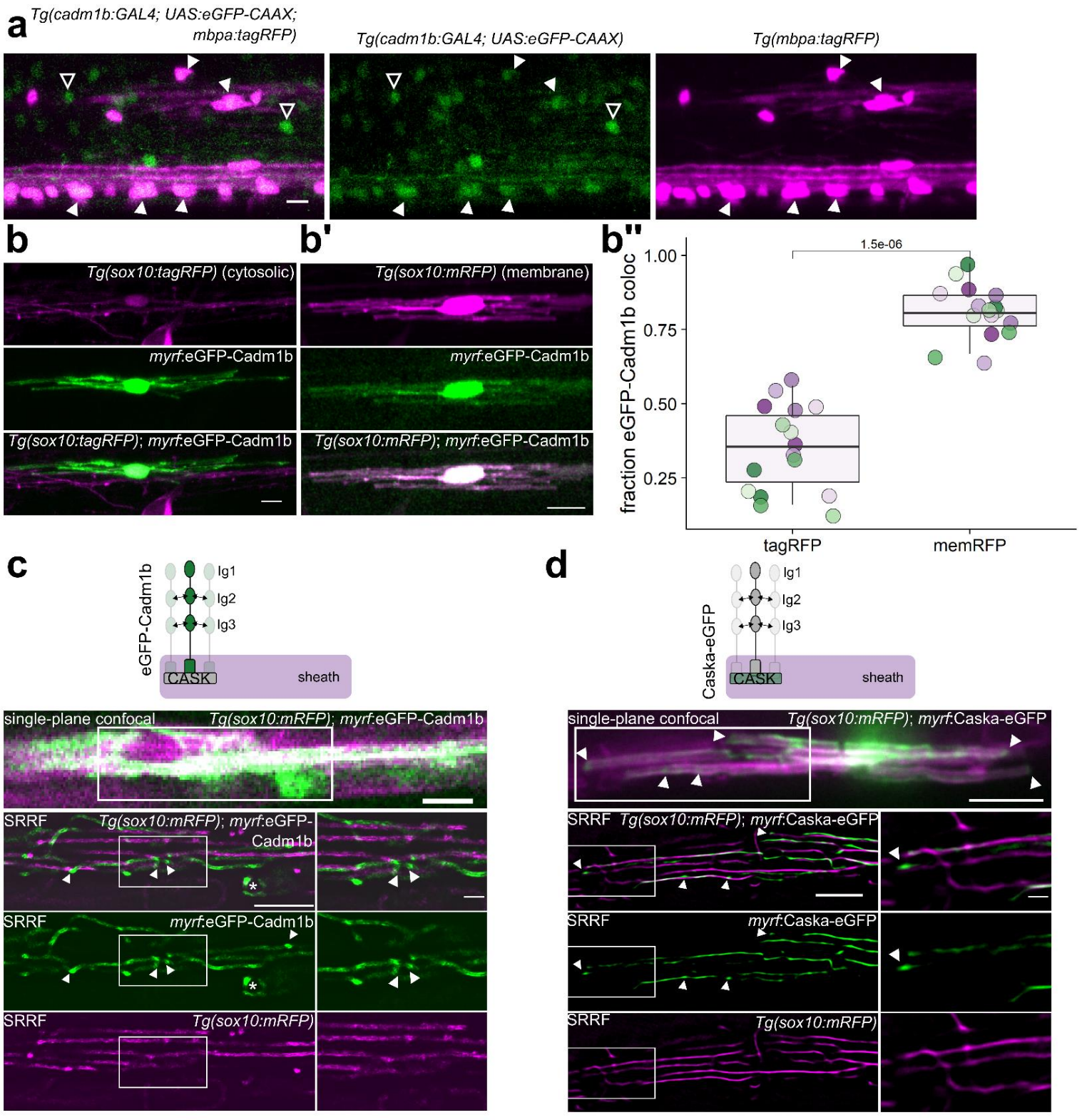
a
Tg(cadm1b:GAL4; UAS:eGFP-CAAX; mbpa:tagRFP)
Tg(cadm1b:GAL4; UAS:eGFP-CAAX)
Tg(mbpa:tagRFP)
b
b'
b''
Tg(sox10:tagRFP) (cytosolic)
Tg(sox10:mRFP) (membrane)
myrf:eGFP-Cadm1b
Tg(sox10:tagRFP); myrf:eGFP-Cadm1b
Tg(sox10:mRFP); myrf:eGFP-Cadm1b
1.5e-06
fraction eGFP-Cadm1b coloc
1.00
0.75
0.50
0.25
tagRFP
memRFP
c
d
eGFP-Cadm1b
Caska-eGFP
Ig1
Ig2
Ig3
CASK
sheath
single-plane confocal
SRRF
Tg(sox10:mRFP); myrf:eGFP-Cadm1b
Tg(sox10:mRFP); myrf:Caska-eGFP
myrf:eGFP-Cadm1b
myrf:Caska-eGFP
Tg(sox10:mRFP)

Figure 2.5. Cadm1b localizes to myelin sheath membrane. (a) CRISPR/Cas9-mediated GAL4 enhancer trap of *cadm1b* reports cells expressing *cadm1b* via *UAS*:eGFP-CAAX expression. Larvae additionally carrying *Tg(mbpa:tagRFP)* reveal *mbp*+ myelinating oligodendrocytes. Closed arrowheads indicate *mbp*+, *cadm1b*+ oligodendrocytes, whereas open arrowheads indicate *mbp*-, *cadm1b*+ cells (likely neurons). Scale bar, 10 µm. (b, b') Expression of *myrf*:eGFP-Cadm1b in *Tg(sox10:tagRFP)* (b) or *Tg(sox10:mRFP)* (c) co-labeled oligodendrocytes. (b'') Fraction of eGFP-Cadm1b colocalized with RFP (Mander's colocalization coefficient) for *Tg(sox10:tagRFP)* (tagRFP) and *Tg(sox10:mRFP)* (memRFP). n=16 cells (tagRFP),16 cells (memRFP), Wilcox rank-sum test. Colored dots represent individual cells. (c) Confocal single-plane (top) and super resolution radial fluctuations (SRRF) (bottom 3 panels) imaging of a eGFP-Cadm1b expressing oligodendrocyte in a *Tg(sox10:mRFP)* larva. Arrowheads indicate eGFP-Cadm1b puncta that are not present in mRFP SRRF. Asterisk marks a sheath going in to the plane of view with circular edges surrounded by eGFP-Cadm1b puncta. Scale bars 5 µm except for innermost inset, 1 µm. (d) Similar to (c) for an oligodendrocyte expressing Caska-eGFP. Scale bars 10 µm (top), 5 µm (left SRRF), 1 µm (SRRF insets).

To resolve eGFP-Cadm1b localization in sheaths, we used super resolution radial fluctuations imaging (SRRF) (Gustafsson et al., 2016). We used Fourier ring correlation analysis to determine that SRRF yields resolution of ~120 nm in cells in live zebrafish (Supplementary Fig. 2.2). SRRF reveals eGFP-Cadm1b puncta primarily at the terminal ends of sheaths (Fig. 2.5c). To determine whether SRRF would report this labeling pattern for any membrane-associated protein, we performed SRRF imaging of cells expressing both *sox10:*mRFP and *myrf*:eGFP-Cadm1b (Fig. 2.5c). Most eGFP-Cadm1b puncta are not associated with mRFP puncta, suggesting that eGFP-Cadm1b enrichment at sheath ends is specific to Cadm1b rather than a general feature of membrane-associated proteins. We similarly analyzed the PDZ scaffold that anchors Cadm1b, Caska/CASK (Biederer et al., 2002). Caska-eGFP occupies a similar position as eGFP-Cadm1b at the ends of sheaths (Fig. 2.5d). These data suggest that the synaptic features of the axon-myelin interface are primarily present at the terminal ends of sheaths, a location that also harbors axon-myelin adhesive complexes including glial NF155 binding to axonal Caspr and Contactin (Tait et al., 2000).

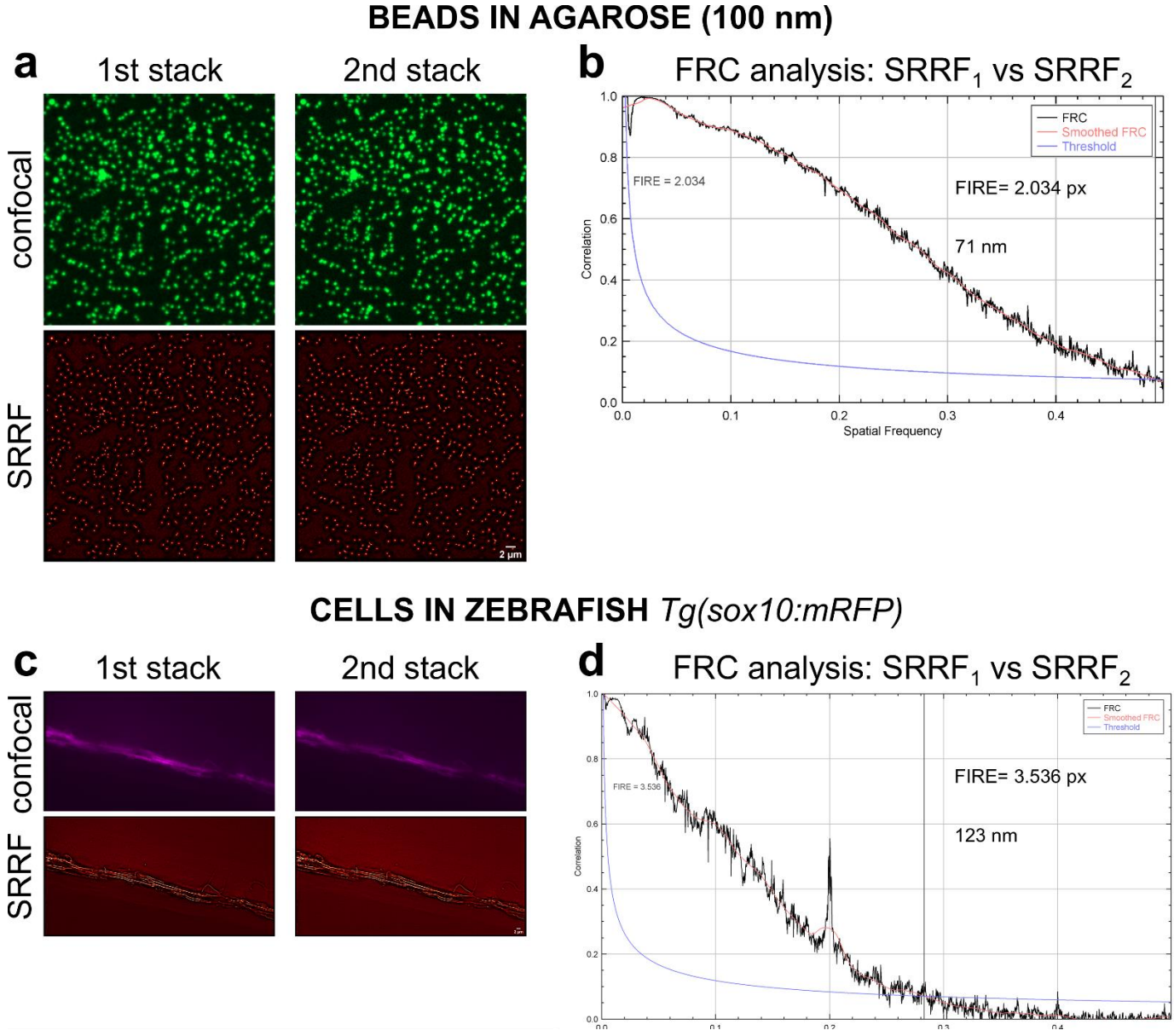

Supplementary Figure 2. 2. Fourier ring correlation (FRC) analysis of resolution achieved by super-resolution radial fluctuation (SRRF) processing. (a) Single optical sections (75 frames) of fluorescent 100 nm beads suspended in agarose were acquired in two independent acquisitions (top) to generate SRRF reconstructions (bottom). (b) SRRF reconstructions were compared by 3-sigma FRC analysis to generate FRC curves and resolution values in both pixels and nanometers (71 nm resolution) (c) Single optical sections (109 frames) of oligodendrocytes in a live *Tg(sox10:mRFP)* agarose-mounted larva acquired twice and processed with SRRF. (d) SRRF reconstructions were compared by 3-sigma FRC analysis to generate FRC curves and resolution values in both pixels and nanometers (123 nm resolution). Scale bars, 2 µm.

Sheath membrane localization is consistent with Cadm1b functioning as a transmembrane protein, possibly bridging the periaxonal space to interact with an axonal partner. Although Cadm proteins can interact transsynaptically both homo- and heterophilically, Cadm1 binds most strongly to Cadm2 (Fogel et al., 2011), a protein previously found to exclusively label myelinated axons in the CNS and to adhere to an unknown partner in oligodendrocytes (Pellissier et al., 2007). To test the possibility that oligodendrocyte Cadm1b interacts with axonal Cadm2, we generated eGFP-Cadm2a and drove expression in reticulospinal neurons. eGFP-Cadm2a localizes under sheaths (Fig. 2.6a) raising the possibility that Cadm2a and Cadm1b interact across the axon-myelin interface. However, this does not exclude the possibility that Cadm1b interacts with other axonal Cadm partners. To test whether Cadm1b interacts with an axonal partner to drive myelination, we generated a second dominant-negative allele designed to prevent adhesion to transsynaptic partners. This allele, Ig1-dnCadm1b, lacks the extracellular distalmost Ig-like domain (Ig1) that specifically interacts transsynaptically with Cadm partners located on other cells (Fogel et al., 2011). We excised Ig1 while preserving the rest of the extracellular domain because the proximal Ig-like domains (Ig2, Ig3) allow Cadm1b to be incorporated into *cis* oligomers with other Cadm1b molecules. In this way, Ig1-dnCadm1b is predicted to bind endogenous Cadm1b via lateral Ig2 and Ig3 interactions, but to interfere with adhesion in *trans* (Fogel et al., 2011) (Fig. 2.6b).

Expression of Ig1-dnCadm1b in oligodendrocytes produces a phenotype distinct from expression of the wt form or the PDZ binding dominant-negative (hereafter called PDZIIb-dnCadm1b) (Fig. 2.6c). Ig1-dnCadm1b oligodendrocytes generate sheaths that

are significantly shorter than wt and wtCadm1b-expressing oligodendrocytes but longer than those made by PDZIIb-dnCadm1b oligodendrocytes (Fig. 2.6d). Furthermore, the number of sheaths may be modestly increased, but not significantly different than wt or wtCadm1b sheath number (Fig. 2.6e). The myelinating capacity of cells expressing each of the constructs is unchanged (Fig. 2.6f), indicating that both extracellular adhesion and PDZ binding tune how oligodendrocytes distribute myelin among sheaths rather than influencing myelin production.

Because PDZIIb-dnCadm1b specifically disrupts downstream Cadm1b interactions with scaffolds including CASK, syntenin, and Mpp3 (Biederer et al., 2002; Murakami et al., 2014), whereas Ig1-dnCadm1b disrupts extracellular adhesion without changing PDZ interactions (Fogel et al., 2011), these data suggest that Cadm1b has roles in both “postsynaptic” signaling within sheaths as well as transsynaptic adhesion-induced signaling with the axon to tune ensheathment. At synapses, the Ig1 domain of postsynaptic Cadm1 functions both to adhere the pre- and postsynapse and to induce presynaptic assembly in the presynaptic neuron (Biederer et al., 2002). Does the Ig1 domain of Cadm1b function to induce presynaptic vesicle clustering in the axon? We first tested whether oligodendrocyte Cadm1b apposes neuronal synaptic vesicles by expressing Syp-mScarlet pan-neuronally in axons and eGFP-Cadm1b in oligodendrocytes, and found that Syp-mScarlet puncta cluster near sites of eGFP-Cadm1b signal (Fig. 2.6g). Because synaptic vesicle exocytosis promotes sheath growth (Hines et al., 2015; Mensch et al., 2015; Wake et al., 2015), we next tested the possibility that Ig1-dnCadm1b oligodendrocytes form shorter sheaths due to impaired vesicle clustering. We labeled either wt or Ig1-dnCadm1b oligodendrocytes in pan-

neuronal Syp-mScarlet larvae and observed axonal Syp-mScarlet wrapped by myelin sheaths (Fig. 2.6h, h'). Unlike the sparse labeling of *phox2b*+ neuronal synaptic vesicles (Fig. 1c), this pan-neuronal labeling allowed us to examine all synaptic vesicles but precluded us from measuring vesicle signal intensity in individual sheaths due to surrounding labeled vesicles. We instead employed Mander's colocalization to assess the 3D fraction of oligodendrocyte-labeled territory that was also positive for Syp-mScarlet signal at 4 dpf, when vesicle clustering is evident (Fig. 2.1d). Colocalization values for sheaths expressing Ig1-dnCadm1b are more variable than values for control sheaths but differences between the two groups are not statistically significant using the standard of $p < 0.05$ (Fig. 6i). This result suggests that disruption of Cadm1b function alters sheath growth independently of presynaptic assembly. Importantly, Ig1-dnCadm1b oligodendrocytes continue to exhibit abnormal ensheathment later in development (Fig. 2.6j, k, l), indicating that compromised axon-myelin adhesion blocks, rather than delays, sheath growth.

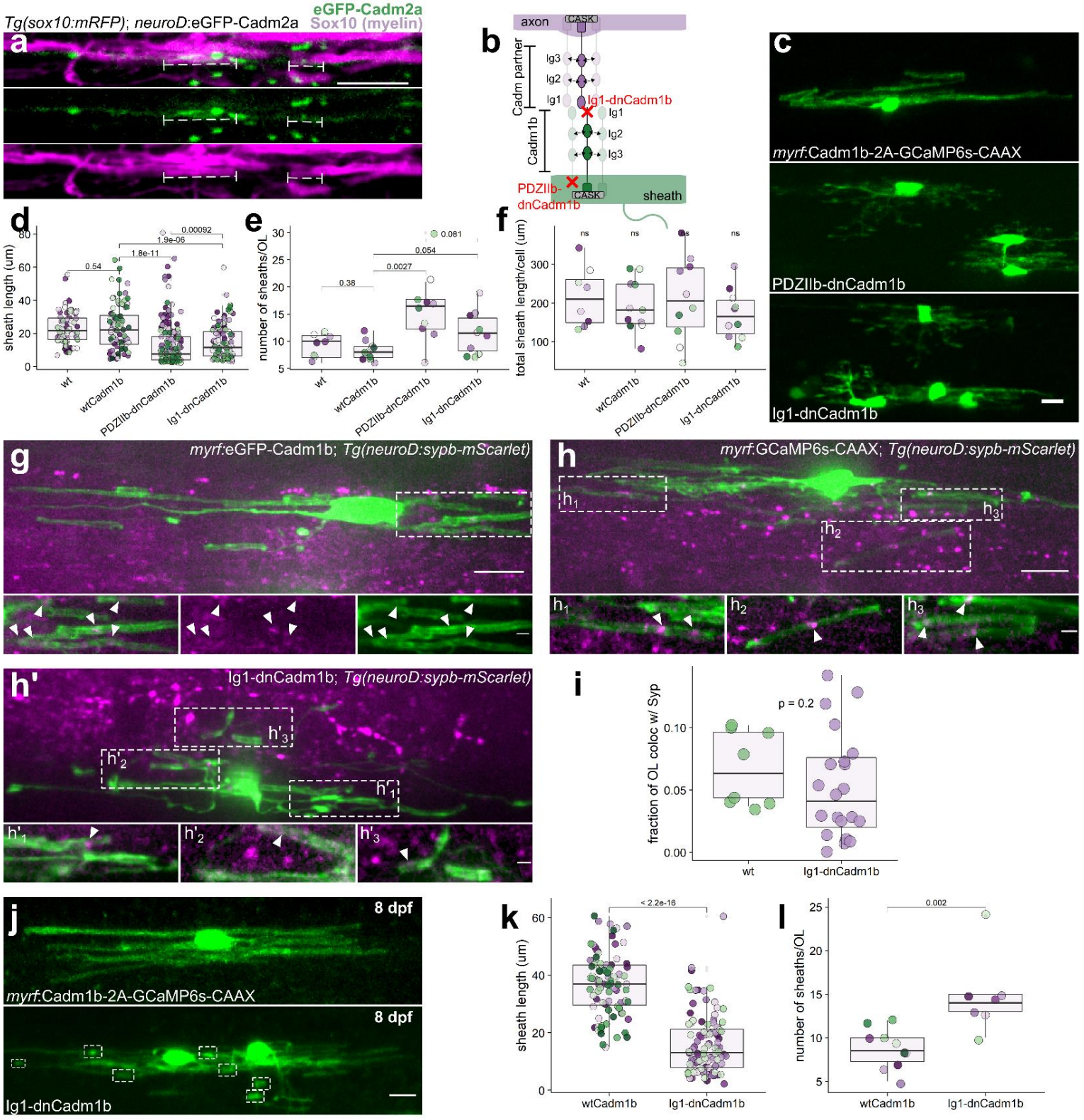
Tg(sox10:mRFP); neuroD:eGFP-Cadm2a
eGFP-Cadm2a
Sox10 (myelin)
a
b
axon
CASK
Cadm partner
Ig3
Ig2
Ig1
Ig1-dnCadm1b
Cadm1b
PDZIIb-dnCadm1b
sheath
c
myrf:Cadm1b-2A-GCaMP6s-CAAX
PDZIIb-dnCadm1b
Ig1-dnCadm1b
d
sheath length (um)
0.54
1.8e-11
1.9e-06
0.00092
wt
wtCadm1b
PDZIIb-dnCadm1b
Ig1-dnCadm1b
e
number of sheaths/OL
0.38
0.0027
0.054
0.081
f
total sheath length/cell (um)
ns
g
myrf:eGFP-Cadm1b; Tg(neuroD:sypb-mScarlet)
h
myrf:GCaMP6s-CAAX; Tg(neuroD:sypb-mScarlet)
h1
h2
h3
h'
Ig1-dnCadm1b; Tg(neuroD:sypb-mScarlet)
h'1
h'2
h'3
i
fraction of OL coloc w/ Syp
p = 0.2
wt
Ig1-dnCadm1b
j
8 dpf
myrf:Cadm1b-2A-GCaMP6s-CAAX
Ig1-dnCadm1b
k
sheath length (um)
< 2.2e-16
wtCadm1b
Ig1-dnCadm1b
l
number of sheaths/OL
0.002

Figure 2.6. The extracellular, trans-acting adhesion domain (Ig1) of Cadm1b promotes myelin sheath growth. (a) Neuronal eGFP-Cadm2a puncta (green) localize under myelin sheaths (magenta, brackets). Scale bar, 10 µm. (b) Schematic of dominant-negative oligodendrocyte Cadm1b variants, PDZIIb-dnCadm1b and Ig1-dnCadm1b, interacting with partner Cadm located on neurons. (c) Representative examples of oligodendrocytes expressing wildtype Cadm1b, PDZIIb-dnCadm1b, and Ig1-dnCadm1b with GCaMP6s-CAAX to label sheath membrane. Scale bar, 10 µm. (d) Sheath lengths for wt, wtCadm1b-, PDZIIb-dnCadm1b-, and Ig1-dnCadm1b-expressing oligodendrocytes. Note that PDZIIb-dnCadm1b is the same allele presented in Fig. 4. n (cells/sheaths) = 8/74 (wt), 11/91 (wtCadm1b), 10/159 (PDZIIb-dnCadm1b), 10/115 (Ig1-dnCadm1b), Wilcox rank-sum test with Bonferroni-Holm correction for multiple comparisons. Dots of the same color indicate sheaths belonging to the same cell and match those in plots (e) and (f). (e) Sheath number for wt, wtCadm1b-, PDZIIb-dnCadm1b-, and Ig1-dnCadm1b-expressing oligodendrocytes. Same n and statistical test as in (d). (f) Total sheath length generated per cell is unchanged by all alleles, Kruskal-Wallis test. (g, h, h') Max projection image of *myrf*:eGFP-Cadm1b oligodendrocyte in *Tg(neuroD:sypb-mScarlet)* larvae, in which Syp-mScarlet is expressed pan-neuronally. Inset is a substack projection of 6 slices (0.31µm/slice) containing eGFP-Cadm1b-labeled sheaths wrapping Syp-mScarlet puncta. Arrowheads indicate colocalized oligodendrocyte eGFP-Cadm1b and neuronal Syp-mScarlet signal. (h, h') *myrf*:GCaMP6s-CAAX (wt) (h) or Ig1-dnCadm1b (h') oligodendrocytes in *Tg(neuroD:sypb-mScarlet)* larvae. Insets are substack projections of 2-8 slices containing sheaths wrapping Syp-mScarlet puncta. In (g, h, h') scale bars are 10 µm/2 µm in insets. (i) Mander's colocalization coefficient displaying the fraction of GCaMP6s-CAAX oligodendrocyte signal that is positive for Syp-mScarlet signal in wt and Ig1-dnCadm1b cells in 4 dpf larvae. n=8 cells (wt) and n=20 cells (Ig1-dnCadm1b), Wilcox rank-sum test. (j, k, l) By 8 dpf, Ig1-dnCadm1b-expressing oligodendrocytes still exhibit numerous stunted myelin sheaths (boxes) compared to wildtype Cadm1b-expressing cells. Sheath length (k) and number (l) for n (cells/sheaths) at 8 dpf = 10/87 (wtCadm1b) and 7/104 (Ig1-dnCadm1b), Wilcox rank-sum test. Scale bar, 10 µm.

Discussion

The data and conclusions that we present in this manuscript add to previous evidence of synaptic-like communication between neurons and oligodendrocyte lineage cells. Oligodendrocyte precursor cells (OPCs) that express the proteoglycan NG2 receive *bona fide* synaptic input from pyramidal neurons and interneurons in hippocampus (Bergles et al., 2000; Lin and Bergles, 2004), axons in corpus callosum (Etxeberria et al., 2010), and climbing fibers in cerebellum (Lin et al., 2005). However, neurotransmitter ceases to evoke somatic currents in oligodendrocytes following their differentiation from NG2 glia (Etxeberria et al., 2010; Kukley et al., 2010), suggesting that synapses on to OPCs are disassembled upon myelination. Recently, live imaging revealed neuronal activity-evoked calcium transients in nascent sheaths (Baraban et al.,

2018; Krasnow et al., 2018), indicating that neuronal activity continues to elicit local ion flux in oligodendrocyte sheaths after somatic currents are no longer detectable. In the optic nerve, axo-myelinic synapses mediated by axonal glutamate release onto myelinic NMDA receptors might allow axons to dynamically control metabolic support provided by overlaying myelin (Micu et al., 2016; Saab et al., 2016). Potentially, synaptic-like communication between axons and oligodendrocyte lineage cells at distinct stages of differentiation mediates distinct features of myelin plasticity and function, such as OPC number, choice of axons for ensheathment, myelin coverage of axons, and metabolic transfer.

Despite the evidence for synaptic-like communication between axons and oligodendrocyte lineage cells, the molecular mechanisms that mediate it have not been determined. If axons communicate to oligodendrocytes via secreted neurotransmitters and trophic factors, then oligodendrocytes might utilize canonical postsynaptic molecular assemblies to receive it. Oligodendrocytes express the postsynaptic scaffold PSD95, shown by immunoblot (Brasko et al., 2017) and RNA-seq (Hrvatin et al., 2017; Marques et al., 2016; Zhang et al., 2014), but the subcellular localization of the protein was not known. We used a genetically-encoded intrabody and an antibody to label endogenous PSD95 in oligodendrocytes and discovered heterogeneity in the labeling of sheaths of individual oligodendrocytes. Some sheaths exhibited end labeling only, while others exhibited a periodic spread of puncta along the length of the sheath. Still other sheaths exhibited no defined labeling. Why this diversity? Perhaps sheaths, like dendritic spines, use different scaffolds to anchor unique subsets of receptors and signaling molecules required for autonomous interaction with the presynaptic axon. For

example, excitatory synapses use PSD95 to anchor NMDA receptors, whereas inhibitory synapses primarily use Gephryin (Gphn) to anchor GABA receptors (Allison et al., 2000). Oligodendrocytes also express Gphn and other scaffolds (Zhang et al., 2014), raising the possibility that sheaths labeled poorly for PSD95 might instead utilize other protein scaffolds, perhaps to support sheaths on different classes of neurons. We also found diverse patterns of vesicle distribution within myelinated axons, including repeated examples in which vesicles appeared clustered near the ends of overlying nascent myelin sheaths, distributed along the length of axons coincident with overlying sheaths or distributed uniformly along both ensheathed and bare portions of axons. Although we do not know the functional significance of these distinct localization patterns, they might reflect distinctions in neuron class, neurotransmitter type or mechanism of signal release.

The presence of these canonical synaptic structures at the axon-myelin interface is consistent with the possibility that these proteins function similarly as they do at neuronal synapses, participating in exocytosis of neurotransmitter and anchoring of receptors to support communication. However, other functions are also possible for these features. For example, “synaptic” vesicles are identified, by us and by others, by the presence of membrane proteins such as Synaptophysin (Syp) that are generally absent in non-synaptic vesicles. A limitation of this classification is that Syp presence in a vesicle membrane indicates nothing about the cargo contained. It is possible that the Syp-labeled vesicles docked under myelin represent a distinct pool from the recycling pool that is shared among presynaptic boutons (Darcy et al., 2006), and may contain distinct cargo intended for myelin, such as pro-myelinating factors. A similar argument

applies to our observation that canonical postsynaptic scaffolds, including PSD95 and CASK, are present in myelin sheaths. While these scaffolds could be anchoring receptors and signaling molecules as they do at synapses, myelinating oligodendrocytes downregulate expression of many receptors, raising the possibility that these scaffolds anchor other proteins or serve other functions. One functional similarity that we did observe is that of the synaptogenic adhesion molecules: interruption of these proteins in neurons disrupts synapse size and number, and we observed a reduction in myelin sheath length. These proteins are sufficient for presynaptic assembly when expressed in non-neuronal cells. However, we observed a severe reduction in myelin sheath length upon expression of dominant-negative that did not diminish presynaptic vesicle clustering, indicating that adhesion may be a more important function for these molecules at the axon-myelin interface.

Why have presynaptic and postsynaptic machinery not been discovered at the axon-myelin interface by transmission electron microscopy (EM), a technique that has been used to identify synapses for over 30 years? One possibility is that EM identifies mature synapses, but frequently misses small, nascent, and diverse synapses that do not resemble classic EM synapses (Burette et al., 2015). Wake et al. (2015) used EM to assess axon-OPC contacts *in vitro*. While they observed presynaptic vesicles docked at axon-OPC contacts, they did not identify a postsynaptic density (PSD), which led them to conclude that the junction is nonsynaptic (Wake et al., 2015). By contrast, by using a non-EM approach, we have detected PSD95 in sheaths. What explains this difference? Perhaps axon-OPC junctions have PSDs on par with immature synapses, which lack an EM-resolvable PSD until maturity, or perhaps maturity of axon-OPC junctions was not

achieved in culture. Another possible reason that synaptic features of axon-oligodendrocyte contacts may go unnoticed by EM is diversity: perhaps synaptic features are not equally present at all axon-oligodendrocyte junctions. Like Wake et al. (2015), Doyle et al. (2018) identified docked axonal vesicles under myelin, but not all myelinated axons had sub-myelin docked vesicles (Doyle et al., 2018). This is consistent with the observation that vesicular release from certain axons profoundly modulates their myelin profiles, whereas vesicular release is dispensable for the myelination of other classes of axons (Koudelka et al., 2016). Furthermore, while we found PSD95 localization in most sheaths, there was substantial heterogeneity between sheaths of individual cells. Together, these studies raise the possibility that axon-oligodendrocyte contacts are diverse in their usage of synaptic elements, perhaps as broad in scope as the variety of synapses. This prompts a significant need for alternatives to EM to identify diverse synapses. Burette et al. (2015) set out recommendations for single-synapse analysis for those synapses missed by EM, including fluorescence microscopy and optophysiology approaches (Burette et al., 2015), both of which we have used here.

To test whether these synaptic similarities are integral to normal myelination, we manipulated synaptic adhesion proteins in oligodendrocytes that disrupt synapse formation in neurons. We tested dominant-negative alleles of candidate transsynaptic adhesion molecules expressed by oligodendrocytes and measured oligodendrocyte sheath length, number, and total sheath length generated per cell. We discovered specific requirements for PDZ binding of Cadm1b, Lrrtm1, and Lrrtm2 in oligodendrocyte sheath length. Lrrtm1 and Lrrtm2 bind to the PDZ domains of PSD95

(Linhoff et al., 2009), but Cadm1b is instead anchored by the related scaffold CASK, which also anchors the major oligodendrocyte protein Claudin11 (Anitei, 2006). Like PSD95, we found that Cadm1b and its interacting scaffold Caska appear to be concentrated near the ends of nascent myelin sheaths during development. This raises the possibility that the ends of sheaths are sites of axonal signal reception and intracellular signal transduction that promote sheath growth (Fig. 2.7). Consistent with this possibility, oligodendrocyte expression of a form of Cadm1b lacking the intracellular PDZ domain, which mediates intracellular protein interactions, produced abnormally short sheaths. Oligodendrocyte expression of a different Cadm1b variant designed to interfere with binding to transsynaptic adhesion partners also produced shorter myelin sheaths, but the change was less extreme than that caused by the PDZ deletion variant. Thus, Cadm1b might have distinct signaling and adhesion-based functions in myelin sheath growth. Although we did not find evidence that disruption of Cadm1b function alters presynaptic assembly, as manifested by axonal vesicle clustering, multiple transsynaptic adhesion systems are thought to operate in parallel at synapses (Brose, 2009; Fowler et al., 2017), and redundancy within and between families can obscure how individual adhesion proteins contribute to synapse formation. Intriguingly, oligodendrocyte expression of a Cadm4 variant, a protein with structural similarity to Cadm1b, consisting of the extracellular and transmembrane domains, predicted to promote adhesion, resulted in a large excess of short sheaths (Elazar et al., 2018). Thus, axon-oligodendrocyte interactions that promote sheath growth might be mediated by numerous adhesion molecules.

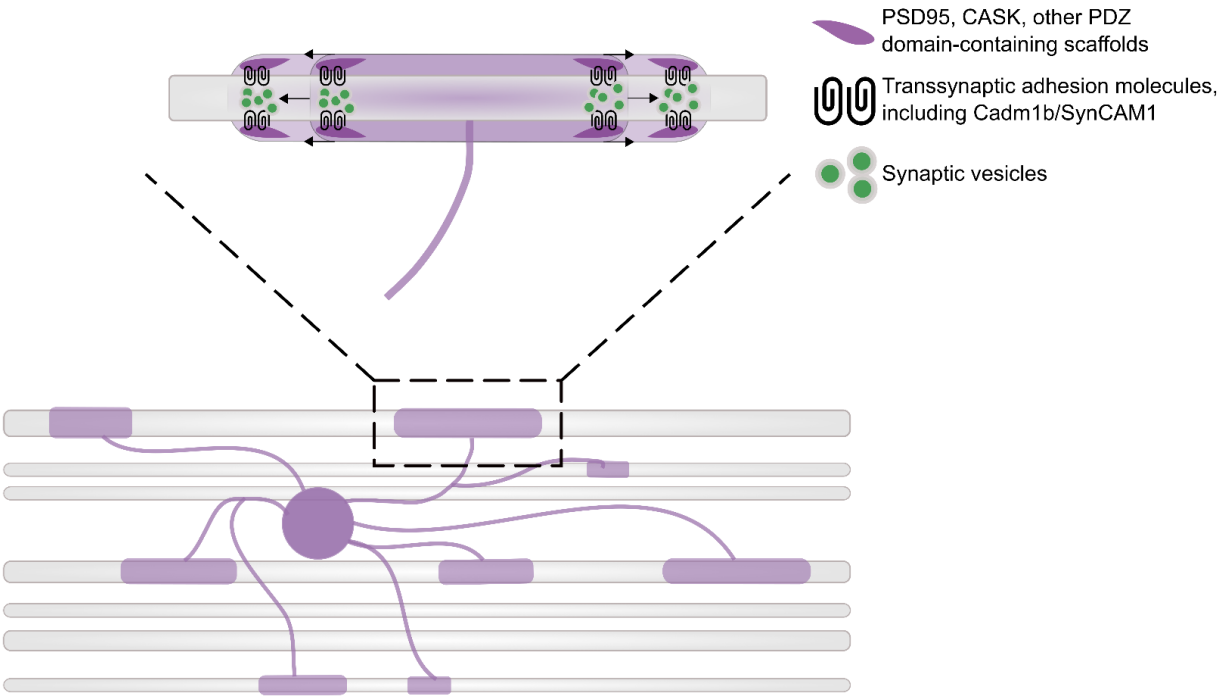

Figure 2.7. Working model of adhesion-promoted sheath growth. PSD95 and other PDZ domain-containing scaffolds expressed by oligodendrocytes, including CASK and Dlg1, anchor transsynaptic adhesion molecules that adhere to and induce presynaptic assembly in the ensheathed axon. The accumulation and exocytosis of synaptic vesicles at ensheathment sites promotes the elongation of nascent sheaths, possibly via neurotransmitter- and/or neurotrophin-induced intracellular signaling in the sheath.

We have shown that synaptic features are present at the axon-myelin junction and that synaptogenic adhesion molecules have a previously underappreciated role in shaping myelination. Is this similarity to synaptogenesis biologically significant? Dendrites and oligodendrocytes utilizing similar mechanisms to establish stable contacts with axons raises the possibility that oligodendrocytes may be vulnerable to pathology in psychiatric disease, where mutations in synaptic genes are likely drivers of pathogenesis (Lips et al., 2012). Indeed, ultrastructural analysis of postmortem brain tissue from patients with schizophrenia reveals myelin and oligodendrocyte defects (Uranova et al., 2011) and diffusion tensor imaging of patients living with schizophrenia (White et al., 2009) and autism (Wolff et al., 2012) reveal white matter defects. Together, these findings raise the intriguing possibility that mutations in synaptic genes could affect oligodendrocytes cell-autonomously to disrupt myelination, which may then contribute to disease progression via reduced neuronal support or conduction velocity. Alternatively, mutations in synaptic genes could impair synaptic transmission and thus change neuronal activity in a way that disrupts oligodendrocyte maturation, myelination, or survival. We have shown that a number of synaptic proteins are expressed at the axon-myelin interface and that disruption of some of these proteins in oligodendrocytes disrupts myelination. This finding supports the former possibility, that synaptic genes cell-autonomously regulate myelination in oligodendrocytes. However, because the oligodendrocyte lineage is sensitive to perturbations in neuronal activity (Demerens et al., 1996), it is also possible that reduced myelination resulting from synaptic protein dysfunction in oligodendrocytes causes aberrant or asynchronous neuronal activity which then further disrupts the oligodendrocyte lineage. Untangling the relationship

between neuronal activity and oligodendrocyte myelination is crucial for understanding nervous system function in both health and disease. Our work draws structural and functional parallels between synaptogenesis and myelination and provides new targets for investigating the mechanistic basis of developmental myelination.

Methods

1. Zebrafish lines and husbandry

All animal work was approved by the Institutional Animal Care and Use Committee at the University of Colorado School of Medicine. Zebrafish embryos were raised at 28.5°C in embryo medium and staged according to hours or days post-fertilization (hpf/dpf) and morphological criteria. *Tg(sox10:mRFP)*^{vu234}, *Tg(sox10:tagRFP)*^{co26}, *Tg(phox2bb:GAL4)*^{co21}, *Tg(UAS:syp-eGFP)*(Heap et al., 2013), *Tg(mbpa:tagRFP)*^{co25} *, Tg(mbpa:eGFP-CAAX)*, and *Tg(UAS:eGFP-CAAX)*^{co18} transgenic lines were used. Additionally, we generated and used the new lines *Tg(cadm1b:GAL4)*^{co53}, *Tg(dlg4b:GAL4)*^{co54} (see section on enhancer trapping), and *Tg(neuroD:sypb-mScarlet)*^{co55}. All other reporters were expressed by transient transgenesis to achieve sparse labeling for single cell analysis.

2. Plasmid construction and generation of transgenic zebrafish

Tol2 expression plasmids were generated by Multisite Gateway cloning and injected into 1-cell embryos with Tol2 mRNA to generate transient transgenic animals. The following entry clones were used (cited) or made (see Supplementary Table 2.1)

via BP recombination of appropriate pDONR backbone with attB-flanked regulatory elements or coding sequences.

p5E-neuroD, p5E-4xUAS (Kwan et al., 2007)*, p5E-myrf* (gift from Jacob Hines)

pME-eGFP(Kwan et al., 2007)*, pME-GAL4*(Kwan et al., 2007)*, pME-vamp2, pME-sypHy, pME-GCaMP6s-CAAX, pME-cadm1b, pME-Ig1-dnCadm1b, pME-PDZIIb-dnCadm1b, pME-lrrtm1, pME-dnLrrtm1, pME-lrrtm2, pME-dnLrrtm2, pME-dnLrrc4ba, pME-dnNlgn1, pME-dnNlgn2b, pME-PSD95.FingR-GFP-CCR5TC-KRAB(A), pME-caska, pME-sypb*

p3E-polyA (Kwan et al., 2007)*, p3E-eGFP* (Kwan et al., 2007)*, p3E-2A-GCaMP6s-CAAX, p3E-cadm1b, p3E-cadm2a, p3E-2A-BoNT/B, p3E-2A-dnVamp2, p3E-mScarlet*

p3E-2A-GCaMP6s-CAAX, p3E-2A-BoNT/B, and *p3E-2A-dnVamp2* were made by amplifying restriction enzyme site-flanked inserts and subcloning into digested *p3E-2A-mcs*.

Entry clones were LR-recombined with either of destination vectors *pDEST-Tol2-CG2* (green heart marker) or *pDEST-Tol2-CC2* (blue eye marker) as transgenesis indicators(Kwan et al., 2007).

zcUAS:PSD95.FingR-GFP-CCR5TC-KRAB(A) was a gift from Joshua Bonkowsky (Addgene plasmid #72638) and was used to generate *pME-PSD95.FingR-GFP-CCR5TC-KRAB(A)*. *CMV::SypHy A4* was a gift from Leon Lagnado (Addgene plasmid #24478) and used to generate *pME-sypHy*. *pGP-CMV-GCaMP6s* was a gift from Douglas Kim (Addgene plasmid #40753) and used to generate *pME-GCaMP6s-CAAX* and *p3E-2A-GCaMP6s-CAAX*. *14UAS:zfPSD95:GFP* was a gift from Martin Meyer &

Stephen Smith (Addgene plasmid #74314). *pQL86-eGFP-BoNT/B* was a gift from Chandra Tucker and used to generate p3E-2A-BoNT/B. *pmScarlet_C1* was a gift from Dorus Gadella (Addgene plasmid #85042) and used to generate *p3E-mScarlet*.

3. CRISPR/Cas9-mediated enhancer trapping

We knocked in *GAL4* 200-500 bp upstream of the translation start site of *cadm1b* and *dlg4b* using a previously published method (Kimura et al., 2014). Briefly, *mbait-hs-Gal4* plasmid, mBait guide RNA, guide RNA targeting upstream of our genes of interest (*cadm1b*, chr15:18645374-18645393; *dlg4b*, chr23:44280085-44280104 in GRCz11/danRer11 assembly, see primer table for sequences), and Cas9 mRNA were injected into 1-cell *Tg(UAS:eGFP-CAAX)* embryos. Guide RNAs were designed using crispor.tefor.net (Haeussler et al., 2016) with specificity > 99. F0 founders were screened for expression and raised to adulthood. Experiments involving these knock-ins were only performed on stable transgenic (F1 or later) *Tg(cadm1b:GAL4)^{co53}* and *Tg(dlg4b:GAL4)^{co54}* larvae.

4. Dominant negative allele generation

We made zebrafish homologs of published mouse dominant-negative alleles for all candidates. For candidates with duplicate paralogs in the zebrafish genome, we investigated the paralog with higher expression in oligodendrocytes(Ravanelli et al., 2018). We isolated RNA from whole, wildtype AB-strain 4 dpf larvae and synthesized cDNA (iScript) to use as template to high-fidelity (Phusion) PCR amplify attB-flanked coding sequences for candidates, omitting C-terminal PDZ binding sites for Cadm1b (-KEYYI) (Pietri et al., 2008; Sandau et al., 2011), Lrrtm1 and Lrrtm2 (-ECEV) (Linhoff et al., 2009), Nlgn1 and Nlgn2b (-STTRV) (Nam and Chen, 2005), and Lrrc4ba (-ETQI)

(Linhoff et al., 2009). For Lrrtm1/2, we omitted 51 additional C-terminal residues to make alleles similar to those used previously (Linhoff et al., 2009). Full-length sequences were also amplified. AttB-flanked products were recombined with *pDONR-221* to form middle entry vectors, and subsequently recombined with *p5E-myrf*, *p3E-2A-GCaMP6s-CAAX*, and *pDEST-Tol2-CG2* to generate expression constructs.

5. Immunohistochemistry

5 dpf *Tg(mbpa:eGFP-CAAX)* larvae injected at one cell stage with *p.neuroD*:*sypb-mScarlet* were fixed (4% paraformaldehyde/1X PBS) overnight at 4ºC. After rinsing in PBS, larvae were embedded in 1.5% agar/30% sucrose blocks and then soaked in 30% sucrose overnight at 4ºC. Next, the blocks were frozen in 2-methyl butane chilled by immersion in liquid nitrogen. 20 µm sections were cut in sagittal plane and collected on microscope slides. The sections were rehydrated with PBS and then blocked with AB Blocking Solution (2% goat serum/1% bovine serum albumin/1% DMSO/0.25% Triton X-100) for 1 hr at room temperature. Rabbit anti-PSD95 antibody (abcam, ab18258) was applied at 1:1000 dilution in AB Blocking Solution for 20 hr at 4ºC. The sections were washed extensively with PBS and then incubated with Alexa Fluor 647 goat anti-rabbit antibody (Jackson ImmunoResearch, 111-605-003) at 1:200 dilution in AB Blocking Solution for 20 hr at 4ºC. After extensive washing with PBS, the slides were covered with Vectashield and coverslipped. Images were collected using a Zeiss CellObserver Spinning Disk confocal system, C-Apochromat 63x/1.20 NA water immersion objective and Photometrics Prime 95B camera.

6. Imaging & image analysis

We performed live-imaging on larvae embedded laterally in 1.2% low-melt agarose containing either 0.4% tricaine or 0.3 mg/ml pancuronium bromide for immobilization. We acquired images on a Zeiss Axiovert 200 microscope with a PerkinElmer spinning disk confocal system (PerkinElmer Improvision), a Zeiss LSM 880 (Carl Zeiss), or a Zeiss CellObserver Spinning Disk confocal system, C-Apochromat 63x/1.20 NA water immersion objective and Photometrics Prime 95B camera. For Figures 1 and 2, we collected data from one field of view from each animal. For experiments in Figures 3-6 we only used one cell per animal, so n = number of cells and number of fish. After collecting images with Volocity (PerkinElmer) or Zen (Carl Zeiss), we performed all processing and analysis using Fiji/ImageJ. Image analysis was performed blind by using the Fiji plugin Lab-utility-plugins/blind-files.

6.1 Synaptophysin-eGFP clustering

We imaged *Tg(phox2b:GAL4; UAS:syp-eGFP; sox10:mRFP)* larvae at 3, 4, and 5 dpf. Roughly 50% of *phox2b*+ neurons are myelinated (Hines et al., 2015), so we confirmed myelination status of individual *phox2b*+ neurons by taking oversampled z-stacks and examining orthogonal views. We traced individual *phox2b*+ neurons containing Syp-eGFP puncta with Fiji's Plot Profile tool and counted peaks, representing individual puncta, that exceeded 150% of the inter-peak background fluorescence intensity. The number of peaks (puncta) per µm of ensheathed and bare axon were transferred from Fiji to R and density of puncta in both regions was determined by dividing puncta count by length (for bare axon density, we used the length of axon

present in the field of view). Regions were compared age-wise by Wilcox rank-sum test (wilcox.test, R package ggpubr) with no assumption of normality.

6.2 SypHy signatures under myelin sheaths

neuroD:sypHy; *Tg(sox10:mRFP)* larvae were immersed for 1 hour in 1 µM bafilomycin A1 (Tocris, cat 1334) in DMSO vehicle in embryo medium. We then paralyzed embryos by adding pancuronium bromide (Sigma, cat P1918) to the solution to achieve a final concentration of 0.3 mg/ml. We made a small incision to the tip of the tail with a tungsten needle to promote circulation of the paralytic agent. Larvae were monitored for an additional 24h post-experiment to ensure incisions did not cause lasting injury or fatality. The same bafilomycin/pancuronium bromide regimen was followed for larvae expressing *neuroD*:sypHy-2A-BoNT/B and *neuroD*:sypHy-2A-dnVamp2.

We imaged larvae in pancuronium bromide-containing low-melt agarose immersed in the same treated embryo medium (containing bafilomycin and pancuronium). We acquired oversampled z-stacks at a single x-y position, over the yolk extension, for individual larvae (1 z-stack per fish). Determination of whether an axonal sypHy hotspot was wrapped by mRFP+ myelin was made by orthogonal views. Because category designation (punctate, filled, uniform) was subjective we plotted individual observations for transparency.

6.3 PSD95 localization in sheaths

We imaged transient-transgenic *myrf*:GAL4;UAS:PSD95-GFP larvae, *myrf*:PSD95.FingR-GFP-CCR5TC-KRAB(A); *Tg(sox10:mRFP)* larvae, and *myrf*:GAL4;

zcUAS:PSD95.FingR-GFP-CCR5TC-KRAB(A); *Tg(sox10:mRFP)* larvae for examination of PSD95-GFP fusion protein localization as well as transcriptionally unregulated and regulated PSD95.FingR-GFP expression in oligodendrocytes. We designated categories based on transcriptionally-regulated PSD95.FingR-GFP expression. Because category designation (end, periodic, diffuse) was subjective, observations for individual cells were plotted for transparency. Unique cells were examined at each time point; i.e., cell #1 at 3 dpf is not cell #1 at 4 dpf. Sheaths overlapping in x-y space with the soma were frequently blown out so only those that did not overlap in x-y space with the soma were analyzed to prevent incorrect category assignment due to brightness. To test whether the distribution of categories changes over developmental time, we carried out a Chi square test (chisq.test, base R) on the contingency table for category at each age point.

6.4 Dominant-negative tests and sheath measurements

All imaging was performed at 4 dpf at approximately the same time each day (~100-102 hpf) or 8 dpf as a later time point. We predetermined that a sample size of 9-12 cells per candidate would generate a sufficient number of sheaths for both sheath length and number measurements. Sheaths were measured per cell by linear ROIs captured in ImageJ's ROI manager. Length values were exported to R with cell identification numbers to identify the number of lengths (sheaths) per cell. Total sheath length per cell is the sum of sheath lengths per cell identification number and sheath number is the number of lengths associated with an identification number. For all three parameters (total sheath length per cell, sheath length, and sheath number) we first tested for global significance using the Kruskal-Wallis test, and if this was significant, we

made pairwise comparisons between groups using the Wilcox rank-sum test with p-values adjusted for multiple comparisons by the Bonferroni-Holm method.

6.5 Quantitative colocalization

We used the Fiji plugin JACoP (Just Another Colocalization Plugin) (Bolte and Cordelières, 2006) to calculate Mander's Colocalization Coefficients, M1 and M2, which describe the fraction of protein A that colocalizes with protein B and vice versa, respectively (Dunn et al., 2011). We chose to evaluate colocalization on the basis of these coefficients because they are independent of fluorescence intensity, which varies between transient-transgenic cells and animals. To evaluate colocalization of eGFP-Cadm1b with RFPs, single plane images of oligodendrocytes expressing *myrf*:eGFP-Cadm1b on either a membrane-labeling *Tg(sox10:mRFP)* or cytosol-labeling *Tg(sox10:tagRFP)* background were cropped to minimize background and split into separate channels for thresholding. JACoP generated M1 and M2 values, which were then exported to R for analysis. To evaluate colocalization of *myrf*:GCaMP6s-CAAX or *myrf*:Ig1-dnCadm1b-2A-GCaMP6-CAAX with *Tg(neuroD:sypb-mScarlet)*, z-stacks of 50 optical sections spaced 0.31 µm apart centered on individual oligodendrocytes were similarly blinded, cropped, thresholded, and M1 values analyzed in R.

6.6 Super resolution radial fluctuations (SRRF)

For individual cells, 100-200 single z-plane images were acquired with minimal time delay between images (acquisition rate ~5 frames per second). Images were transferred from Zen to Fiji and first corrected for drift (Plugins > Registration > Correct 3D drift). We corrected for slow drifts but did not edge-enhance images to avoid

introducing artifacts. Drift-corrected images were then analyzed using the NanoJ-SRRF plugin with default settings.

Statistics

All statistics were performed in R (version 3.4.1) with RStudio. Plots were generated using dplyr and ggplot2 packages (Wickham, 2017) with cowplot package formatting (Wilke, 2016), and all statistical tests were performed using ggpubr (Kassambara, 2017) except for the Chi square test, which was carried out in base R (Core, 2015). We used the Wilcox rank sum test (also called Mann-Whitney), with no assumption of normality, for all unpaired comparisons. For multiple comparisons, we first assessed global significance using the Kruskal-Wallis test, followed (only if Kruskal-Wallis significant) by pairwise Wilcox rank sum tests with Bonferroni-Holm correction for multiple comparisons.

Acknowledgments

We are grateful to Jacob Hines for cloning *myrf* regulatory DNA and providing it to us, to Christina Kearns for tissue sectioning, and to Dominik Stich for assistance with Fourier ring correlation. We also thank Ethan Hughes and Caleb Doll for valuable comments on the manuscript.

Funding

This work was supported by US National Institutes of Health (NIH) grant R01 NS046668 and a gift from the Gates Frontiers Fund to B.A. and a National Science Foundation Graduate Research Fellowship (DGE-1553798) to A.N.H. The University of

Colorado Anschutz Medical Campus Zebrafish Core Facility was supported by NIH grant P30 NS048154.

Author contributions

A.N.H. and B.A. conceptualized the project. A.N.H. performed all the experiments, with the exception of antibody labeling, which was performed by B.A., and collected and analyzed all the data. A.N.H. wrote and B.A. edited the manuscript.

CHAPTER III

MICROGLIA PHAGOCYTOSE MYELIN SHEATHS TO MODIFY DEVELOPMENTAL MYELINATION[5]

Abstract

During development, oligodendrocytes contact and wrap neuronal axons with myelin. Similar to neurons and synapses, excess myelin sheaths are produced and selectively eliminated, but how elimination occurs is unknown. Microglia, the resident immune cells of the CNS, engulf surplus neurons and synapses. To determine if microglia also prune myelin sheaths, we used zebrafish to visualize and manipulate interactions between microglia, oligodendrocytes, and neurons during development. We found that microglia closely associate with oligodendrocytes and specifically phagocytose myelin sheaths. By using a combination of optical, genetic, chemogenetic, and behavioral approaches we revealed that neuronal activity bidirectionally balances microglial association with neuronal cell bodies and myelin phagocytosis in the optic tectum. Furthermore, multiple strategies to deplete microglia caused oligodendrocytes to maintain excessive and ectopic myelin. Our work reveals a neuronal activity-regulated role for microglia in modifying developmental myelin targeting by oligodendrocytes.

[5] This work is adapted from Hughes, A.N., Appel, B. Microglia phagocytose myelin sheaths to modify developmental myelination. *Nat Neurosci* 23, 1055-1066 (2020). DOI: 10.1038/s41593-020-0654-2

Introduction

Neuronal axon conduction velocity is supported by myelin, a specialized, proteolipid-rich membrane produced by glial cells. During development, oligodendrocytes generate numerous nascent myelin sheaths along axons. Neuronal activity promotes the formation and maturation of myelin sheaths (Gibson et al., 2014; Hines et al., 2015; Mensch et al., 2015) and can bias which axons are selected for myelination (Hines et al., 2015; Mitew et al., 2018). Sensory enrichment and deprivation paradigms in both mice and humans can modify oligodendrogenesis and myelination in relevant brain regions (Hughes et al., 2018; Sampaio-Baptista et al., 2013; Scholz et al., 2009), raising the possibility that changes in myelin support the development of higher cognitive functions. Consistent with this possibility, new myelin is required for at least some types of learning (McKenzie et al., 2014).

An underappreciated dimension of myelin plasticity is myelin elimination. Similar to neurons and synapses of the developing CNS, myelin is first overproduced and then partially eliminated (Liu et al., 2013). How myelin sheaths are removed is unknown. Microglia, the resident immune cell type of the CNS, eliminate surplus neurons and synapses during development. Microglia detect and respond to neuronal activity (Li et al., 2012; Tremblay et al., 2010), notably engulfing synapses in an activity-regulated manner to direct development of the visual system (Schafer et al., 2012). In neurological and neurodegenerative diseases, this synaptic elimination program can reemerge maladaptively to promote disease progression (Hong et al., 2016). Notably, microglial phagocytosis of myelin also is a feature of neural disease and injury (Neumann et al., 2009; Uranova et al., 2011). Therefore, to explain developmental myelin elimination, we

hypothesized that microglia engulf myelin sheaths during development to sculpt myelination.

To test this hypothesis, we manipulated and directly observed interactions between microglia, myelin, and neurons in vivo using zebrafish as a model system. We found that microglia are intimately associated with oligodendrocytes and specifically phagocytose myelin sheaths, leaving cell bodies intact. We used multiple strategies to manipulate neuronal activity and demonstrated that microglia are attracted to active neurons at the expense of myelin phagocytosis and conversely, microglia phagocytose more myelin and contact fewer neurons when neuronal activity is silenced. By eliminating microglia, we found evidence that microglia remove excess myelin sheaths and prevent ectopic myelination of cell bodies. Our data establish that microglia limit developmental myelination and thereby extend our understanding of the mechanistic basis of myelin plasticity.

Results

1. Microglia survey myelinated axon tracts

Our first objective was to determine if a relationship exists between microglia and oligodendrocytes during development. To visualize microglia, we established a transgenic line of zebrafish, *Tg(mpeg1.1:mVenus-CAAX)*, in which *mpeg1.1* regulatory DNA drives expression of membrane-tethered mVenus-CAAX in microglia and macrophages. Crossing this line to animals carrying *Tg(mbpa:mCherry-CAAX)*, a transgene that labels myelinating oligodendrocyte membrane with mCherry, permitted us to see microglia-oligodendrocyte interactions (Fig. 3.1a). In the spinal cord at 4 days post-fertilization (dpf), the time at which *Tg(mbpa:mCherry-CAAX)* expression becomes

visible, spinal cord microglia almost exclusively occupied the myelinated tracts of the dorsal and medial longitudinal fasciculi. By counting microglia in each of these tracts over developmental time, we found that microglia had an early bias for localization in the medial longitudinal fasciculus of the ventral spinal cord but occupied the tracts equally by 8 dpf (Fig. 3.1b). To learn if the change in microglia distribution correlates with a change in oligodendrocyte number, we counted oligodendrocyte cell bodies in dorsal and ventral tracts in a 3.5 hemisegment region. Similarly to microglia, oligodendrocytes were first more numerous in the ventral tract but became more equally distributed between tracts by 8 dpf (Fig. 3.1c, d). Comparing the dorsal to ventral ratio of oligodendrocytes and microglia revealed that they were nearly evenly matched in both locations over developmental time (Fig. 3.1e). Because microglia are motile cells, we sought to determine the extent of their surveillance of the myelinated tracts. To accomplish this, we performed timelapse imaging of the spinal cord and assessed the frequency of microglia migrating through a 3.5 hemisegment region. We found that regions were visited by a migrating microglial cell roughly every 4 h (Fig. 3.1f, g). These observations reveal that spinal cord microglia associate with oligodendrocytes during development and suggest that microglia are sufficiently motile to comprehensively survey myelinated axon tracts.

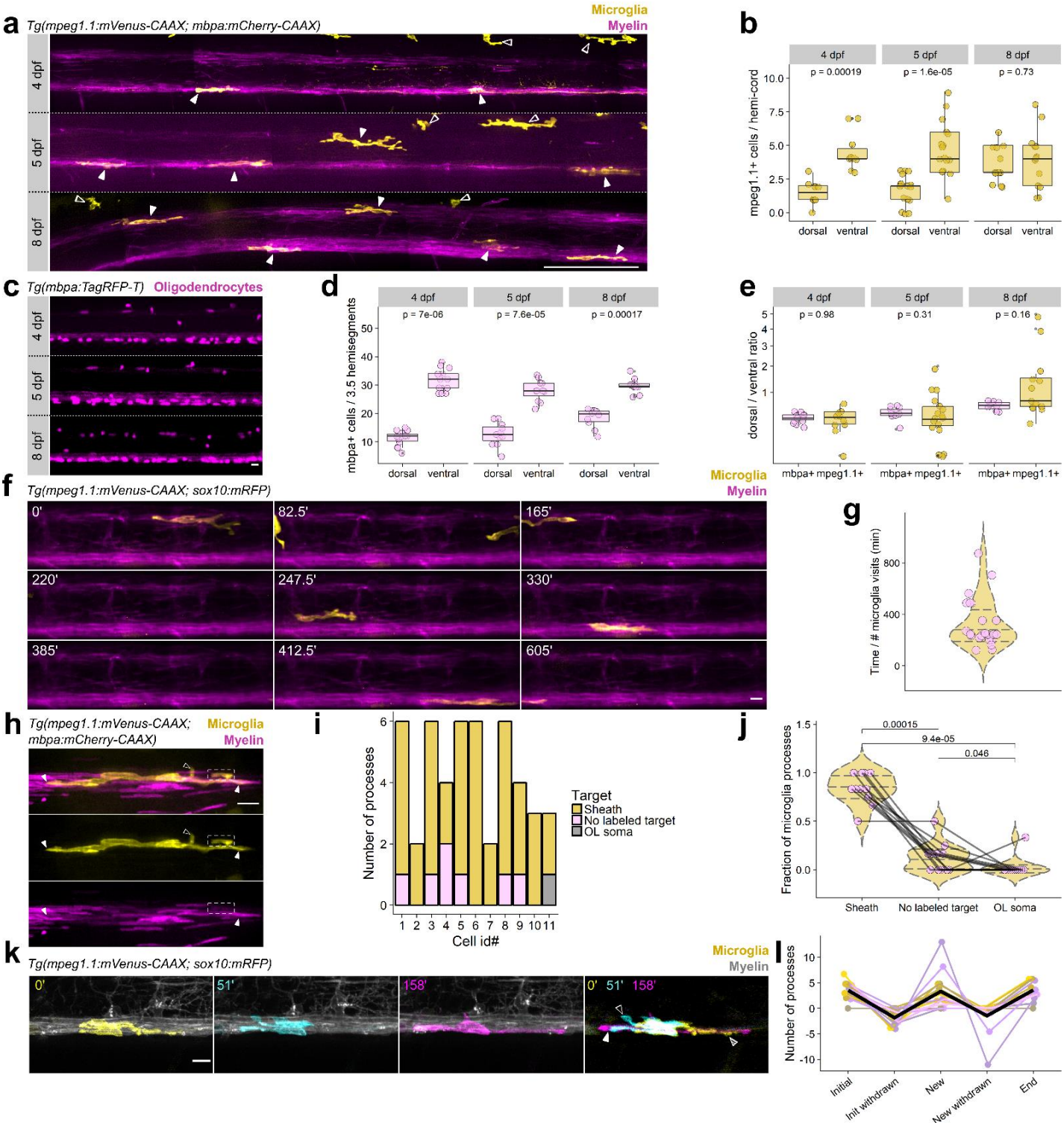

Figure 3.1. Microglia dynamically engage with myelin sheaths in the spinal cord. (a) Lateral tile scans of spinal cords of *Tg(mpeg1.1:mVenus-CAAX; mbpa:mCherry-CAAX)* larvae at 4, 5, and 8 dpf. Closed arrowheads mark microglia and open arrowheads mark peripheral macrophages. Scale bar, 50 µm. (b) Microglia counts in dorsal and ventral tracts (hemi-cord) in 4, 5, and 8 dpf larvae. Wilcox rank-sum

test, n=fish/cells, n=10/60 4 dpf, 17/109 5 dpf, 13/97 8 dpf. (c) Oligodendrocytes in 3.5 hemisegments in the spinal cord of *Tg(mbpa:TagRFP-T)* larvae at 4, 5, and 8 dpf. Scale bar, 10 μm. (d) Oligodendrocyte counts in dorsal and ventral tracts (3.5 hemisegments) in 4, 5, and 8 dpf larvae. Wilcox rank-sum test, n=fish/cells, n=14/602 4 dpf, 11/448 5 dpf, 10/482 8 dpf. (e) Ratios of dorsal/ventral cell counts for *mbpa*$^{+}$ oligodendrocytes and *mpeg1.1*$^{+}$ microglia at 4, 5, and 8 dpf, for cells counted in (b) and (d). Data in (b), (d), and (e) analyzed by Wilcox rank-sum test. (f) Timelapse imaging frames over 10 h in *Tg(mpeg1.1:mVenus-CAAX; sox10:mRFP)* larvae at 4 dpf. (g) Time between microglia visits. Each point represents the timelapse acquisition time divided by the number of microglia visits to the imaging field of view; each point is one larva (n=22 larvae). Violin plot lines mark quantiles (25, 50, 75 percentile) and colors are meaningless. (h) A microglia (yellow) in the dorsal spinal cord of a *Tg(mpeg1.1:mVenus-CAAX; mbpa:mCherry-CAAX)* larva. Closed arrowheads mark close associations of microglial processes with myelin sheaths (magenta rectangles); open arrowheads mark processes extending toward unlabeled targets; dashed box shows a process enveloping a sheath. (i) Distribution of microglial processes per cell associated with myelin sheaths, oligodendrocyte somas, or unlabeled targets for n=11 cells (11 fish). (j) Fraction of microglial processes in (i) plotted per target type, Wilcox rank-sum test with Bonferroni-Holm correction for multiple comparisons. Each point represents one microglia. (k) Timelapse imaging frames of a microglia in a *Tg(mpeg1.1:mVenus-CAAX; sox10:mRFP)* larva, pseudocolored to show cell morphology at three different time points and merged. Striped arrowhead marks a process present at 0' that is absent at 51' (initial, withdrawn); open arrowhead marks a process generated during the imaging period that later disappears (new, withdrawn); closed arrowhead marks a process that is generated during the imaging period and is maintained at the end of the imaging window (new). (l) Number of processes generated and withdrawn by microglia during 1 hour of timelapse imaging; black trace is the mean (n=14 microglia in 14 fish). Scale bars, 10 μm.

We next assessed how microglia interact with oligodendrocytes. During larval stages, microglia have few, mostly primary, processes. We determined that most processes associated with myelin sheaths rather than oligodendrocyte cell bodies or putative targets unlabeled by our transgenic reporters (Fig. 3.1h-j). Timelapse imaging revealed that microglia processes were not static but were continually retracted and extended within myelinated tracts labeled by *Tg(sox10:mRFP)* (Fig. 3.1k, l). These dynamic behaviors are consistent with the possibility that microglia survey a large fraction of nascent myelin sheaths in the spinal cord.

2. Microglia phagocytose myelin sheaths but not oligodendrocytes

To learn if myelin-associated microglia are phagocytic we performed imaging experiments to detect intracellular calcium transients, a signature of phagocytic

microglia and macrophages (Eichhoff et al., 2011; Hishikawa et al., 1991; Pozner et al., 2015). To visualize calcium dynamics, we generated a transgenic line, *Tg(mpeg1.1:GCaMP6s-CAAX)*, which labels microglia membrane with the calcium indicator GCaMP6s-CAAX. By imaging microglia in 4 dpf larvae, we found numerous spontaneous calcium events within process tips, branches, and the cell body. To distinguish calcium transients from membrane fluctuations that occur during cellular movement, we imaged microglia in larvae carrying both GCaMP6s-CAAX and another membrane-tethered fluorophore, mScarlet-CAAX, at 4 dpf and detected and investigated events with the calcium imaging toolbox, AQuA (Fig. 3.2a). We found that calcium events were distinguishable from membrane movement events on the basis of fluorescence change, dF/F (Fig. 3.2b), so we set a threshold for calcium events to include only those exceeding dF/F > 0.05. By this criterion, 100% of microglia exhibited calcium transients during a 10 min acquisition (Supplementary Table 3.1). To determine if these calcium events represent phagocytic activity at microglia-myelin contacts, we next performed calcium imaging on *Tg(mpeg1.1:GCaMP6s-CAAX; sox10:mRFP)* larvae (Fig. 3.2c). Microglia exhibited transients both within processes contacting sheaths and those not contacting sheaths. Of the 645 filtered calcium events we detected in 31 microglia, we further filtered events to examine the sheath-contacting status of the largest calcium events (dF/F > 0.10, area > 3 μm^2), which yielded 41 events in 9/31 cells. These events predominantly occurred at contacts with myelin sheaths (Fig. 3.2d) and were distinguishable from non-sheath-contacting events on the basis of event duration (Fig. 3.2e, Extended Fig. 3.1), consistent with these events representing a specific signaling program within sheath-contacting processes. Indeed, we found that

sheath-contacting processes exhibiting calcium transients were sometimes followed by sheath disappearance (Fig. 3.2f), consistent with calcium signaling as a signature of phagocytic activity.

To investigate phagocytosis of myelin sheaths directly, we next performed timelapse imaging in 4 dpf *Tg(mpeg1.1:mVenus-CAAX; sox10:mRFP)* larvae. Similar to our observations of apparent sheath loss following calcium events (Fig. 3.2f), our timelapse imaging experiments captured occasional whole-sheath engulfment events by microglia (Fig. 3.2g). To determine the relative proportion of sheaths eliminated by engulfment and retraction, we performed timelapse imaging of microglia and their surrounding 3.5 hemisegment territory for 3 h. To identify sheaths that disappeared during timelapse in an semi-automatic and unbiased way, we used the myelin channel frames to generate a series of images in which the exclusive-or (XOR) operation is performed on consecutive frames, creating a series of the signals that change over time (see Methods, Supplementary Table 3.2). Summing these XOR frames and merging with the time-summed myelin channel identified sheaths that disappeared over time, while keeping us blinded to microglia location and thus sheath association (Fig. 3.2h). Tagged sheaths were then tracked in the original timelapse to detect microglial engulfment or lack of microglial contact (retraction). We found that although both engulfment and retraction contribute to sheath elimination, microglia engulfment accounted for the majority (~70%) of sheath elimination at this stage (Fig. 3.2i, j). Furthermore, sheaths engulfed by microglia were longer than those that were retracted (Fig. 3.2k), raising the possibility that engulfment targets more mature sheaths. Consistent with this possibility, timelapse imaging of microglia interacting with *mbpa*$^{+}$

oligodendrocytes revealed similar sheath engulfment (Fig. 3.2l). We validated these observations of myelin phagocytosis using an alternative method to visualize myelin within microglia. Specifically, we performed immunohistochemistry to detect myelin basic protein (Mbp) in tissue obtained from *Tg(mpeg1.1:mVenus-CAAX; mbpa:mCherry-CAAX)* larvae. Nearly all mCherry-CAAX inclusions in microglia were Mbp^{+}, indicating that mCherry-CAAX inclusions represent phagocytosed myelin in living larvae (Fig. 3.2m, n, Extended Fig. 3.2).

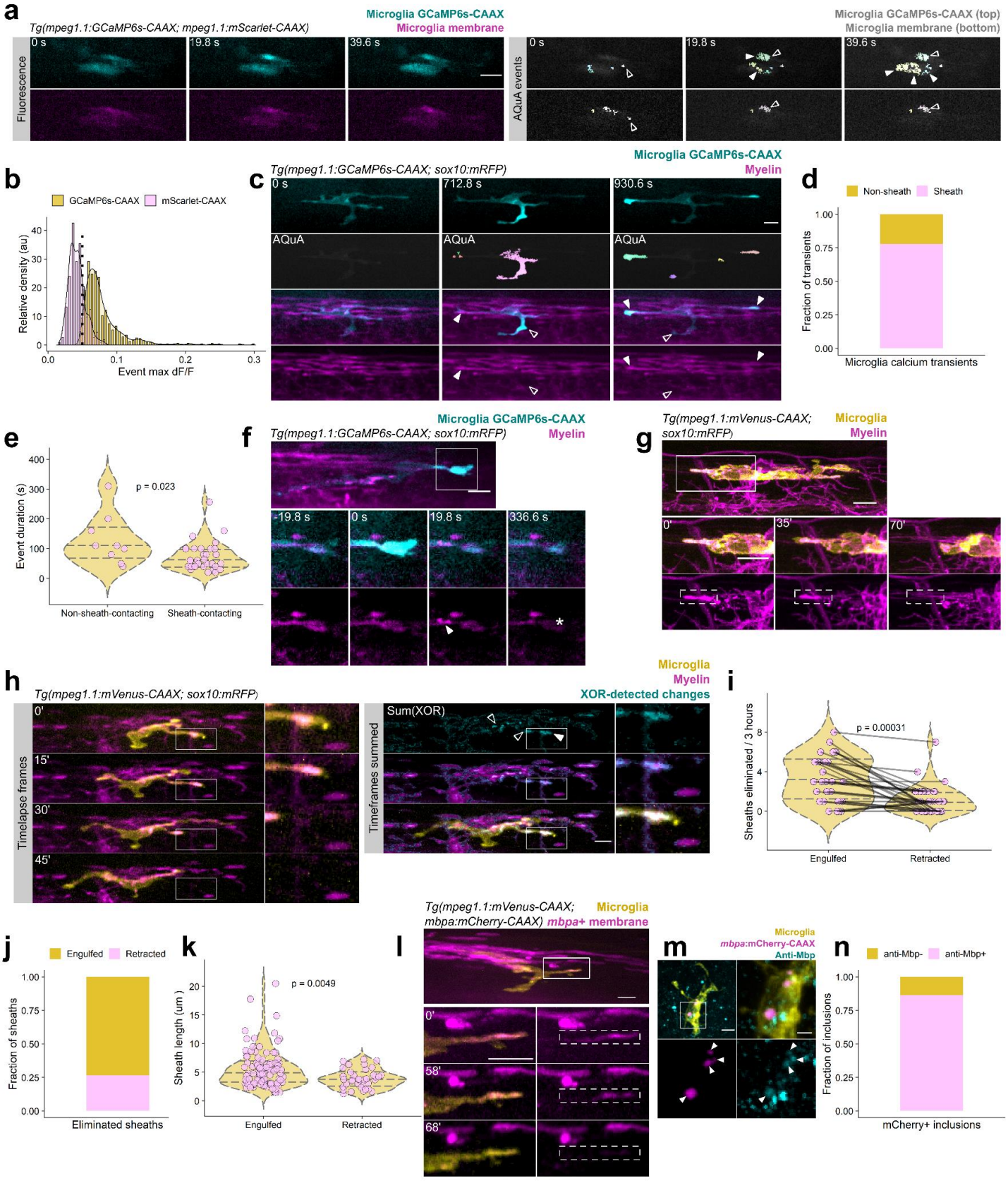
a
Tg(mpeg1.1:GCaMP6s-CAAX; mpeg1.1:mScarlet-CAAX)
Microglia GCaMP6s-CAAX
Microglia membrane
Fluorescence
0 s
19.8 s
39.6 s
AQuA events
Microglia GCaMP6s-CAAX (top)
Microglia membrane (bottom)
b
GCaMP6s-CAAX
mScarlet-CAAX
Relative density (au)
Event max dF/F
c
Tg(mpeg1.1:GCaMP6s-CAAX; sox10:mRFP)
Microglia GCaMP6s-CAAX
Myelin
0 s
712.8 s
930.6 s
AQuA
d
Non-sheath
Sheath
Fraction of transients
Microglia calcium transients
e
Event duration (s)
p = 0.023
Non-sheath-contacting
Sheath-contacting
f
Tg(mpeg1.1:GCaMP6s-CAAX; sox10:mRFP)
Microglia GCaMP6s-CAAX
Myelin
-19.8 s
0 s
19.8 s
336.6 s
g
Tg(mpeg1.1:mVenus-CAAX; sox10:mRFP)
Microglia
Myelin
0'
35'
70'
h
Tg(mpeg1.1:mVenus-CAAX; sox10:mRFP)
Microglia
Myelin
XOR-detected changes
Timelapse frames
Timeframes summed
Sum(XOR)
0'
15'
30'
45'
i
Sheaths eliminated / 3 hours
p = 0.00031
Engulfed
Retracted
j
Engulfed
Retracted
Fraction of sheaths
Eliminated sheaths
k
Sheath length (um)
p = 0.0049
Engulfed
Retracted
l
Tg(mpeg1.1:mVenus-CAAX; mbpa:mCherry-CAAX)
Microglia
mbpa+ membrane
0'
58'
68'
m
Microglia
mbpa:mCherry-CAAX
Anti-Mbp
n
anti-Mbp-
anti-Mbp+
Fraction of inclusions
mCherry+ inclusions

Figure 3.2. Microglia phagocytose myelin sheaths during developmental myelination. (a) Timelapse imaging (left) and AQuA transient detection in a microglia carrying dual reporters for membrane fluorescence (mScarlet-CAAX) and membrane calcium (GCaMP6s-CAAX). Open arrowheads label membrane events present in both channels; closed arrowheads mark calcium transients. (b) Histogram of membrane and calcium event dF/F values (649 calcium events in 31 cells, 228 membrane events in 9 cells) shows that events are separable by dF/F; therefore, only events >0.05 dF/F were considered calcium transients. (c) Timelapse imaging of filtered calcium transients (dF/F > 0.05) in a microglia interacting with myelin. Closed arrowheads mark events occurring at points of contact with sheaths; open arrowheads mark events at non-sheath-contacting processes. (d, e) Fraction of large calcium events (d) and event duration (e) associated with sheath-contacting and non-contacting processes. Wilcox rank-sum test; n=32/9 filtered events from 9 cells/9 fish. (f) Timelapse imaging of a microglia calcium transient and phagocytosis of contacted material (arrowheads mark blebbing; asterisk marks loss of signal). (g) Timelapse imaging of a microglia engulfing a nascent myelin sheath. (h) Analysis scheme for detecting myelin sheaths eliminated by phagocytosis or retraction. Timelapse frames (left) are processed by consecutive exclusive-or (XOR) calculation to generate an image of lost sheaths (cyan); those engulfed by microglia are engulfed (closed arrowheads) whereas those lost but not contacted are retracted. (i) Paired comparison of number of sheaths lost by engulfment and retraction in 3 h in 30 microglia from 30 animals. Each pair-connected line is one animal; Wilcox-rank sum test. (j) Relative fractions of sheaths across all timelapse acquisitions that were engulfed or retracted. (k) Lengths of sheaths eliminated by engulfment vs retraction; Wilcox rank-sum test (n=135 sheaths from 30 cells/30 fish). (l) Representative example of myelin sheaths in *mbpa*$^{+}$ oligodendrocytes eliminated by microglia. (m, n) Immunohistochemistry and quantification of anti-Mbp (cyan) inclusions within microglia in animals carrying *Tg(mbpa:mCherry-CAAX)* to label oligodendrocyte membrane. n=44 mCherry-CAAX+ inclusions in 11 cells in 7 fish. All scale bars, 10 μm.

Following engulfment, fluorescent material was only briefly visible within microglia before fluorescence disappears, limiting our ability to estimate the fraction of microglia that phagocytose myelin during development (Fig. 3.3a). This rapid disappearance likely results from degradation by phagosome acidification. We therefore predicted that inhibiting the acidification of phagosomes would delay the breakdown of phagocytosed myelin and allow us to determine the fraction of microglia that phagocytose myelin membrane (Fig. 3.3a, b). To inhibit phagosome acidification, we treated 4 dpf larvae with bafilomycin A1 for 1 h prior to imaging. Microglia in *Tg(mpeg1.1:mVenus-CAAX; mbpa:mCherry-CAAX)* larvae treated with bafilomycin had more and brighter myelin inclusions than microglia of larvae treated with vehicle (Fig. 3.3b). We confirmed that myelin inclusions were contained within microglia by viewing cells in 3D. Morphological segmentation allowed us to obtain measurements of these

inclusions (Fig. 3.3c). We found that when larvae were treated with DMSO control, myelin inclusions were evident in about 2/3 of all microglia, with the remaining 1/3 containing no detectable inclusions. However, treatment with bafilomycin to acutely delay myelin breakdown revealed that all microglia contained myelin inclusions, suggesting that all spinal cord microglia participate in myelin pruning by phagocytosis (Fig. 3.3d). Bafilomycin did not change the area of individual inclusions (Fig. 3.3e), but the total area of inclusions per microglia was increased (Fig. 3.3f), consistent with stalled myelin breakdown within microglia. Because oligodendrocytes can start myelinating at any time between 4 and 8 dpf, we also tested whether myelin phagocytosis detectable by bafilomycin might change over developmental time. We found no difference in the number of myelin inclusions per microglia at 4, 5, or 8 dpf, consistent with continuous myelin pruning by microglia over the course of developmental myelination (Fig. 3.3g).

Although we only observed microglial phagocytosis of individual myelin sheaths, in principle, microglia might also engulf entire oligodendrocytes. To investigate this possibility, we first labeled oligodendrocytes undergoing apoptosis using the vital dye acridine orange (Fig. 3.3h). We found that *mbpa*$^{+}$ oligodendrocyte apoptosis was rare and that the frequency was not changed by bafilomycin (Fig. 3.3h-k, Extended Fig. 3.3). Therefore, dying oligodendrocytes are not likely the source of mCherry-CAAX inclusions in microglia. Next, we tested the possibility that microglia engulf entire live oligodendrocytes. To do so, we repeated our mCherry-CAAX engulfment experiments using an additional oligodendrocyte reporter line, *Tg(mbpa:TagRFP-T)*, in which the same *mbpa* regulatory DNA drives expression of cytosolic TagRFP-T. Because most

oligodendrocyte cytosol is extruded from myelin sheaths, this line primarily labels oligodendrocyte cell bodies (Fig. 3.3l). We predicted that if microglia phagocytose entire oligodendrocytes then this oligodendrocyte somatic label would also be detectable within microglia. However, we very rarely detected TagRFP-T within microglia in DMSO or bafilomycin-treated larvae (Fig. 3.3m, n). These data suggest that microglia specifically engulf myelin sheaths with negligible phagocytosis of oligodendrocyte cell bodies.

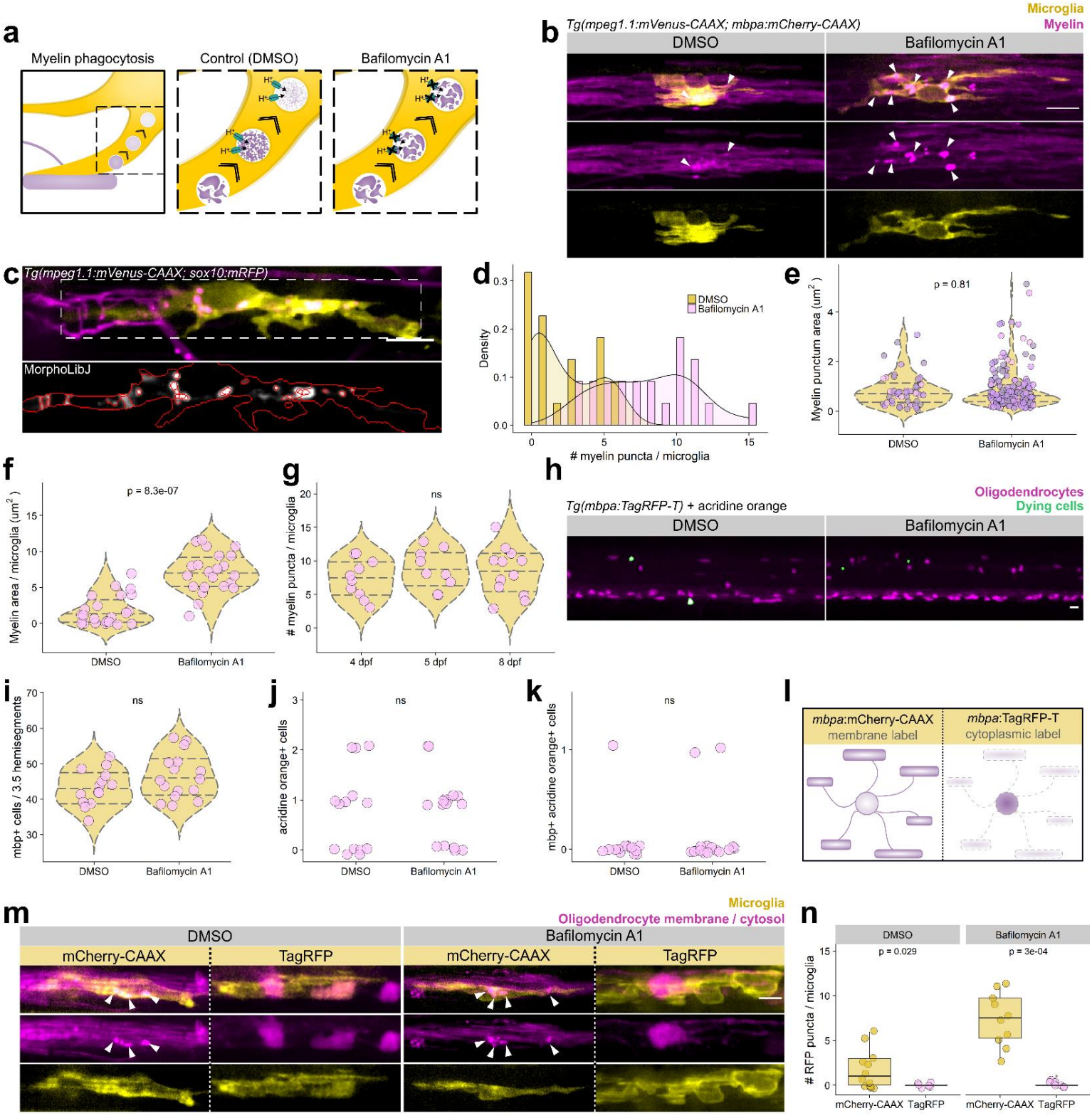
a
Myelin phagocytosis
Control (DMSO)
Bafilomycin A1
b
Tg(mpeg1.1:mVenus-CAAX; mbpa:mCherry-CAAX)
Microglia
Myelin
DMSO
Bafilomycin A1
c
Tg(mpeg1.1:mVenus-CAAX; sox10:mRFP)
MorphoLibJ
d
Density
DMSO
Bafilomycin A1
myelin puncta / microglia
e
p = 0.81
Myelin punctum area (um2)
DMSO
Bafilomycin A1
f
p = 8.3e-07
Myelin area / microglia (um2)
DMSO
Bafilomycin A1
g
ns
myelin puncta / microglia
4 dpf
5 dpf
8 dpf
h
Tg(mbpa:TagRFP-T) + acridine orange
Oligodendrocytes
Dying cells
DMSO
Bafilomycin A1
i
ns
mbp+ cells / 3.5 hemisegments
DMSO
Bafilomycin A1
j
ns
acridine orange+ cells
DMSO
Bafilomycin A1
k
ns
mbp+ acridine orange+ cells
DMSO
Bafilomycin A1
l
mbpa:mCherry-CAAX
membrane label
mbpa:TagRFP-T
cytoplasmic label
m
Microglia
Oligodendrocyte membrane / cytosol
DMSO
Bafilomycin A1
mCherry-CAAX
TagRFP
n
DMSO
Bafilomycin A1
p = 0.029
p = 3e-04
# RFP puncta / microglia
mCherry-CAAX
TagRFP

Figure 3.3. Microglia phagocytose myelin sheaths with minimal phagocytosis of oligodendrocyte somas. (a) Strategy for delaying the breakdown of phagocytosed myelin with bafilomycin A1. (b) Microglia in *Tg(mpeg1.1:mVenus-CAAX; mbpa:mCherry-CAAX)* larvae treated with DMSO or bafilomycin (1 µm) for 1 hour prior to imaging. Arrowheads mark round myelin inclusions inside microglia. (c) Example sum-projected image of a microglia containing mRFP inclusions (top) with morphological segmentation performed using MorphoLibJ to identify inclusions (bottom). (d) Histogram depicting the number of myelin inclusions per microglia in DMSO and bafilomycin-treated larva. (e-g) Morphological segmentation on sum-projected images of microglia in 4 dpf *Tg(mpeg1.1:mVenus-CAAX; mbpa:mCherry-CAAX)* larvae that were treated with either DMSO or bafilomycin prior to imaging. Each point represents one inclusion (e) or microglia (f, g); points shaded so overlapping points are visible (DMSO, n=22 cells from 22 larvae containing 48 inclusions; bafilomycin, n=22 cells/22 larvae/175 inclusions). (e) Area (μm^2) of myelin inclusions inside microglia, Wilcox rank-sum test. (f) Total myelin inclusion area (μm^2) per microglia, Wilcox rank-sum test. (g) Number of myelin inclusions per microglia in bafilomycin-treated larvae over the course of developmental myelination (4-8 dpf). Kruskal-Wallis test, n=fish/cells/inclusions, n=10/10/74 4 dpf, 9/9/79 5 dpf, 12/12/101 8 dpf. (h) Max-projection images of spinal cord oligodendrocytes (magenta) in larvae treated with either DMSO or bafilomycin A1 and live-stained with acridine orange (green). (i-k) Quantification of *mbpa*$^+$ cells (i), acridine orange cells (j), and *mbpa*$^+$ cells stained by acridine orange (k) in 3.5 hemisegments and analyzed by Wilcox rank-sum test for n=fish/cells, n=14/602 DMSO, 16/742 bafilomycin. (l) Schematic of transgenic oligodendrocyte reporters that label either oligodendrocyte membrane (mCherry-CAAX) or cytosol (TagRFP). (m) Examples of microglia in either *Tg(mpeg1.1:mVenus-CAAX; mbpa:mCherry-CAAX)* or *Tg(mpeg1.1:mVenus-CAAX; mbpa:TagRFP-T)* 4 dpf larvae, treated with either DMSO or bafilomycin A1 prior to imaging. Arrowheads mark myelin inclusions. (n) Number of mCherry-CAAX and TagRFP inclusions per microglia in each of the four groups presented in (m), Wilcox rank-sum test (n=fish/cells/inclusions, n=12/12/18 mCherry-CAAX DMSO, 10/10/74 mCherry-CAAX bafilomycin, 6/6/0 TagRFP DMSO, 8/8/1 TagRFP bafilomycin). Scale bars, 10 µm.

3. Myelin phagocytosis is bidirectionally regulated by neuronal activity

Microglia contact numerous myelin sheaths (Fig. 3.1f-j) but do not phagocytose all sheaths. What determines the amount of myelin that microglia phagocytose? Previous data showed that neuronal activity can both promote and suppress microglial interactions with cellular targets. For example, active neuronal cell bodies were more frequently contacted by microglia in zebrafish optic tectum (Li et al., 2012). By contrast, inhibiting retinal ganglion cell activity increased microglia engulfment of synapses from axons projecting to lateral geniculate nucleus (Schafer et al., 2012). Together, these observations suggest that elevated neuronal activity can shift microglia away from interaction with synapses and toward neuronal cell bodies. We therefore hypothesized that neuronal activity similarly tunes microglial interaction with neuronal cell bodies and

myelinated axons, thereby regulating myelin sheath phagocytosis by microglia. To test this, we investigated microglia in the periventricular neuronal cell body layer of optic tectum (Fig. 3.4a, a'). Approximately 10 microglia occupy the cell body layer of each tectal hemisphere (Sieger et al., 2012), positioned between the somas of unmyelinated periventricular neurons and a separate population of heavily myelinated axons that comprise the tectal commissure (Bai et al., 2011) (Fig. 3.4a). We thus tested the possibility that microglia interacting with active neuronal somas would be less likely to phagocytose myelin from the commissural axons, and conversely, that silencing cell body layer somas would predispose microglia to interact with and phagocytose commissural myelin.

We first tested the effects of manipulating neuronal activity on microglia interactions with neuronal somas. To do so, we silenced a subset of cell body layer neurons marked by fluorescent protein expression. Specifically, we injected 1-cell stage *Tg(mpeg1.1:mVenus-CAAX; mbpa:mCherry-CAAX)* embryos with a plasmid designed to bicistronically express dominant-negative Vamp2 (dnVamp2), a variant lacking the transmembrane domain, or botulinum toxin (BoNT/B) with mTagBFP-CAAX under control of a pan-neuronal driver. As a control, we mosaically labeled neurons with mTagBFP-CAAX alone. Because expression was mosaic pan-neuronal, we excluded larvae in which tectal commissure axons were labeled so that we could specifically test the role of cell body layer inhibition. We acquired z-stack confocal images of the tectal cell body layer at 4 dpf and determined the fraction of labeled neuronal somas contacted by microglia (Fig. 3.4b). Whereas neuronal inhibition did not change the number of microglia, microglia made fewer contacts on the cell bodies of inhibited

neurons than on control neurons (Fig. 3.4c, d), consistent with the possibility that reducing neuronal activity reduces microglia interaction with somas.

To determine if neuronal activity biases microglia to contact somas, we mosaically activated cell body layer neurons by expressing the capsaicin-gated channel, TRPV1 (*Rattus norvegicus*) fused to mTagBFP in *Tg(mpeg1.1:mVenus-CAAX)* larvae. At 4 dpf, we treated larvae for 2 h with capsaicin (1 µM) to activate neurons expressing the channel, or with DMSO as a control, and then determined the fraction of TRPV1-mTagBFP^{+} neurons contacted by microglia. Neurons activated by capsaicin more frequently received somatic contact by microglia (Fig. 3.4e, f), despite an unchanged number of available microglia (Fig. 3.4g). To learn how microglia acutely respond to soma activation, we locally increased neuronal activity in the cell body layer by photouncaging MNI-glutamate (Fig. 3.4h). We determined that our uncaging protocol elicited neuronal Ca^{2+} transients in sparsely-labeled *neuroD*:GCaMP6s neurons most reliably within a 20 µm distance (Fig. 3.4i, i', Extended Fig. 3.4), consistent with previous findings (Li et al., 2012). We then used this measurement to determine the distance between microglia and our uncaging target sites. We uncaged MNI-glutamate or DMSO control within 20 µm of microglia and performed timelapse imaging of process extension and retraction toward and away from the uncaging point (Fig. 3.4j). We found that microglia in both groups underwent the same number of process movements (Fig. 3.4k), but glutamate uncaging caused microglia to elaborate processes in the direction of uncaging and to retract processes from the opposite side (see Methods) (Fig. 3.4l). Together, these data demonstrate that activity bidirectionally governs microglial interactions with neuronal somas.

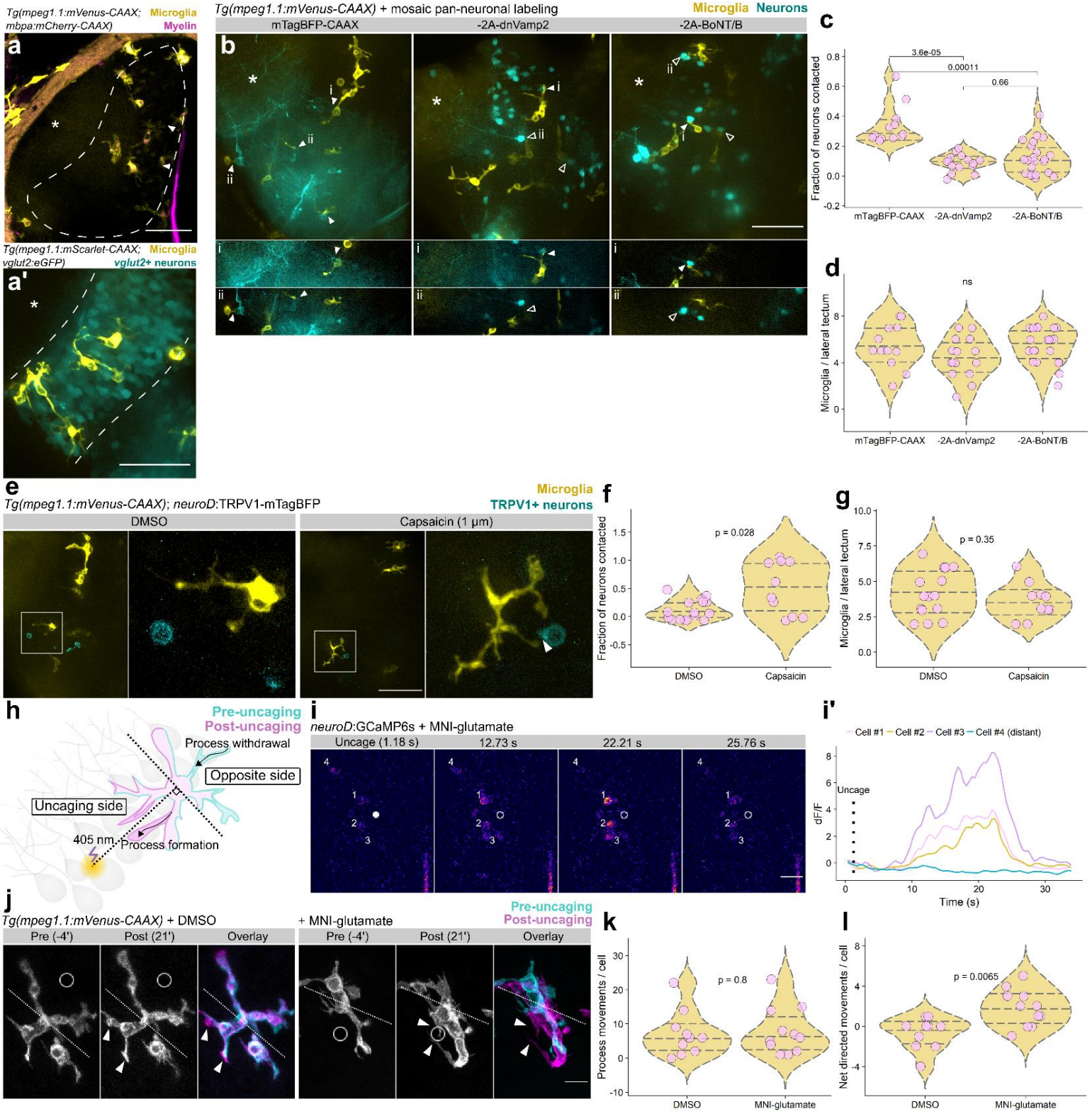
Tg(mpeg1.1:mVenus-CAAX; mbpa:mCherry-CAAX)
Microglia
Myelin
a
Tg(mpeg1.1:mScarlet-CAAX; vglut2:eGFP)
Microglia
vglut2+ neurons
a'
Tg(mpeg1.1:mVenus-CAAX) + mosaic pan-neuronal labeling
Microglia Neurons
mTagBFP-CAAX
-2A-dnVamp2
-2A-BoNT/B
b
c
Fraction of neurons contacted
3.6e-05
0.00011
0.66
mTagBFP-CAAX
-2A-dnVamp2
-2A-BoNT/B
d
Microglia / lateral tectum
ns
e
Tg(mpeg1.1:mVenus-CAAX); neuroD:TRPV1-mTagBFP
Microglia
TRPV1+ neurons
DMSO
Capsaicin (1 µm)
f
Fraction of neurons contacted
p = 0.028
DMSO
Capsaicin
g
Microglia / lateral tectum
p = 0.35
h
Pre-uncaging
Post-uncaging
Process withdrawal
Opposite side
Uncaging side
405 nm
Process formation
i
neuroD:GCaMP6s + MNI-glutamate
Uncage (1.18 s)
12.73 s
22.21 s
25.76 s
i'
Cell #1
Cell #2
Cell #3
Cell #4 (distant)
Uncage
dF/F
Time (s)
j
Tg(mpeg1.1:mVenus-CAAX) + DMSO
+ MNI-glutamate
Pre-uncaging
Post-uncaging
Pre (-4')
Post (21')
Overlay
k
Process movements / cell
p = 0.8
DMSO
MNI-glutamate
l
Net directed movements / cell
p = 0.0065
DMSO
MNI-glutamate

Figure 3.4. Neuronal activity regulates microglia-neuron interactions. (a) Coronal view of microglia and myelin in one hemisphere of optic tectum in a live *Tg(mpeg1.1:mVenus-CAAX; mbpa:mCherry-CAAX)* 5 dpf larva. Dashed line marks the cell body layer, asterisks marks the neuropil layer, and arrowheads indicate the tectal commissure. (a') Lateral view of microglia in the cell body layer. Microglia labeled by *Tg(mpeg1.1:mScarlet-CAAX)* and cell body layer glutamatergic neurons labeled by *Tg(vglut2:eGFP)*. (a) and (a') are representative images from 10 larvae. Scale bars, 50 µm. (b) Top panels, max projection images of optic tectum (lateral view) in *Tg(mpeg1.1:mVenus-CAAX)* larvae mosaically expressing *neuroD*:mTagBFP-CAAX or *neuroD*:mTagBFP-CAAX-2A-dnVamp2/BoNT/B (-2A-dnVamp2, -2A-BoNT/B). Panels below show single optical sections containing microglial-neuron contacts (closed arrowheads) or absence of contact (open arrowheads). Asterisks mark neuropil. Scale bar, 50 µm. (c) Fraction of neuron somas contacted per tectal field of view in each of the groups in (b), analyzed by Wilcox rank-sum test with Bonferroni-Holm correction for multiple comparisons. (d) Number of microglia per tectal field of view for each group in (b), analyzed by Kruskal-Wallis test. For (b-d), n=fish/neurons/microglia, n=12/166/65 mTagBFP-CAAX, 15/487/66 -2A-dnVamp2, 22/398/121 -2A-BoNT/B. (e) Max-projection images of microglia (yellow) and neurons sparsely expressing TRPV1-mTagBFP (cyan) in optic tectum of larvae treated with DMSO vehicle or 1 µm capsaicin. Closed arrowhead marks a microglia-neuron contact. Scale bar, 50 µm. (f, g) Quantification of the fraction of TRPV1-mTagBFP+ neurons contacted by microglia (f) and the number of microglia per lateral tectum field of view (g). Each dot represents one larval tectum, analyzed by Wilcox rank-sum test (n=fish/neurons, n=16/62 DMSO, 10/19 capsaicin). (h) Schematic of glutamate uncaging and analysis of microglial motility. (i, i') Example frames of glutamate uncaging near neurons sparsely-labeled with GCaMP6s. Closed dot marks the point of uncaging, open dot shows the position after uncaging, and cell numbers match transient traces in (i'). Representative example from one of 9 larvae (Extended Fig. 3.4). Scale bar, 20 µm. (j) Timelapse imaging frames of microglia in larvae treated with DMSO vehicle or MNI-glutamate, before and after focal 405 nm uncaging at the open circle. Dotted line divides microglia into uncaging and opposite sides (described in (h)) and arrowheads indicate newly formed processes. Scale bar, 10 µm. (k, l) Total process extensions and retractions per cell in each group (k) and net movements toward the uncaging point (l). Wilcox rank-sum test, n=fish/microglia, n=10/10 DMSO, 11/11 MNI-glutamate.

If neuronal activity regulates microglial interaction with neuronal somas, could activity also reciprocally determine microglial phagocytosis of myelin from the tectal commissure? To test this possibility, we measured the amount of myelin phagocytosed by microglia upon neuronal inhibition with dnVamp2 and BoNT/B (Fig. 3.5a). Similarly to spinal cord, optic tectum microglia contained phagocytosed myelin (Fig. 3.5a). However, when neurons were silenced with either dnVamp2 or BoNT/B, optic tectum and spinal cord microglia contained many more myelin inclusions (Fig. 3.5b), and the total area of myelin inclusions per microglia was increased (Fig. 3.5c), despite no appreciable changes in microglial area or the size of myelin inclusions (Fig. 3.5d, e). Together, these

data indicate that microglia engulf more myelin from the tectal commissure when neuronal cell body layer activity is suppressed.

To test if sustained increased activity in the cell body layer is sufficient to reduce myelin phagocytosis from the tectal commissure, we used a strong water current paradigm, in which a magnetic stir bar generates strong water currents that force larvae to orient themselves and swim against the currents. Such visuomotor behaviors activate optic tectum (Nevin et al., 2010) and this specific paradigm upregulated proteins associated with the optic tectum, consistent with tectal activation (Langebeck-Jensen et al., 2019). We placed *Tg(mpeg1.1:mVenus-CAAX; mbpa:mCherry-CAAX)* larvae in strong water currents for two consecutive days, followed immediately by live-imaging of myelin inclusions in tectal microglia (Fig. 3.5f-g). We found that exposing larvae to strong water currents did not alter the morphology or size of tectal microglia (Fig. 3.5h), but microglia engulfed less myelin (Fig. 3.5i). Taken together with our observations that microglia engulfed more myelin upon inhibition of cell body layer neurons (Fig. 3.5a-c), these data suggest that microglia phagocytose myelin in a bidirectional neuronal activity-regulated manner.

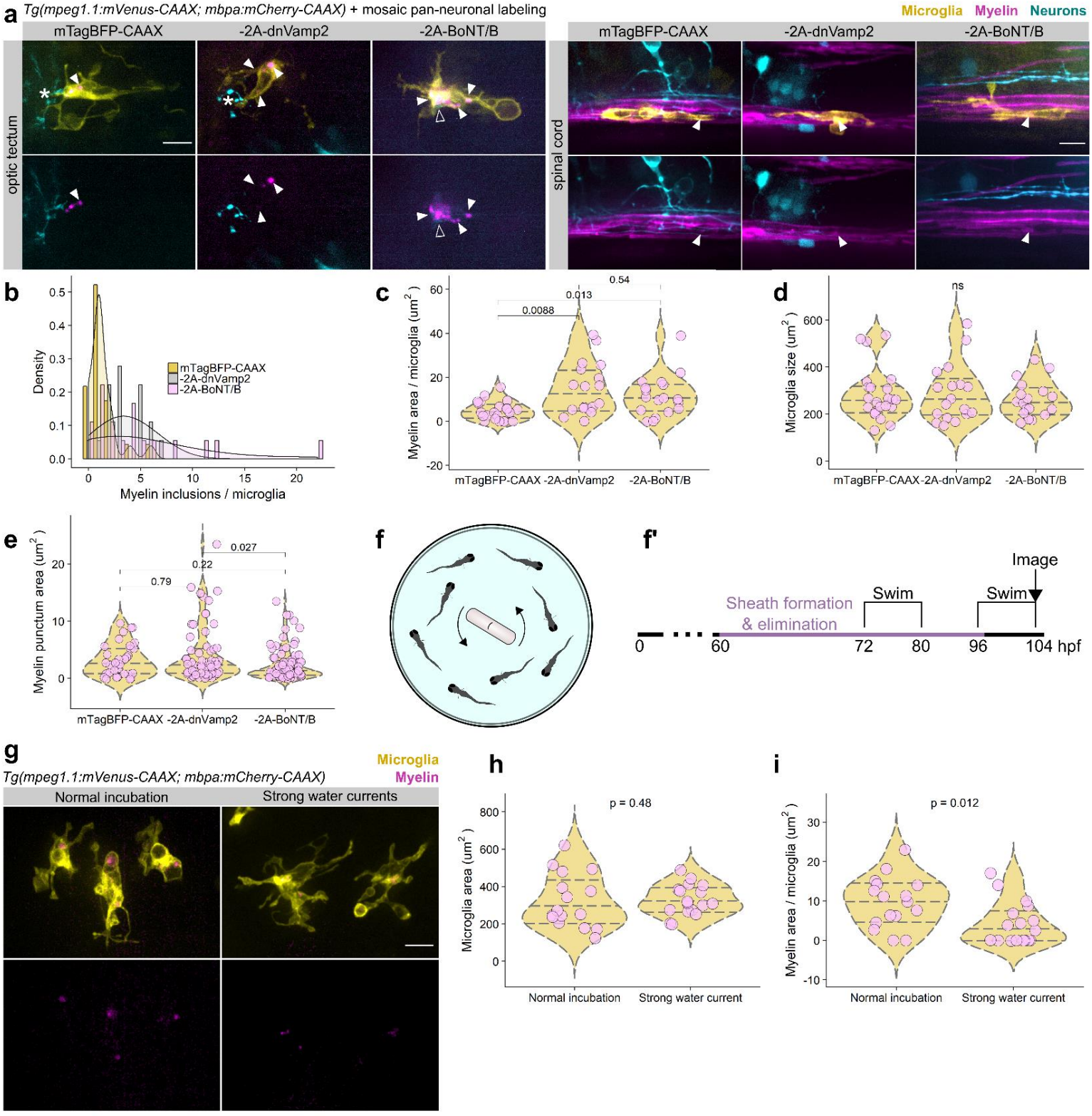
a
Tg(mpeg1.1:mVenus-CAAX; mbpa:mCherry-CAAX) + mosaic pan-neuronal labeling
Microglia Myelin Neurons
mTagBFP-CAAX
-2A-dnVamp2
-2A-BoNT/B
optic tectum
spinal cord
b
Density
Myelin inclusions / microglia
mTagBFP-CAAX
-2A-dnVamp2
-2A-BoNT/B
c
Myelin area / microglia (um2)
0.54
0.013
0.0088
d
Microglia size (um2)
ns
e
Myelin punctum area (um2)
0.027
0.22
0.79
f
f'
Image
Sheath formation & elimination
Swim
Swim
0
60
72
80
96
104 hpf
g
Tg(mpeg1.1:mVenus-CAAX; mbpa:mCherry-CAAX)
Microglia
Myelin
Normal incubation
Strong water currents
h
Microglia area (um2)
p = 0.48
Normal incubation
Strong water current
i
Myelin area / microglia (um2)
p = 0.012
Normal incubation
Strong water current

Figure 3.5. Neuronal activity regulates myelin phagocytosis by microglia. (a) Microglia in the optic tectum and spinal cord in larvae carrying Tg(mpeg1.1:mVenus-CAAX; mbpa:mCherry-CAAX) to label microglia and myelin and mosaically expressing either neuroD:mTagBFP-CAAX or neuroD:mTagBFP-CAAX-2A-dnVamp2/BoNT/B (-2A-dnVamp2, -2A-BoNT/B). Closed arrowheads mark myelin inclusions inside microglia (magenta); open arrowheads mark neuronal inclusions (cyan); asterisks mark microglial processes contacting neurons. Scale bars, 10 µm. (b-e) MorphoLibJ morphological segmentation on sum-projected images of optic tectum microglia in 4 dpf in each group in (a). Each point represents one microglia (c, d) or inclusion (e) (n=fish/microglia/inclusions, n=18/23/30 mTagBFP-CAAX, 18/18/63 -2A-dnVamp2, 18/18/87 -2A-BoNT/B). (b) Histogram depicting the number of myelin inclusions inside microglia. (c) Total myelin inclusion area per microglia, Wilcox rank-sum test with Bonferroni-Holm correction for multiple comparisons. (d) Microglia area, Kruskal-Wallis test. (e) Area of individual myelin inclusions inside microglia, Wilcox rank-sum test. (f, f') Schematic and timeline of strong water current-induced forced swimming to increase neuronal activity in optic tectum. (g) Representative examples of microglia containing myelin inclusions in normal incubation and forced swim paradigms. Scale bar, 10 µm. (h, i) Microglia area (h) and myelin inclusion area (i) per cell in each group, Wilcox rank-sum test (n=fish/microglia, n=12/16 normal, 13/17 strong currents).

4. Microglia regulate myelin targeting by oligodendrocytes

Microglia eliminate some, but not all myelin sheaths (Fig. 3.2), and microglia phagocytose myelin in a neuronal activity-regulated manner (Fig. 3.5). Does microglial myelin phagocytosis refine myelin sheath number or targeting? To answer this, we eliminated microglia using three independent approaches and measured myelination by individual oligodendrocytes (Fig. 3.6a, b). First, we used an antisense morpholino oligonucleotide (MO) designed to block translation of mRNA encoding interferon regulatory factor-8 (Irf8), which is required for macrophage specification and microglia development (Shiau et al., 2015). Second, we targeted Csf1r function, which is required for macrophage invasion of the CNS and microglial distribution (Herbomel et al., 2001), by using a Csf1r inhibitor that has been used previously in larval zebrafish (Green et al., 2019). Because both of these methods eliminate microglia early in development, and microglia support OPC development (Giera et al., 2018; Wlodarczyk et al., 2017), we took a third strategy to eliminate microglia specifically after myelination onset. We generated a transgenic line, *Tg(mpeg1.1:NTR-IRES-eGFP-CAAX)*, in which microglia

express an enhanced variant of *E.coli* nitroreductase (*NfsB*$^{T41Q/N71S/F124T}$) (NTR) to induce *mpeg1.1*$^{+}$ cell death upon treating larva with the actuator, metronidazole. We quantified microglial ablation by each of these three strategies by adapting a neutral red assay previously used for quantifying microglia (Herbomel et al., 2001) and determined that they eliminate ~95, ~45, and ~75% of microglia, respectively (Fig. 3.6c, d).

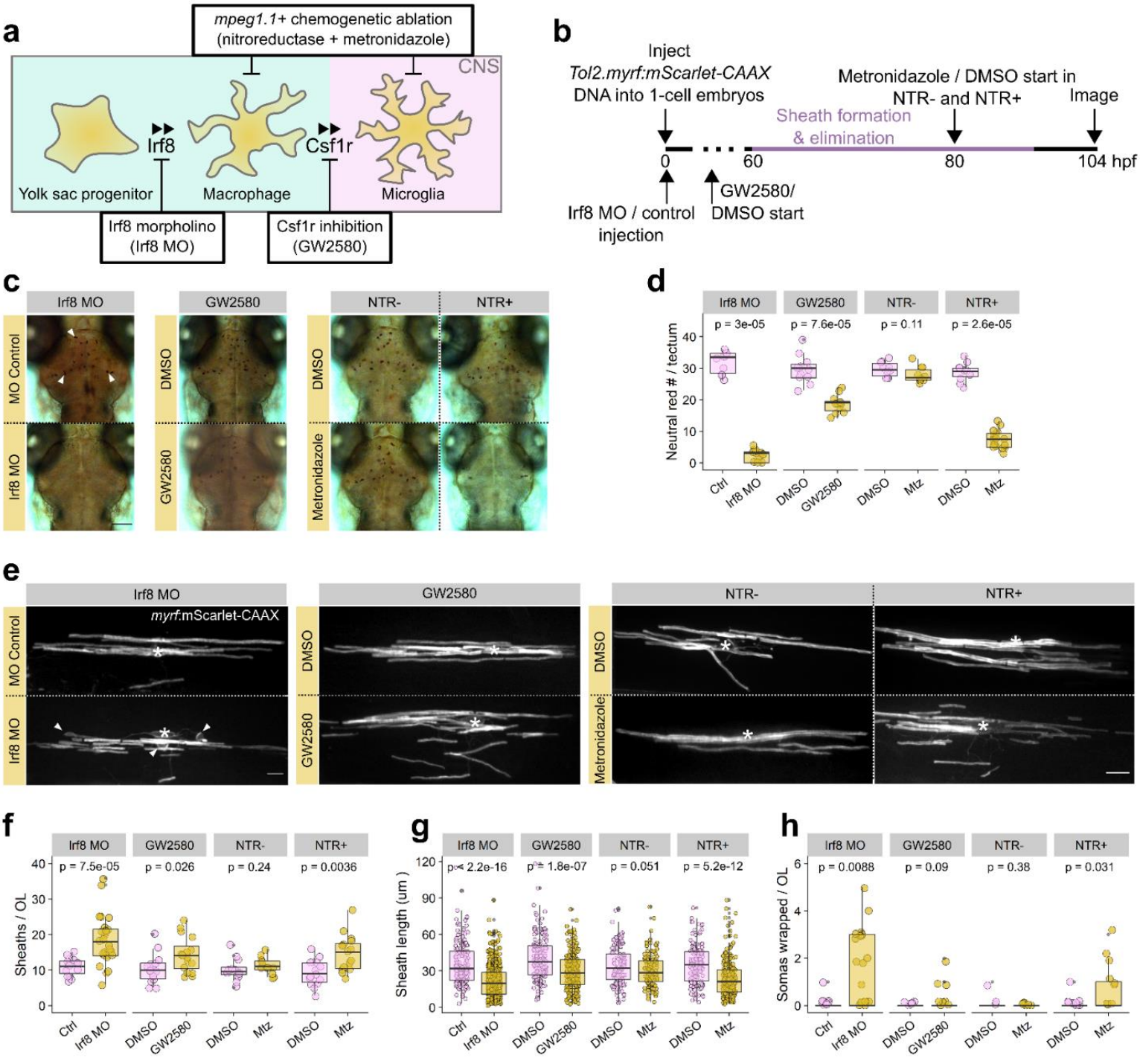
a
mpeg1.1+ chemogenetic ablation
(nitroreductase + metronidazole)
CNS
Irf8
Csf1r
Yolk sac progenitor
Macrophage
Microglia
Irf8 morpholino
(Irf8 MO)
Csf1r inhibition
(GW2580)
b
Inject
Tol2.myrf:mScarlet-CAAX
DNA into 1-cell embryos
Metronidazole / DMSO start in
NTR- and NTR+
Image
Sheath formation
& elimination
0
60
80
104 hpf
Irf8 MO / control
injection
GW2580/
DMSO start
c
Irf8 MO
GW2580
NTR-
NTR+
MO Control
Irf8 MO
DMSO
GW2580
DMSO
Metronidazole
d
Irf8 MO
GW2580
NTR-
NTR+
p = 3e-05
p = 7.6e-05
p = 0.11
p = 2.6e-05
Neutral red # / tectum
Ctrl
Irf8 MO
DMSO
GW2580
DMSO
Mtz
DMSO
Mtz
e
Irf8 MO
GW2580
NTR-
NTR+
myrf:mScarlet-CAAX
MO Control
Irf8 MO
DMSO
GW2580
DMSO
Metronidazole
f
Irf8 MO
GW2580
NTR-
NTR+
p = 7.5e-05
p = 0.026
p = 0.24
p = 0.0036
Sheaths / OL
g
Irf8 MO
GW2580
NTR-
NTR+
p = 2.2e-16
p = 1.8e-07
p = 0.051
p = 5.2e-12
Sheath length (um)
h
Irf8 MO
GW2580
NTR-
NTR+
p = 0.0088
p = 0.09
p = 0.38
p = 0.031
Somas wrapped / OL

Figure 3.6. Microglial ablation during myelination increases myelin sheath number. (a) Schematic of microglial development and three approaches to ablate microglia. (b) Timeline for labeling individual oligodendrocytes by microinjection at the 1-cell stage and ablating microglia either by coinjection with Irf8 translation blocking morpholino, treatment with Csf1r inhibitor GW2580, or nitroreductase (NTR) treatment with metronidazole (Mtz). (c) Brightfield images of live neutral red-stained larvae in each of three ablation groups. Arrowheads mark examples of neutral red-labeled microglia in optic tectum (small red dots). Scale bar, 100 µm. (d) Quantification of neutral red-labeled microglia in the optic tectum of larvae in each group. Each dot represents the microglia count in one larva. Wilcox rank-sum test, left to right, n=fish/microglia, n=10/319, 15/35, 12/357, 11/206, 10/296, 10/279, 10/288, 16/120. (e) Example spinal cord oligodendrocytes labeled by *myrf*:mScarlet-CAAX in each group. Asterisks mark oligodendrocyte somas and arrowheads indicate myelinated cell bodies. Scale bar, 10 µm. (f, g, h) Quantification of sheath number (f), length (g), and ectopic soma wraps (h, example in (e)) in each group. Each point represents one oligodendrocyte (f), sheath (g), or soma wrap (h). Wilcox rank-sum test, left to right, n=cells/fish/sheaths, n=15/15/163, 27/27/503, 15/15/156, 16/16/229, 12/12/121, 11/11/124, 15/15/139, 15/15/223). Scale bars, 10 µm.

To assess how microglia might refine myelin sheath formation, we examined formation of myelin sheaths by individual oligodendrocytes in larvae in which microglia were eliminated using these approaches. To do so, we microinjected *Tol2.myrf:mScarlet-CAAX* DNA into 1-cell stage embryos to scatter-label oligodendrocytes via Tol2-mediated transgenesis (Fig. 3.6b). At 104 hpf, we imaged oligodendrocytes in each of the eight groups (Fig. 3.6e, Extended Fig. 3.5a). We found that microglial depletion did not change *mbpa*$^{+}$ oligodendrocyte number or distribution (Extended Fig. 3.5b,c). However, tracing myelin sheaths formed by individual oligodendrocytes revealed that upon microglial depletion (Irf8 MO, GW2580, NTR+/metronidazole) oligodendrocytes had more sheaths than oligodendrocytes in corresponding control groups (Fig. 3.6e, 6f) and these sheaths were also shorter in length (Fig. 3.6g). Furthermore, oligodendrocytes in the two severe depletion groups (Irf8 MO, NTR+/metronidazole) formed a number of spherical ensheathments, a phenomenon recently described as ectopic ensheathment of neuronal cell bodies

(Almeida et al., 2018) (Fig. 3.6h). These data indicate that microglial sheath pruning corrects myelin targeting and refines myelination by oligodendrocytes.

Discussion

Our work identifies microglia as mediators of myelin refinement by pruning sheaths during development. Previous work established that microglial signaling to adhesion G protein-coupled receptors on oligodendrocyte precursor cells (OPCs) promotes their differentiation, survival, and myelinogenesis (Giera et al., 2018; Wlodarczyk et al., 2017). Recently, single cell RNA-seq analysis of rodent microglia detected *Mbp* mRNA, a myelin transcript that is enriched in myelin sheaths, within white matter microglia (Li et al., 2019). This finding raised the possibility that microglia also engulf myelin under normal physiological conditions. By directly observing microglia-myelin interactions over development, we have discovered that microglia selectively phagocytose myelin sheaths to sculpt myelination.

What regulates the amount of myelin phagocytosed by microglia? We tested the possibility that neuronal activity regulates myelin engulfment and found that microglial myelin phagocytosis is increased upon neuronal silencing and decreased with activation (Fig. 3.5). This is reminiscent of previous studies that showed reducing neuronal activity limits myelin coverage of axons and increasing activity can bias axons for myelination and promote myelin growth (Gibson et al., 2014; Mitew et al., 2018). Our work suggests that myelin plasticity is not confined to the axon-myelin unit but is additionally modifiable by other cell types, including microglia. How might microglia locate developing myelinated tracts? Volume transmission of extra-synaptic ATP from axons to oligodendrocyte lineage cells has been hypothesized to promote the myelination of

white matter tracts (Fields, 2004). In addition to signaling to oligodendrocyte lineage cells, ATP is sufficient to promote microglial translocation (Davalos et al., 2005) and process extension in zebrafish optic tectum (Li et al., 2012). If such volume cues to OPCs also are sensed by microglia, ATP might regulate myelination by steering microglia toward or away from target neurons. Our work in the optic tectum suggested that the activity of one population of neurons, those in the periventricular cell body layer, dictated the microglial phagocytosis of myelin from a different population of axons, those in the tectal commissure (Fig. 3.5). This raises the intriguing possibility that the firing patterns of specific populations of neurons may regulate the myelination of nearby populations by directing microglial target interactions, perhaps contributing to the stereotyped myelination patterns of different axon tracts (Extended Fig. 3.6).

If microglia contribute to myelin plasticity, then brain regions with different densities of microglia, or different microglial states, might exhibit differences in myelin plasticity. During the larval stages we examined, microglia are present in the retina and optic tectum, and sparsely in the spinal cord and forebrain, but are largely absent from other regions (Herbomel et al., 2001). Recent work indicates that the myelination of at least one population of spinal cord neurons, the commissural primary ascending (CoPA) interneurons, is myelinated despite expression of tetanus neurotoxin to suppress activity (Koudelka et al., 2016). CoPA axons project within the DLF and are myelinated earlier than other neuron types (Nelson et al., 2019). One possibility for the insensitivity of CoPA myelination to silenced neuronal activity is that very few dorsal microglia are present at this stage (Fig. 3.1a, b), possibly preventing activity-regulated myelin phagocytosis. Somewhat conversely, treating mice with clinically-relevant doses of

methotrexate, a chemotherapeutic agent that induces persistent inflammatory microglia (CD68+, Iba1+), was sufficient to counteract activity-dependent myelin growth upon optogenetic stimulation (Geraghty et al., 2019; Gibson et al., 2014). Together, these data support a role for microglial availability and state in regulating the dynamic range of activity-dependent myelination available to different brain regions.

Previously, the elimination of nascent myelin wraps was attributed to oligodendrocyte membrane resorption, a process referred to as “retraction” (Baraban et al., 2018; Hines et al., 2015; Hughes et al., 2018; Mensch et al., 2015). Here, we have shown that microglia also participate in myelin refinement by phagocytosing myelin sheaths (Fig. 3.2h-k). How do cell autonomous process retraction and microglial pruning work together to guide myelin patterning during development? We have learned some properties of microglia-myelin interactions that may distinguish roles for each of these mechanisms. A larval zebrafish that has ~160 oligodendrocytes in the spinal cord may elaborate upwards of 2400 nascent wraps prior to elimination. It is thus unlikely that the ~12 spinal cord microglia (Fig. 3.1b) are numerous and motile enough to assess each nascent wrapping attempt. Indeed, extrapolating from our timelapse motility data, the average number of processes per microglia and the number of microglia, we estimate that spinal microglia contact ~1600 sheaths over a 24 h period. However, nearly all microglia we examined contained phagocytosed, Mbp^{+} myelin (Fig. 3.2m, n, Extended Fig. 3.2) and microglial depletion consistently increased sheath number and ectopic wrapping (Fig. 3.6). Additionally, the activity-regulated effects on myelin phagocytosis we describe here are similar to effects reported on sheath retraction, with neuronal silencing both increasing myelin elimination by phagocytosis (Fig. 3.5) and nascent

sheath retraction (Hines et al., 2015). Together, these observations suggest that microglial myelin pruning complements autonomous retraction of newly forming myelin sheaths. Why might multiple mechanisms be necessary to eliminate nascent myelin? During wrapping, synthesized myelin is thought to spread over the axon surface like a liquid droplet (Nawaz et al., 2015), raising the possibility that oligodendrocyte processes that begin synthesizing myelin may not be easily retracted. Additionally, the formation of adhesive contacts between nascent sheaths and axons may preclude facile withdrawal (Elazar et al., 2018; Hughes and Appel, 2019), requiring pruning to disrupt attachment. Consistent with these possibilities, we found that sheaths engulfed by microglia were longer than those that were retracted (Fig. 3.2k). These observations raise the possibility that microglial myelin elimination extends the period of elimination after a developmental window for autonomous retraction has closed, perhaps due to the fluidity or adhesion of myelin.

What molecular cues might regulate phagocytosis? Mice deficient for multiple components of the classical branch of the complement cascade had extra synapses (Stevens et al., 2007) and reduced synapse engulfment by microglia (Schafer et al., 2012), raising the possibility that complement may also tag myelin sheaths for elimination. Consistent with this possibility, the outer lamellar myelin protein myelin oligodendrocyte glycoprotein (MOG) binds the complement initiator C1q directly (Brunner et al., 1989), myelin phagocytosis in vitro was augmented by complement (van der Laan et al., 1996), and multiple sclerosis lesions in postmortem brain tissue were immunoreactive for C3d, a cleavage product of complement component C3 (Barnett et al., 2009). However, just as recent work indicates that microglial synapse engulfment is

complement-independent in some brain regions (Gunner et al., 2019), studies of myelin phagocytosis have produced a number of complement-independent candidates that also appear to regulate myelin phagocytosis, including Fc-receptor gamma and scavenger receptor-AI/II (Rotshenker et al., 2008). Identifying the cues responsible for directing myelin removal, and the possibility that such a code may also be used by synapses, will likely inform strategies for treating myelin phagocytosis in disease.

Microglia are increasingly recognized for their roles in normal CNS development. Within the last two decades, we have learned that microglia dynamically survey their environment in the absence of injury (Nimmerjahn et al., 2005), in a manner that was recently unveiled to be directed by local noradrenergic tone (Liu et al., 2019b; Stowell et al., 2019). Microglial interactions with both neurons and glia support development of the nervous system by eliminating structures and secreting trophic factors (Brown and Neher, 2014; Schafer et al., 2012), influenced by and potentially contributing to regionalization of the brain (De Biase et al., 2017). Recently, a 10 month-old patient with a lethal mutation in CSF1R, a receptor required for microglial survival, was found to lack microglia and had epilepsy, agenesis of the corpus callosum, and leukodystrophy, underscoring the important and numerous roles that microglia serve in development of the nervous system (Oosterhof et al., 2019). By revealing that microglia tune CNS myelination, our study now raises the possibility that interactions between microglia, neurons, and oligodendrocytes contribute to the development of brain function.

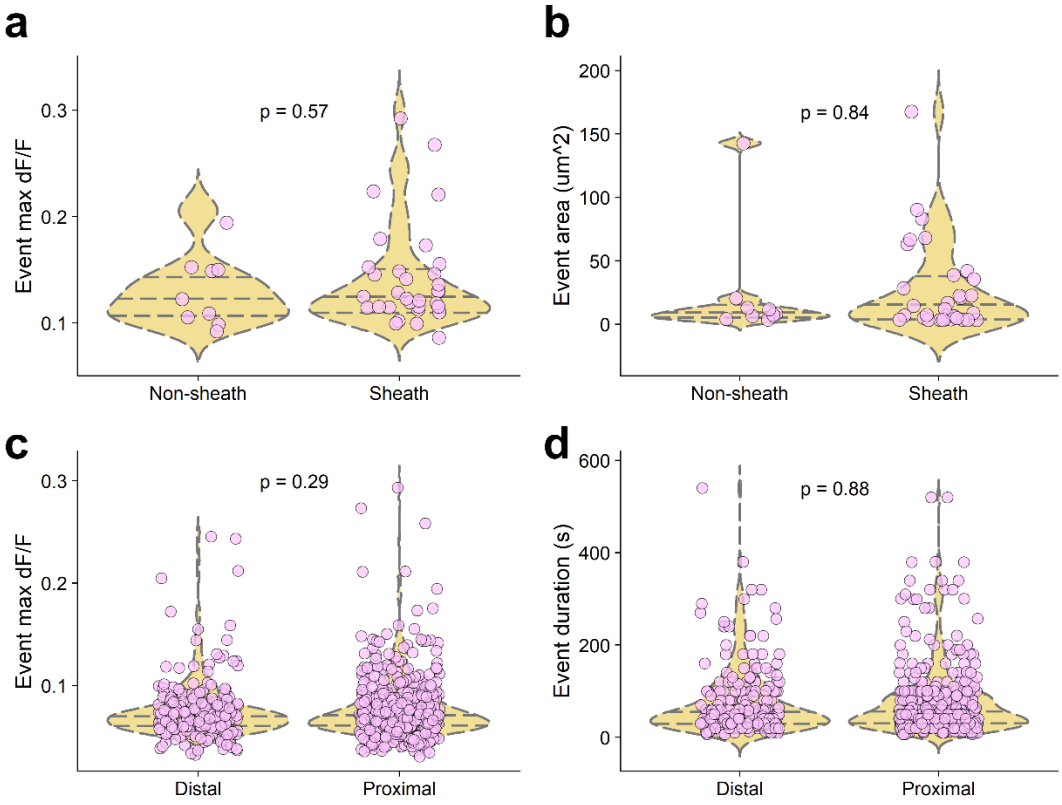

Extended Figure 3.1. Calcium events in microglia contacting myelin sheaths compared to non-sheath contacting processes and comparison with proximal vs distal events. (a, b) Max dF/F (a) and event area (b) for large events (dF/F >0.1, area > 3 μm^2) at non-sheath-contacting and sheath-contacting processes of microglia at 4 dpf in *Tg(mpeg1.1:GCaMP6s-CAAX; sox10:mRFP)* larvae. Wilcox rank-sum test, n=41 events from 9 microglia in 9 fish. (c, d) To distinguish if distance from cell soma is responsible for sheath-contacting vs non-contacting event differences, we split 645 events that occurred in 31 cells (31 fish) into distal and proximal halves and assessed event dF/F (c) and duration (d); both ns by Wilcox rank-sum test.

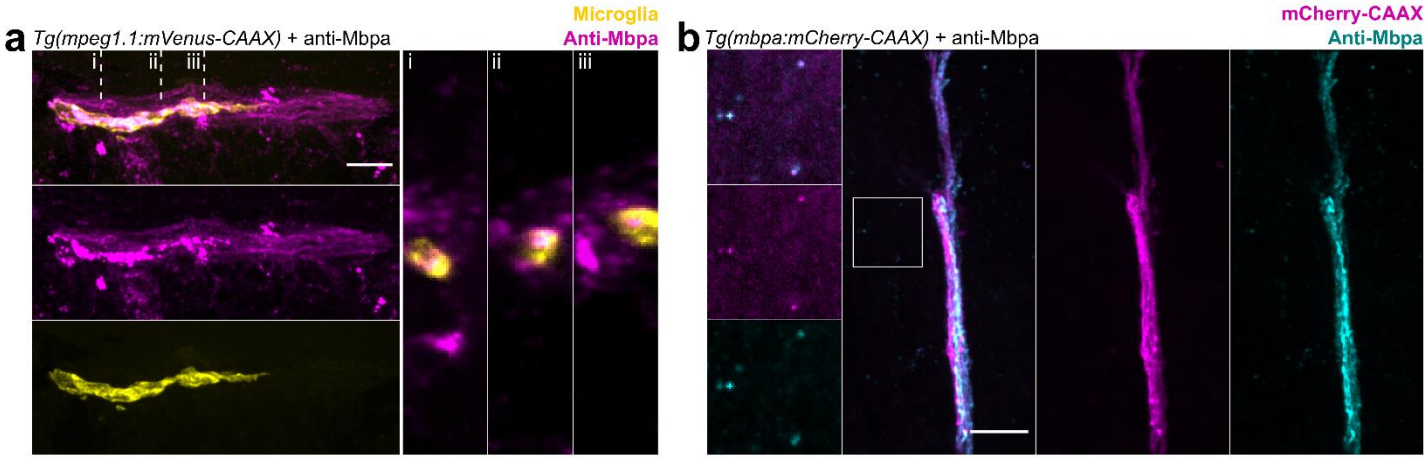

Extended Figure 3.2. Anti-Mbpa detects myelin within microglia. (a) Coronal section of *Tg(mpeg1.1:mVenus-CAAX)* 6 dpf larval spinal cord stained with anti-Mbpa to detect myelin. Note anti-Mbpa inclusions (magenta) within microglia (yellow) in orthogonal views (right panels) taken at the locations marked (i), (ii), (iii). (b) Coronal section of *Tg(mbpa:mCherry-CAAX)* 6 dpf tectal commissure stained with anti-Mbpa (cyan) to detect myelin. Oligodendrocyte membrane (mCherry-CAAX) colocalizes with anti-Mbpa (cyan), both in the intact commissure and as a limited amount of extracellular debris (inset). Scale bars, 10 µm.

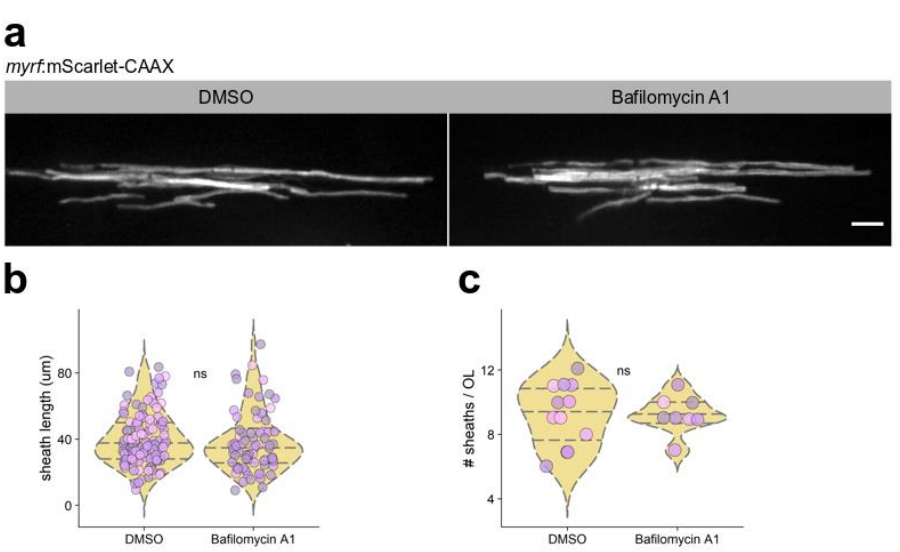

Extended Figure 3.3. Acute treatment of larvae with bafilomycin A1 does not affect oligodendrocyte myelination. (a) Individual oligodendrocytes in transient-transgenic myrf:mScarlet-CAAX expressing larvae treated with bafilomycin A1 or DMSO. Scale bar, 10 µm. (b, c) Quantification of sheath length and number of oligodendrocytes in each treatment group. n=12 larvae/12 fish (DMSO), 8 larvae/8 fish (bafilomycin A1). Data in (b) and (c) analyzed by Wilcox rank-sum test.

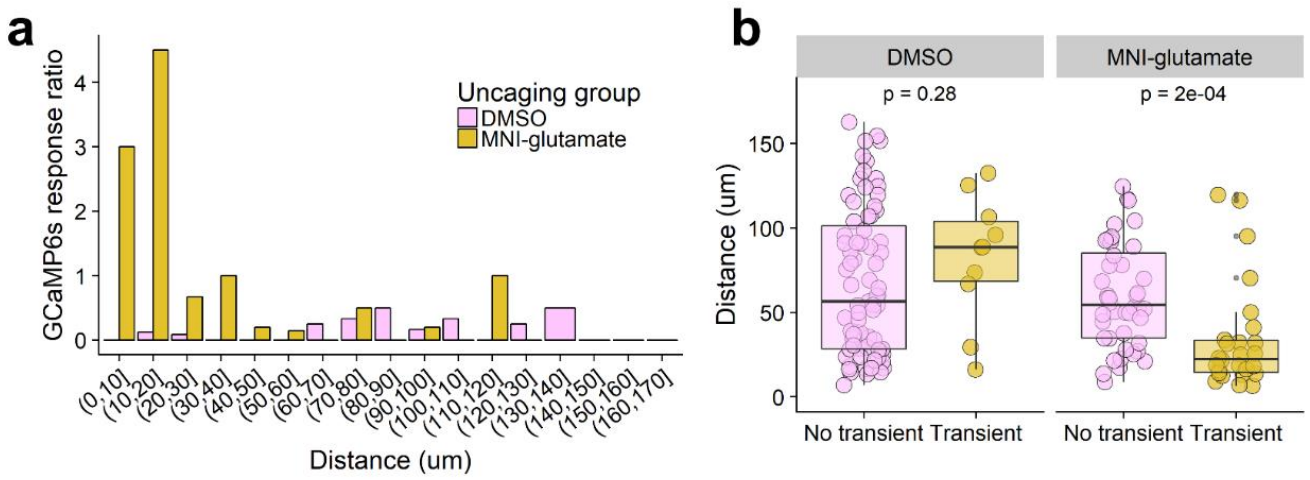

Extended Figure 3.4. Glutamate uncaging evokes Ca^{2+} transients most reliably in neurons located < 20 µm away from the uncaging site. (a) Ratio of Ca^{2+} transient-experiencing neurons to those without transients binned in 10 µm bins from the uncaging site. (b) Distance of neurons with Ca^{2+} transients (defined as dF/F>0.5) or no transients from the uncaging point in larvae treated with DMSO or MNI-glutamate, analyzed by Wilcox rank-sum test (n=fish/neurons, n=5/85 DMSO, 9/70 MNI-glutamate).

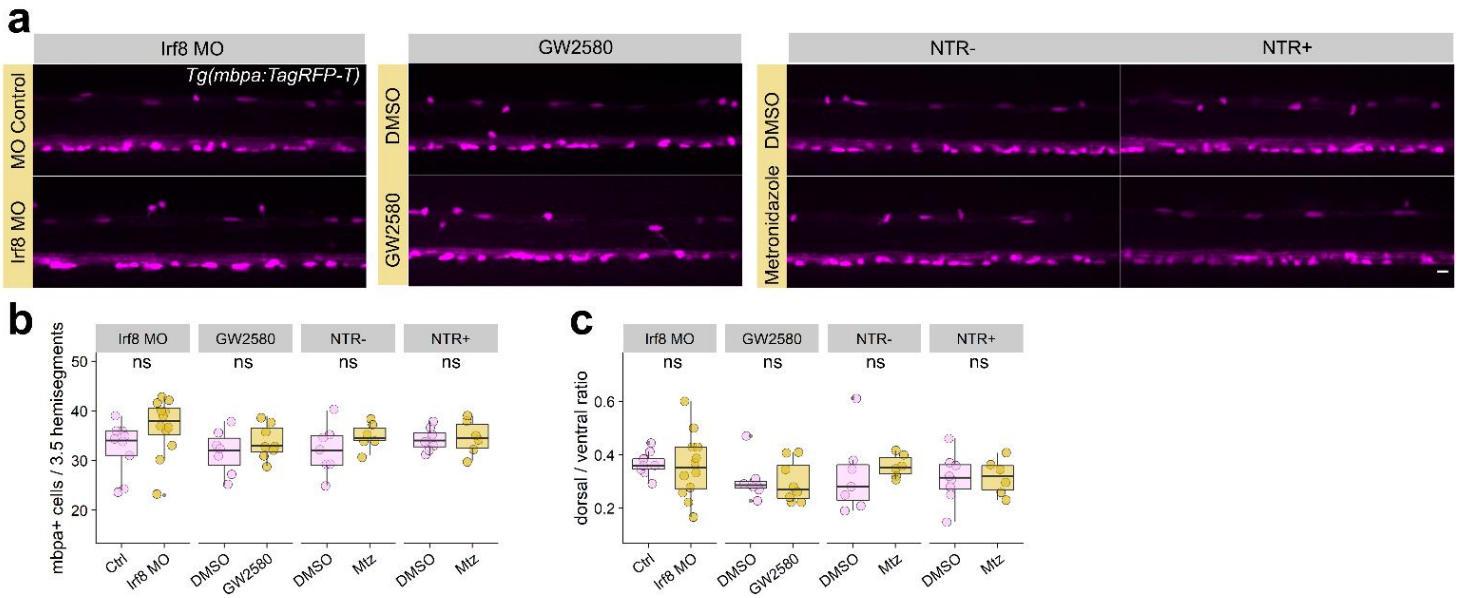

Extended Figure 3.5. Microglia ablation does not change oligodendrocyte number or distribution. (a) Max projection images of hemi-spinal cords in 4 dpf *Tg(mbpa:TagRFP-T)* larvae in each microglia ablation group and controls. Scale bar, 10 µm. (b, c) Total number (b) and dorsal/ventral distribution (c) of oligodendrocytes per 3.5 hemisegments in each ablation group paired with corresponding controls, analyzed by Wilcox rank sum test (n=fish/oligodendrocytes, groups left to right, n=9/293, 12/442, 7/222, 8/271, 7/225, 6/209, 8/274, 6/208).

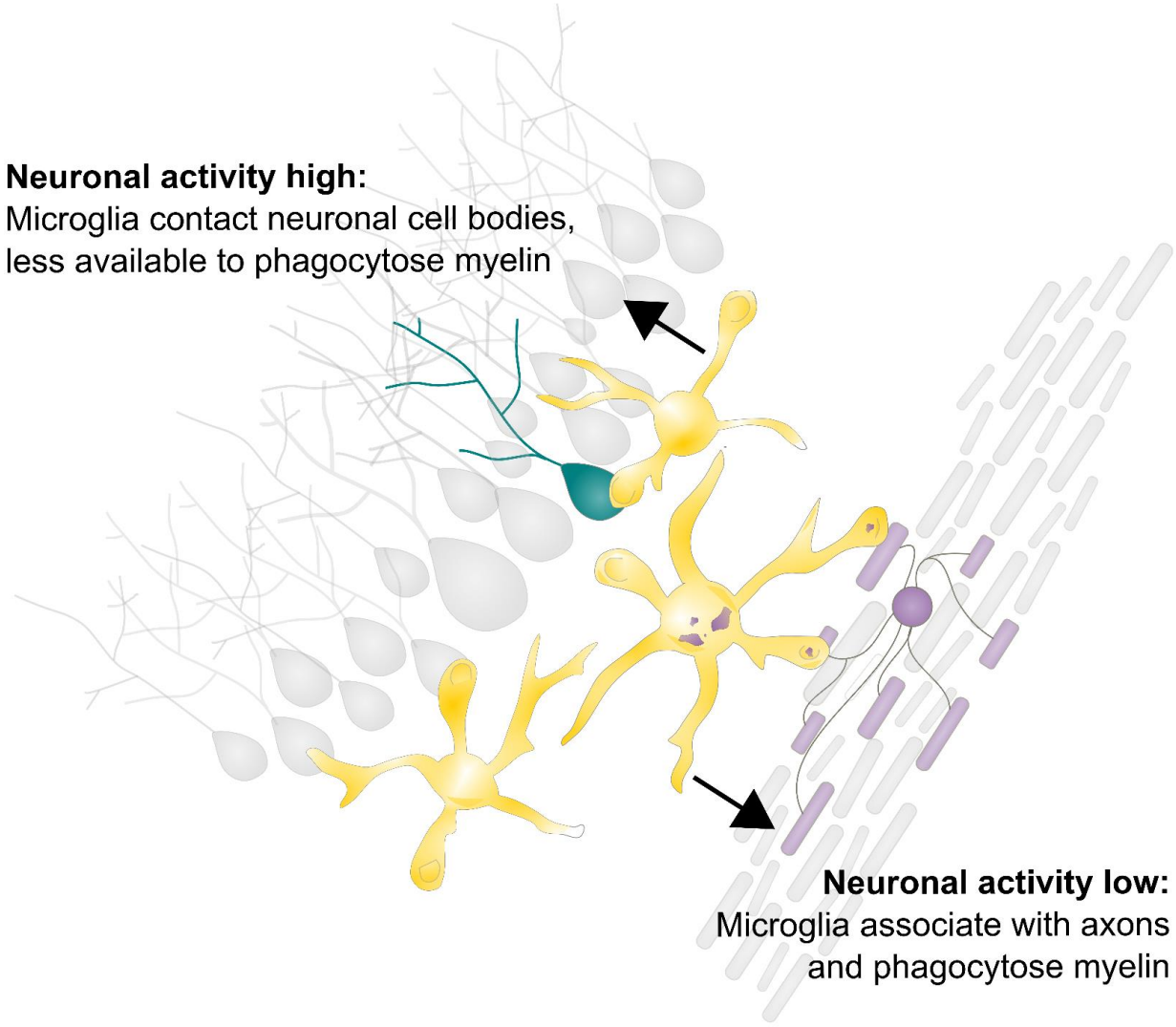

Extended Figure 3.6. Working model of activity-regulated myelin phagocytosis by microglia. Microglia phagocytose myelin to regulate myelin sheath number and targeting. Neuronal activity attracts microglia to contact neuronal cell bodies and reduces the amount of myelin that microglia can phagocytose, whereas reductions in neuronal activity promote myelin phagocytosis from axons.

Methods

1. Zebrafish lines and husbandry

All animal work was approved by the Institutional Animal Care and Use Committee at the University of Colorado School of Medicine. Zebrafish embryos were raised at 28.5°C in embryo medium and staged according to hours or days post fertilization (hpf / dpf) and morphological criteria (Kimmel et al., 1995).

We used the previously established transgenic lines *Tg(sox10:mRFP)*^{vu234}, *Tg(mbpa:tagRFP)*^{co25}, *Tg(vglut2:eGFP)*(Higashijima et al., 2004), and *Tg(mbpa:mCherry-CAAX)*^{co13}.

We also generated and used the new lines *Tg(mpeg1.1:mVenus-CAAX)*^{co56}, *Tg(mpeg1.1:NTR-IRES-eGFP-CAAX)*^{co57}, *Tg(mpeg1.1:mScarlet-CAAX)*^{co62}, and *Tg(mpeg1.1:GCaMP6s-CAAX)*^{co65}. All other reporters were expressed by transient transgenesis to achieve sparse labeling.

2. Plasmid construction and generation of transgenic zebrafish

Tol2 expression plasmids were generated by Multisite Gateway cloning and injected into 1-cell embryos with Tol2 mRNA to generate transient transgenic animals. The following entry clones (Kwan et al., 2007) were used in LR recombination reactions to generate expression plasmids:

p5E-neuroD, *p5E-myrf*, *p5E-mpeg1.1* (Ellett et al., 2011)

pME-NTR (*NfsB*$^{T41Q/N71S/F124T}$) (Mathias et al., 2014), *pME-mTagBFP-CAAX* no stop, *pME-mTagBFP-CAAX* with stop, *pME-mVenus-CAAX*, *pME-mScarlet-CAAX*, *pME-*

GCaMP6s-CAAX (Hughes and Appel, 2019), *pME-GCaMP6s*, *pME-TRPV1* (*Rattus norvegicus*) (Chen et al., 2016)

p3E-polyA, *p3E-2A-dnVamp2* (Hughes and Appel, 2019), *p3E-2A-BoNT/B* (Hughes and Appel, 2019), *p3E-IRES-eGFP-CAAX*, *p3E-mTagBFP*

pDEST-Tol2-pA, *pDEST-Tol2-CG2* (green heart marker), *pDEST-Tol2-CR2* (red heart marker)

To generate *pME-GCaMP6s* and *pME-TRPV1* we PCR amplified attB1-attB2 flanked coding sequences of GCaMP6s and TRPV1 using templates *pGP-CMV-GCaMP6s* (Addgene #40753) and *UAS:TRPV1-TagRFP*(Chen et al., 2016) and the following primers:

attB1-GCaMP6s:

GGGGACAAGTTTGTACAAAAAAGCAGGCTACCATGGGTTCTCATCATCATCA

attB2-GCaMP6s:

GGGGACCACTTTGTACAAGAAAGCTGGGTTCTTCGCTGTCATCATTTGTACA

attB1-TRPV1:

GGGGACAAGTTTGTACAAAAAAGCAGGCTACCATGGAACAACGGGCTAGCTTA

attB2-TRPV1:

GGGGACCACTTTGTACAAGAAAGCTGGGTTTTTCTCCCCTGGGACCATGG

attB1-attB2-flanked amplicons were gel purified, recombined with pDONR-221 to generate pMEs, Sanger sequenced, and then LR-recombined with entry vectors to

generate Tol2 expression plasmids *neuroD:GCaMP6s-pA-CR2* and *neuroD:TRPV1-mTagBFP-pA-CR2.*

3. Drug treatments

- Bafilomycin A1 (Tocris, cat. 1334) was diluted in DMSO and larvae were treated with 1 μM in embryo medium for 1 hour at 28.5º before mounting larvae in agarose for live imaging. An equivalent volume of DMSO (0.1%) was used as vehicle control.
- Metronidazole (Sigma, M1547) was diluted to 10 mM in 0.1% DMSO in embryo medium immediately prior to use for nitroreductase-mediated cell ablation(Mathias et al., 2014). Metronidazole is light sensitive, so all four treatment groups were kept in the incubator in the dark starting at administration (80 hpf).
- Neutral red (Sigma, N7005) was diluted to 2.5 μg/ml in embryo medium and administered to 4 dpf larvae, raised in 0.003% PTU (Sigma, P7629) to prevent pigmentation, for 2.5 hours at 28.5º in the dark(Herbomel et al., 2001; Shiau et al., 2013). Following staining, larvae were washed 2-3 times in fresh media and monitored until nonspecific tissue redness washed out (30 min-1 hour) before mounting larvae dorsal-down in low-melt agarose for widefield, brightfield imaging (10x) of optic tectum microglia.
- GW2580 (ApexBio, A1655) was diluted in DMSO and administered at 100 μm in embryo medium to 48 hpf larvae with drug refresh every 24 h. An equivalent volume of DMSO (0.2%) was used as vehicle control.

- Capsaicin (Sigma, M2028) was diluted in DMSO and administered at 1 µm in embryo medium 2 h prior to imaging. An equivalent volume of DMSO (0.1%) was used as vehicle control.
- MNI-glutamate (Tocris, cat. 1490) was diluted in DMSO to 50 mM and administered at 1 µm in embryo medium 1 h prior to imaging. An equivalent volume of DMSO (0.02%) was used as vehicle control. After 1 h, a small incision was made to larval tails to assist pancuronium bromide NMJ paralysis for timelapse imaging (see Imaging & image analysis). Larvae were kept in the dark as much as possible during treatment, paralysis, and agarose mounting. MNI-glutamate and DMSO were focally uncaged with a 405 nm laser applied to a circular ROI (~2.5 µm radius) in the center of the acquired z-stack (microglia) or in the same plane of imaging (neurons).
- Acridine orange (Sigma, A6014) was diluted in embryo medium to 3 µg/ml and larvae were treated for 30 min, washed twice, and immediately live-imaged(Almeida and Lyons, 2016).

4. Strong water currents / forced swim paradigm

Larvae were placed in 30 mm dishes with or without a stir bar and maintained at 28.5º on a stir plate at 350 rpm for 8 hours a day for two consecutive days, at 3 and 4 dpf (Langebeck-Jensen et al., 2019), followed immediately by live-imaging of myelin inclusions in tectal microglia.

5. Morpholino injections

A published translation-blocking antisense morpholino oligodendrocyte directed against *Irf8* (Li et al., 2011) (GeneTools) (TCAGTCTGCGACCGCCCGAGTTCAT) was diluted to 2 mM in water and used to prepare a 1.5 ng/nl injection solution that also contained *Tol2* mRNA and *Tol2.myrf:mScarlet-CAAX* DNA for oligodendrocyte labeling. 3 nl of injection solution was injected into the yolk of 1-cell stage embryos. Control injection solution was similar except morpholino was replaced with an equivalent volume of water.

6. Immunohistochemistry

6 dpf *Tg(mpeg1.1:mVenus-CAAX; mbpa:mCherry-CAAX)* larvae were fixed at 4 °C overnight in 4% paraformaldehyde/1X PBS. Larvae were washed in PBS and embedded in 1.5% agar/30% sucrose blocks placed in 30% sucrose overnight at 4 °C. Blocks were frozen in 2-methyl butane chilled by immersion in liquid nitrogen. 20 µm sections were cut and collected on microscope slides. Sections were rehydrated with PBS, washed with PBS containing 0.1% Triton X-100 (PBSTx), and then blocked with 2% goat serum/2% bovine serum albumin in PBSTx for 1 h at room temperature. Rabbit anti-Mbpa antibody(Kucenas et al., 2009) was applied at 1:200 dilution in blocking solution overnight at 4 °C. The sections were washed with PBSTx and then incubated with Alexa Fluor 647 goat anti-rabbit antibody (Jackson ImmunoResearch, 111-606-044) at 1:200 dilution in blocking solution for 2 h at room temperature. Slides were washed again with PBSTx, covered with Vectashield, and coverslipped.

7. Statistics & Reproducibility

All statistics were performed in R (version 3.4.1) with RStudio. Plots were generated using dplyr and ggplot2 packages with cowplot package formatting and all statistical tests were performed using ggpubr functions. We used the two-tailed Wilcox rank-sum test (Mann-Whitney), with no assumption of normality, for all unpaired comparisons. For multiple comparisons, we first assessed global significance using the Kruskal-Wallis test, followed by pairwise Wilcox rank-sum tests with Bonferroni-Holm correction for multiple comparisons. Violin plots and box plots show quantiles (25, 50, 75%) with the central line marking the median. Violin plot colors are not meaningful and only the axes specify the groups. For other plot types, including stacked bar plots and histograms, legends are provided to explain grouping colors. We considered $p<0.05$ the threshold for statistical significance and provided exact p-values; p-values > 0.05 are listed as ns. All representative images that are shown are derived from the data sets analyzed, so the number of *n* biological replicates is the number of times each imaging experiment was performed. Embryos and larvae were randomly allocated to groups. All image analysis was performed blind by using the Fiji plugin Lab-utility-plugins/blind-files. Image acquisition was not blinded but identical anatomical regions were imaged in all larvae.

8. Imaging & image analysis

We performed live-imaging on larvae embedded in 1.2% low-melt agarose containing either 0.02% tricaine or 0.3 mg/ml pancuronium bromide (Sigma, P1918) for immobilization. We acquired images using a Plan Apochromat 20x/0.8 NA (with 1.6x optivar) air, C-Apochromat 40x/1.1 NA water, and 63x/1.2 NA water immersion

objectives on a Zeiss LSM 880 and a Zeiss CellObserver Spinning Disk confocal system equipped with a Photometrics Prime 95B camera. We collected images of neutral red-stained larvae using a Zeiss AxioObserver microscope. After collecting images with Zen (Carl Zeiss), we performed all processing and analysis using Fiji/ImageJ.

8.1 Neuronal calcium imaging

Embryos were injected at the 1-cell stage with *Tol2* mRNA and *Tol2.neuroD:GCaMP6s.* Mosaically-labeled neurons in the hindbrain and midbrain were imaged at ~4 Hz for 50 s following uncaging of MNI-glutamate or DMSO. Identifiable cell bodies were traced in Fiji, along with a background ROI, and mean fluorescence intensity values for each cell at each time point were background-subtracted and divided by the average fluorescence intensity of frames prior to uncaging (baseline) to generate dF/F values. We considered dF/F events over 0.5 as transients, which generally correlated with visible changes in GCaMP6s fluorescence. The distance of each cell centroid to the uncaging point was measured by linear ROI to determine the distance of cells vs likelihood of exhibiting a transient in response to uncaging.

8.2 Microglia calcium imaging

4 dpf larvae were timelapse-imaged using a 20x air objective with 1.6x optivar. Z-stacks of 5 slices with Nyquist (oversampled) spacing were acquired every 5-20 s for 10-20 min. Single-channel images were processed in AQuA (Wang et al., 2019) (Fiji) with parameters listed in Supplementary Table 3.3. For mScarlet-CAAX events, all events were used for analysis. Following determination that most of these membrane “events” fell below dF/F <0.05, we filtered GCaMP6s-CAAX events such that dF/F

>0.05. A smaller filtered dataset, containing only events with dF/F > 0.10 and area > 3 μm^2 was generated in R and used to assess sheath-contacting and non-contacting process transients.

8.3 Sheath engulfment vs retraction analysis

Tg(mpeg1.1:mVenus-CAAX; sox10:mRFP) 4 dpf larvae were timelapse-imaged using a 20x air objective with 1.6x optivar. Z-stacks of uniform (Nyquist) slice number and spacing were acquired in the spinal cord every 10-15 min for 3 hours. At each time point, slices were sum-projected to preserve all signal for intensity-based analysis. Then, frames were registered to correct for drift and corrected for photobleaching using the exponential fit method. To identify myelin changes over time in an automated and unbiased way, the myelin channel was then subjected to a custom written progressive exclusive-or (XOR) processing scheme (Supplementary Table 3.2), in which the Image Calculator performs the XOR operation on consecutive timelapse frames and generates a new series of frames containing only signal present in frame i or frame i+1 but not both, therefore only including signal from the myelin transgene that changes over time in the original timelapse. This progressive XOR series was then sum-projected to generate an output image containing all changes in the myelin transgene signal over time. Merging with the original timelapse, projected into a single frame, marked sheaths that had disappeared (or appeared) during the timelapse acquisition. We then examined the fate of these XOR-identified sheaths in the original timelapse. Sheaths that appeared or disappeared were examined for microglial contact in the original timelapse: those that appeared to be engulfed and were marked by our XOR series were counted as phagocytosed. Non-contacted sheaths that disappeared were counted as retracted.

8.4 Microglia process motility analysis

Larvae were immobilized by immersion in pancuronium bromide (Sigma, P1918) 0.3 mg/ml, aided by a small incision at the tip of the tail, prior to mounting in agarose. Timelapse z-stack frames were acquired every 2.5 min for 1 hour. Movies were max-projected at every time frame, registered to correct for drift, and cells were manually tracked from frame to frame for process maintenance, withdrawal, or formation of new processes. Events occurring at distalmost (usually primary or secondary) processes were tracked. In response to glutamate uncaging, two values were calculated: total process movements, and net directed process movements. Total process movements = uncaging new + uncaging lost + opposite new + opposite lost, and net directed process movements = (uncaging new + opposite lost) – (uncaging lost + opposite new), where the uncaging side is the side of the microglia facing (orthogonal to) the uncaging site, and the opposite side is the side of the microglia facing away.

8.5 Myelin inclusion measurements

Z-stack images of microglia, acquired with uniform optical sectioning and number of slices, were sum-projected in Fiji. The microglia border was manually traced, and the background was cleared. The channels were split and the myelin channel was subjected to morphological segmentation using the Fiji plugin MorphoLibJ (Legland et al., 2016). Specific parameters were: object image, gradient type=morphological, gradient radius=1px, watershed segmentation tolerance=60 (spinal cord) or 20 (optic tectum). Watershed segmentation values were predetermined on sample images of microglia from each of the two regions. Following segmentation, the wand tool was used

to trace watershed ROIs and ROI and total cell area values were saved for downstream analysis in R.

8.6 Sheath length measurements

Z-stack images of oligodendrocytes, acquired with uniform optical sectioning, were traced in 3D using the Fiji plugin Simple Neurite Tracer (Longair et al., 2011). The number of paths (sheaths) belonging to a single oligodendrocyte is the number of sheaths per cell and the path length in 3D is the sheath length. Default parameters were used, except cursor snapping = 2 XY pixels. Path lengths were exported to R for analysis.

Acknowledgments

We thank M Preston (InVivo Biosystems, Eugene, OR) and J Hines (Winona State University, Winona, MN) for providing *pME-NTR* and *p5E-myrf* plasmids, respectively, and W Macklin, E Hughes, and S Bromley-Coolidge for comments on the manuscript.

Funding

This work was supported by US National Institutes of Health (NIH) grant R01 NS095679 and a gift from the Gates Frontiers Fund to B.A. and a National Science Foundation Graduate Research Fellowship (DGE-1553798) to A.N.H. The University of Colorado Anschutz Medical Campus Zebrafish Core Facility was supported by NIH grant P30 NS048154.

Author contributions

A.N.H. and B.A. conceptualized the project. A.N.H. designed and performed the experiments and collected and analyzed the data. A.N.H. wrote and B.A. edited the manuscript.

CHAPTER IV

MYELIN SHEATH LENGTH REGULATES TIMING IN THE MAUTHNER NEURON – MOTOR NEURON ESCAPE CIRCUIT

Abstract

Rapid escape responses are important for animal survival. Escaping predation, for example, requires that an animal can detect a threat and immediately reorient. In zebrafish, a single action potential in the Mauthner neuron elicits a whole-body C-bend that allows the fish to rapidly turn around to escape. Two bilateral Mauthner neurons innervate motor neurons along the body axis and the Mauthner axons are myelinated. How does myelin patterning on the Mauthner axons regulate the kinematics of the escape response? To assess the role of Mauthner axon myelination in the escape response, I used the NEURON simulation environment to create a model of a Mauthner neuron that innervates motor neurons, based on documented measurements of these structures in larval zebrafish. I elicited a single action potential in the Mauthner soma and recorded postsynaptic action potentials in output motor neurons along the body axis, while varying myelin sheath length. I found that shorter, but more numerous myelin sheaths on the Mauthner axon increased the latency between motor neuron action potentials, predictive of a slower and less angular escape trajectory. This result raises the possibility that myelin patterning regulates the shape and timing of the zebrafish escape response.

Introduction

The escape response in teleost fish is driven by Mauthner neurons, a pair of large reticulospinal neurons with cell bodies positioned in rhombomere 4 of the hindbrain (Eaton et al., 1977; Hecker et al., 2020). A stimulus on one side of the animal elicits axial muscle contractility on the contralateral side of the fish, such that the fish's head turns away from the stimulus and toward the ideal direction of escape. The Mauthner cells receive multiple types of sensory input, allowing for the detection and response to threatening stimuli via acoustic, visual, and other input modalities (Eaton et al., 1977; Hale et al., 2016; Thompson et al., 2016; Zottoli et al., 1987).

Whereas much work has investigated how inputs to the Mauthner cell regulate the escape response, considerably less attention has focused on how the Mauthner axon coordinates the escape trajectory. To execute the C-bend shape of the escape response, motor neurons that line the body axis receive synaptic input from the Mauthner axon to drive axial muscle contraction on the side of the body opposite the stimuli. This fast and coordinated contraction has the effect of shortening one side of the fish (to create the characteristic C-shape), turning the head away from the stimulus such that resumption of swimming propels the larva away from the stimulus. Conduction along the axon is essential for this response (Hecker et al., 2020) but the factors that regulate conduction velocity, axon diameter and myelination, have not been investigated directly. The Mauthner axon has the largest diameter of any spinal cord axon, approximately 5-6 μm in a 4 dpf larval zebrafish (Buckley et al., 2010), and it is also entirely myelinated, the first axon to receive myelination during development

(Almeida et al., 2011). How myelin sheath patterning on the Mauthner axon contributes to the escape response is unknown.

To test the contribution of myelin patterning to the escape response, I used the NEURON simulation environment to generate a model of a Mauthner axon that innervates an array of motor neurons. I elicited single action potentials in the Mauthner axon and recorded membrane voltages in the output motor neurons, while varying the myelin patterning on the Mauthner axon. I found that the myelin patterning typically seen in vivo generates the fastest modeled escape response, manifested here as the shortest latency between the first (most rostral) and last (most caudal) motor neuron firing. Reducing myelin sheath length, even while maintaining total myelin coverage, delayed the onset of the first motor neuron firing but maintained the latency. Reducing both sheath length and total coverage significantly slowed the response.

Results & Discussion

1. Model generation in the NEURON simulation environment

To generate a model of the Mauthner cell and its motor neuron targets, I used the NEURON simulation environment to create eleven neurons, one Mauthner neuron (named soma[0] in the hoc code) and ten motor neurons (soma[1-10]) which receive input along the length of the Mauthner axon (Fig. 4.1). A real Mauthner axon forms synapses onto far more than ten motor neurons, but this model allowed me to assess how motor neurons located varying distances down the axon might receive input at different time scales. The Mauthner axon's parameters were selected from biophysical parameters previously reported, including the axon diameter (Buckley et al., 2010), the axon reversal potential, and the capacitance and conductance of myelin membrane

(Shen et al., 1999). I distinguished nodes of Ranvier from segments of bare axon by equipping nodes with NEURON's default excitable channel mechanisms (sodium and potassium channels, Hodgkin-Huxley channels) in addition to passive leak channels, whereas bare axon segments and myelinated axon segments received only passive leak channels. Motor neurons had 10 μm diameter somas and received synapses from the Mauthner axon at NetCon network connections, in which voltage exceeding threshold in the presynapse (the connected region of the axon) would activate an ExpSyn, exponentially decaying synapse, on the postsynaptic motor neuron.

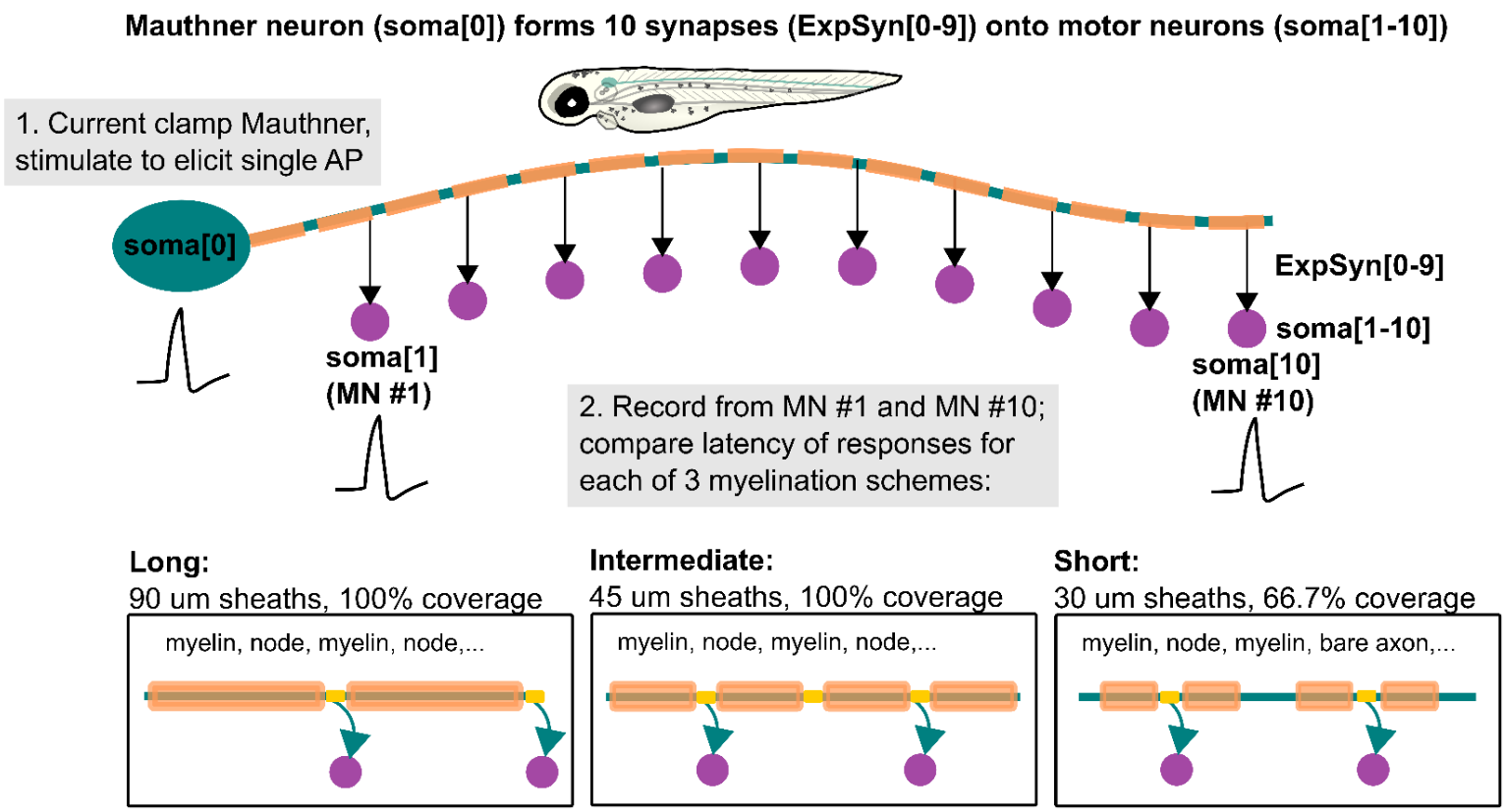

Figure 4.1. Schematic of NEURON model. A model of the Mauthner neuron (teal, position shown in a larval zebrafish) was built in NEURON with a soma, initial segment, a variably myelinated axon, and synapses on to 10 motor neurons. Current clamp stimulation of the Mauthner soma to generate a single action potential is detected by recording postsynaptic potentials in the motor neurons. Three models of myelin patterning are tested: “long” represents the typical myelination of the Mauthner axon in vivo, “intermediate” tests what happens when complete myelination (coverage) is maintained but sheaths are shorter, and “short” reduces both sheath length and coverage.

With this invariant base circuit set up, I next created three different myelination patterns to add to the Mauthner axon. The first, called “long”, refers to the myelin patterning that is typical *in vivo*: myelin sheaths on the Mauthner axon are long (90 µm) compared to typical myelin sheaths on other axons (~30 µm) and the Mauthner axon is myelinated along its entire length (Fig. 4.2a, a’), with only interruptions for nodes of Ranvier (2 µm length). The second paradigm, “intermediate,” tests what would happen if myelin sheaths were half the length (45 µm) but doubly numerous and still myelinated the entire axon. This “intermediate” phenotype is reminiscent of how several oligodendrocyte manipulations have produced more numerous, but shorter, myelin sheaths (Hughes and Appel, 2019). The third paradigm, “short” has significantly shorter sheaths (30 µm) and incomplete axon coverage (66.7% myelinated), which may be reflective of early Mauthner axon myelination prior to sheath elongation and maturation.

2. Myelin sheath length regulates escape response onset and latency

To stimulate the Mauthner neuron, I current clamped the Mauthner soma and delivered 1 nA of current for 5 ms, 10 ms after the onset of recording from the motor neurons. I recorded action potentials from the first and last motor neurons (#1 and #10) and found that they occurred near-coincidently in the model for long- and intermediate-length sheaths, but were visibly offset with short sheaths (Fig. 4.2.b), suggesting a significant delay before the last motor neuron fires. Detecting the time at which the action potential peak voltage occurred for the first and last motor neuron revealed that short sheaths increased this latency 9-fold relative to the other conditions (Fig. 4.2.c, c’), from 0.05 ms to 0.45 ms. In a larval fish, such a latency between the first and last motor neuron firing may cause rostral muscles to contract and extend before caudal muscles

contract, potentially widening the angle of the C-bend. Additionally, whereas latency was unchanged between the long and intermediate sheath conditions, the first motor neuron in the intermediate condition fired 0.1 ms later than the first motor neuron in the long condition (Figure 4.2.c), raising the possibility that this shift in myelin patterning would manifest in a slightly delayed, albeit kinematically normal escape response.

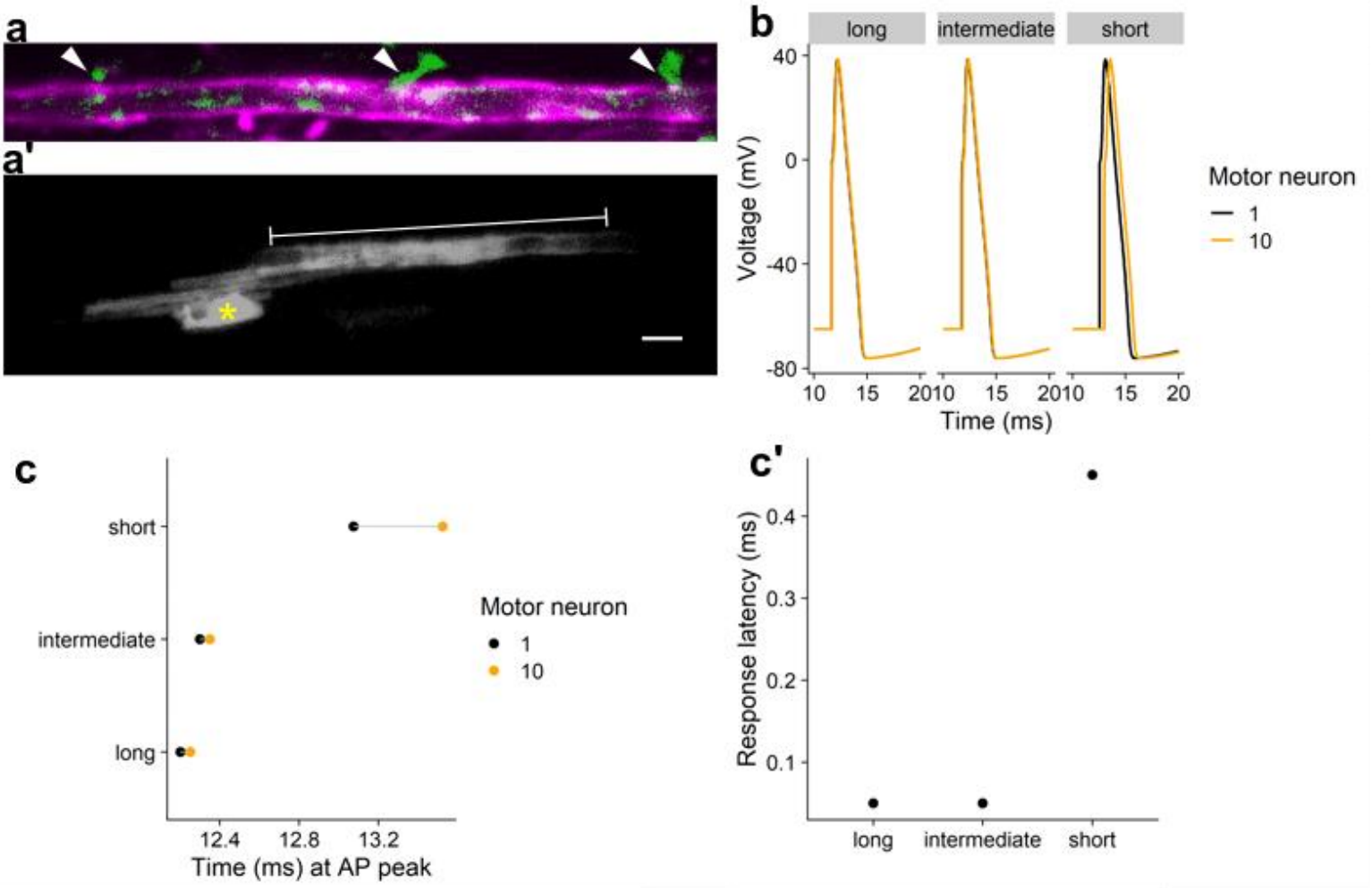

Figure 4.2. Mauthner axon myelin sheath length changes the latency of motor neuron responses. (a) Myelinated Mauthner neuron (magenta) expressing synaptophysin-pHluorin (green) in a 4 dpf zebrafish larva, *Tg(sox10:mRFP)* with mosaic *neuroD*:sypHy. Arrowheads indicate putative presynaptic termini (motor neurons not labeled). (a') A single oligodendrocyte in the ventral spinal cord labeled by mosaic expression of *myrf*:TagBFP-CAAX. Bracket indicates a 90 µm sheath formed on the Mauthner axon (identified by its large diameter) and asterisk labels the oligodendrocyte cell body. Scale bar, 10 µm. (b) Representative action potentials from the first (black) and last (orange) motor neurons innervated by the Mauthner axon in each of the three myelin conditions (long, intermediate, short) in the NEURON model. Current clamp stimulation was delivered to the Mauthner soma 10 ms after recording started, so time windows start at 10 ms. (c) Time at action potential peaks in the first and last motor neurons in each of the three myelin conditions; grey line segments indicate the latencies between peaks and are plotted in (c').

Modeling myelination on the Mauthner cell predicts that myelin sheath patterning regulates the speed and shape of the escape response, but this awaits experimental testing *in vivo*. In the future, I may adapt this model to vary myelin thickness to determine the relative contributions of myelin length and thickness to conduction velocity or synaptic output to the motor neurons. Furthermore, myelin in this model is currently based on measurements of myelin capacitance and conductance, but I could adapt recent and more biologically accurate models of myelin that account for number of myelin wraps (Zbili and Debanne, 2020) and the conductivity of the sub-myelin space (Cohen et al., 2020). Another improvement may be to incorporate other cell types to better model the circuit, such as including both bilateral Mauthner cells, interneurons that they interact with, and adapting extracellular mechanisms to model ephaptic coupling at the Mauthner axon cap.

Acknowledgments

I started this project during a course, NRSC 7612, Nervous System Modeling with NEURON. I am grateful to Alon Poleg-Polsky and Jesse Gilmer for their input and suggestions.

CHAPTER V

FUTURE DIRECTIONS

Thinking beyond myelin sheath parallelism to neuronal synapses

During my graduate training, I had the opportunity to explore the biology of both myelin sheath formation and elimination. These projects were connected by a joint appreciation that axon-myelin interactions at the myelin sheath are alike, in many ways, to the interactions between axons and dendrites at synapses. While this parallel lens can generate hypotheses, oligodendrocytes are not neurons. That is not to call them lesser: oligodendrocytes serve roles in the CNS that neurons are simply not equipped to fulfill. Several potential functions will be missed if oligodendrocytes continue to be viewed in the shadow of Cajal's first element. In this chapter, it is my goal to highlight some outstanding questions about myelin sheath formation and elimination in which a broader view, beyond parallelism to neurons, may be helpful.

Synaptic proteins in oligodendrocytes may regulate trophic support of axons

In Chapter II, I described a dominant-negative candidate screen to identify transsynaptic adhesion proteins that regulate myelination. I identified a few proteins that regulate myelin sheath length and number, and a few that do not. Does this indicate that those adhesion proteins that do not change sheath length or number are dispensable for myelination or oligodendrocyte function? A similar argument has been previously used to assert that NMDA receptors are dispensable for myelination: De Biase et al. (2011) found no overt myelination changes upon oligodendrocyte lineage-specific deletion of the obligate NMDA receptor subunit NR1 and concluded that this receptor does not play a role in myelination or oligodendrogenesis. It was later found that

signaling downstream of NMDAR activation in oligodendrocytes supports the provision of trophic support to axons (Fünfschilling et al., 2012; Krasnow and Attwell, 2016; Lee et al., 2012; Saab et al., 2016). Using a similar NR1 conditional deletion approach, Saab et al. (2016) found that NMDAR activation on oligodendrocytes increased membrane insertion of the glucose transporter GLUT1 (Krasnow and Attwell, 2016; Saab et al., 2016), which may regulate the transport of glucose to axons (Fünfschilling et al., 2012; Lee et al., 2012; Meyer et al., 2018; Nave, 2010). In addition to trophic support, oligodendrocytes serve other functions uncoupled from morphology, such as K^+ uptake. An oligodendrocyte-specific Kir4.1 knockout mouse reportedly has overtly normal oligodendrocytes and myelin, but animals exhibited ataxia and spontaneous seizures due to poor K^+ uptake by oligodendrocytes (Larson et al., 2018). Together, these data indicate that measuring sheath length and number, or myelin morphology, may be insufficient to test whether synaptic proteins are required for oligodendrocyte function. Instead, future work on synaptic proteins in oligodendrocytes might aim to include readouts of axon health or metabolic transfer. For example, biosensors for lactate, like Laconic, have been used to visualize lactate transport from astrocytes to neurons in mouse cortex (Mächler et al., 2016; Zuend et al., 2020). Is lactate transport from oligodendrocytes to axons impaired upon disruption of transsynaptic adhesion proteins, similar to NR1 deletion in oligodendrocytes? Expressing biosensors to detect energy supply from oligodendrocytes, or to detect health or function of axons, would allow us to learn how axon-myelin communication supports axon physiology in a more comprehensive way than measurement of sheath length and number.

1. Myelin sheath calcium imaging as a readout of axon-myelin signaling

A potential additional readout for detecting axon-myelin signaling, in additional to measuring myelin sheath length and number, is myelin sheath calcium imaging. Intracellular calcium signaling has been implicated in OPC development (reviewed in (Paez and Lyons, 2020)), and as a second-messenger downstream of neurotransmitter receptor activation, sheath calcium appears in principle to be a promising readout for axon-myelin signaling. Two complementary papers released in early 2018 used zebrafish to study calcium transients in myelinating oligodendrocytes during normal development (Baraban et al., 2018; Krasnow et al., 2018). The groups used a transgenic line that expressed GCaMP6s in oligodendrocyte lineage cells and found frequent calcium transients in sheaths: over 50% of sheaths exhibited at least one transient per hour (Baraban et al., 2018) with average dF/F of ~1.0 (100% increase in fluorescence) and duration ~20 s. Krasnow et al. (2018) reported that sheath transients occurred roughly once every 10 min, with similar increase in dF/F and duration as reported by Baraban et al. (2018), and additionally found that TTX or hindbrain stimulation could decrease or increase the rate of transients, respectively (Krasnow et al., 2018). The presence of transients was associated with later sheath growth, but the highest amplitude events preceded sheath shortening or elimination.

I sought to use calcium transients as a readout of axon-myelin signaling upon the disruption of transsynaptic adhesion molecules (Chapter II)[6]. To do so, I expressed cytosolic GCaMP6s, the genetically-encoded calcium indicator used by Baraban and

[6] This is the reason that sheath length and number was measured in cells using GCaMP6s-CAAX and not an ordinary membrane-tethered fluorophore: I had done all of the cloning and most of the static imaging to assess sheath length and number before attempting calcium imaging.

Krasnow et al. (2018) or membrane-tethered GCaMP6s-CAAX, which might better label myelin sheaths, in myelinating (*myrf*+) oligodendrocytes. I performed timelapse imaging at the same developmental stage, using the same acquisition frequency and optical parameters described by the groups, with the same anesthetic from the same supplier, and I obtained a protocol to use the anesthetic from the lab so that I would use it in the same way. A difference that I knowingly did not account for is that the groups used zebrafish that lack melanocytes (*mitfa*-/-) but I otherwise followed all described methods. In a transgenic line in which all myelinating oligodendrocytes express GCaMP6s-CAAX, I never observed any calcium transients in myelin sheaths (0/44 oligodendrocytes) (Fig. 5.1). I did not devote significant time to imaging or analyzing calcium transients in sparsely-labeled OPCs or premyelinating cells, but I did observe premyelinating cells exhibit flickering calcium activity in filopodia.

I do not know the source of the discrepancy between my findings and those reported by Baraban and Krasnow et al. (2018). I later visualized and measured calcium transients in neurons and microglia (Chapter III) and from these experiments I learned more about calcium dynamics typical of both neurons and glia. The duration of the events identified by Baraban and Krasnow et al. (2018) is similar to the duration of events previously detected in OPCs (Wake et al., 2015). However, the change in intensity, dF/F, reported by Baraban and Krasnow et al. (2018), is quite high. The groups both reported that the average event in an oligodendrocyte has dF/F ~1.0, which represents a 100% increase in (doubling of) fluorescence. Using the same calcium indicator (GCaMP6s), I only observed events of this amplitude in neurons (Fig. 3.4i’),

with even visually-obvious events in microglia ranging from 0.05 – 0.20 (5-20% increase) (Fig. 3.2b).

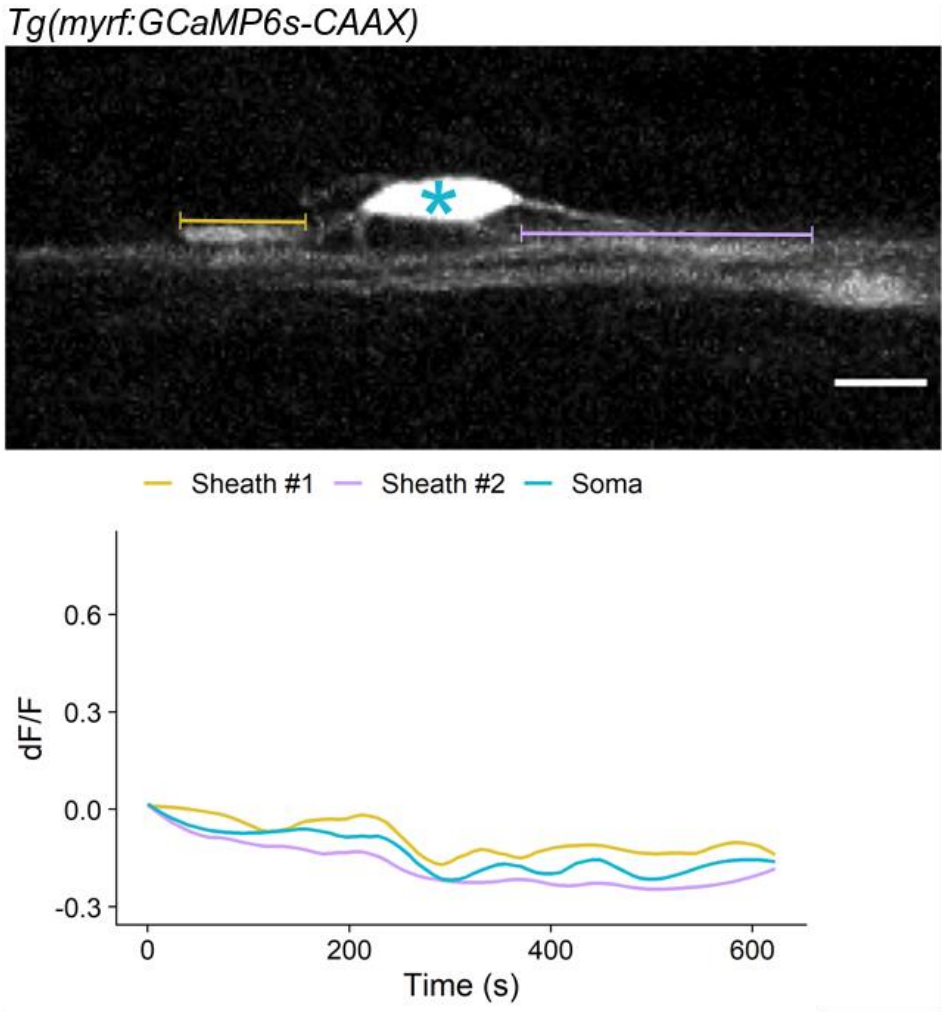

Figure 5.1. Absence of calcium transients in myelin sheaths. (Top) An oligodendrocyte in the dorsal spinal cord of a 4 dpf *Tg(myrf:GCaMP6s-CAAX)* larva, in which all pre- and myelinating oligodendrocytes express the membrane-tethered calcium indicator GCaMP6s-CAAX. Scale bar, 10 µm. (Bottom) dF/F traces over time from the three locations indicated in the image. Acquisition every 2.5 s for 10.5 min, similar to Krasnow et al. (2018). Fluorescence profiles are representative of 44 oligodendrocytes (0/44 oligodendrocytes exhibited sheath or somatic transients).

Later work, in which calcium transients were imaged in myelin sheaths on layer V pyramidal neurons, found transients that were degrees of magnitude different in size and duration from those reported by Krasnow and Baraban et al. (2018). These myelin calcium events lasted ~1.3 s (vs 20 s) and had dF/F <15% (vs 100%) (Battefeld et al., 2019). Whole-cell recording from myelinated neurons further revealed that the sheath calcium transients were independent of neuronal activity (and actually decreased in amplitude following a train of action potentials) and disappeared altogether upon myelin compaction (Battefeld et al., 2019). Blocking the mitochondria permeability pore abolished these calcium events, identifying the source of the myelin calcium transients to be myelin sheath mitochondria. Battefeld et al. (2019) acknowledged the discrepancies between their findings and those of Krasnow and Baraban et al. (2018) and suggested that such discrepancies could arise from different model organisms. However, another recent zebrafish study found that the population of OPCs that differentiate into myelinating oligodendrocytes exhibited the lowest rate of calcium transients (Marisca et al., 2020), consistent with the absence of transients I observed in myelinating oligodendrocytes[7]. At this time, whether calcium transients can be regarded as a functional readout for axon-myelin signaling remains to be determined, and the significance of calcium transients in myelin wrapping is still unclear. In the following section, I provide a preliminary investigation of mitochondria, the source of the fast calcium transients observed by Battefeld et al. (2019) in nascent myelin sheaths.

[7] I did not attempt to detect the fast transients reported by Battefeld et al. (2019), which required imaging at 40 Hz. Across all experiments I imaged at rates between 0.4 – 4.0 Hz, similar to or slightly faster than rates reported by Krasnow and Baraban et al. (2018).

2. Mitochondria as a potential readout of myelin sheath maturation

Mitochondria are abundant in nascent myelin sheaths. Battefeld et al. (2019) found that mitochondria generate the majority of calcium transients in myelin sheaths and suggested that the high rate of transients may ensure adequate mitochondrial ATP production for myelin membrane biosynthesis. Therefore, the presence of mitochondria may be a suitable readout for myelin sheath developmental status, because compacted myelin had fewer mitochondria and calcium transients (Battefeld et al., 2019). To detect mitochondria in myelin sheaths in our system, I cloned zebrafish cytochrome C oxidase subunit 8a (*cox8a*), generated a Cox8a-eGFP fusion protein, and drove expression in myelinating oligodendrocytes. Injecting this plasmid into 1-cell embryos carrying transgenes for oligodendrocytes allowed me to sparsely visualize mitochondria within myelinating cells (Fig. 5.2). Two observations are worth mentioning here. The first is that mitochondria are relatively sparse and easily segmentable and countable within sheaths, which supports their suitability as a readout, although quantification or correlation with developmental time or sheath maturation has yet to be assessed. The second observation is that many oligodendrocyte-derived mitochondria are present outside of oligodendrocytes. Compared to other transient-transgenic labeling experiments using *myrf* regulatory DNA to drive expression, labeling mitochondria in oligodendrocytes consistently leads to several eGFP+ mitochondria present outside the oligodendrocytes or in other cell types, including radial glia and neurons. It is possible that the construct is ectopically expressed in other cell types, but this seldom happens with this driver and extra-oligodendrocyte mitochondria labeling was present in all labeling experiments. With a fair amount of skepticism, I interpret this preliminary data to suggest that oligodendrocyte mitochondria may be released into the extracellular

space or taken up by other cell types. Whether this is biologically significant remains to be tested.

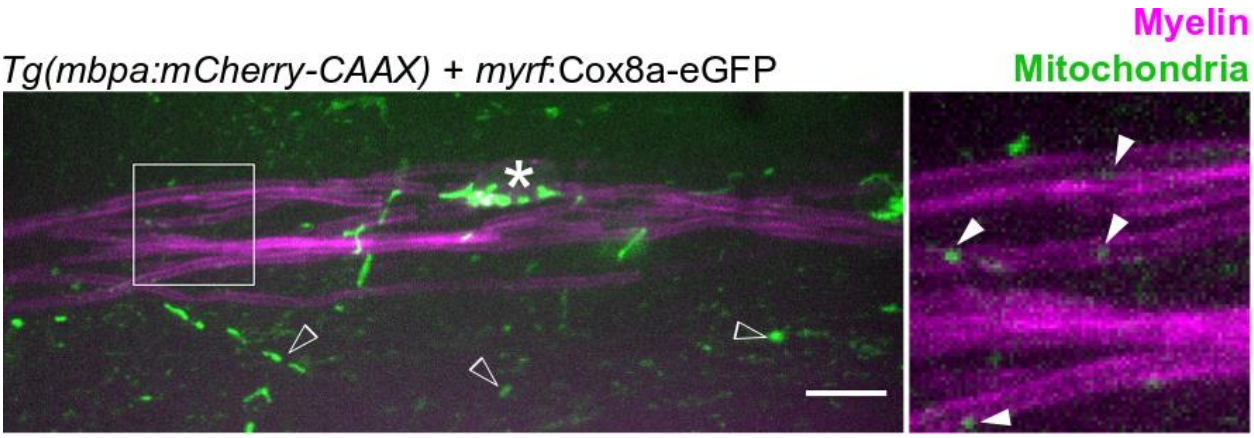

Figure 5.2. Mitochondria in myelin sheaths. Oligodendrocytes mosaically expressing Cox8a-eGFP to label mitochondria in a transgenic larva carrying *Tg(mbpa:mCherry-CAAX)* to label all myelinating oligodendrocytes. Note several mitochondria outside oligodendrocyte (open arrowheads) and enrichment near the soma (asterisk). Box marks inset area with arrowheads indicating mitochondria within myelin sheaths. Scale bar, 10 µm.

How do microglia determine sheaths to eliminate?

Microglia contact many sheaths but do not engulf very many of them. They are responsible for the majority of sheath elimination at 4 dpf (70%), a stage at which most sheaths are stable, and engulf roughly 1 sheath per hour in the spinal cord (Fig. 3.2). Because microglia also eliminate synapses, some possible signaling mechanisms that identify sheaths for elimination may be shared with those cues that localize to engulfment-fated synapses. However, in keeping with the theme of this section, I will also describe potential signaling mechanisms that exist outside of the parallelism to neuronal synapses.

1. Find-me signals recruit microglia

Find-me signaling mechanisms direct microglia to relevant territories, such as regions containing apoptotic cells, whereas eat-me signals flag cells or cellular compartments for direct engulfment. To determine the signals that direct myelin sheaths for elimination, I will discuss both potential find-me signals that entice microglia to myelinated tracts and eat-me signals that may be deposited on individual sheaths for elimination.

ATP is a widely investigated find-me signal for microglia. Helmut Kettenmann's lab first identified that ATP elicits inward currents and calcium transients in microglia via a P2-class ATP receptor (Walz et al., 1993), and ATP's status as a chemoattract was later validated in mouse cortex (Davalos et al., 2005; Nimmerjahn et al., 2005). Other find-me signals, including fractalkine and sphingosine 1-phosphate, can also direct microglial migration. Notably, a receptor for sphingosine 1-phosphate, S1PR2, is the

target of the immunomodulatory multiple sclerosis (MS) drug, fingolimod. In two animal MS models, lysolecithin-induced demyelination and experimental autoimmune encephalitis (EAE), fingolimod decreased macrophage invasion of lesions and promoted oligodendrogenesis and myelination (Seyedsadr et al., 2019). This is consistent with the possibility that sphingosine 1-phosphate signaling in oligodendrocytes also recruits microglia outside of disease contexts (Coelho et al., 2010), but this has not been tested.

To determine if microglia are attracted to ATP in our system, I performed preliminary experiments in which I photouncaged NPE-caged ATP in the ventral spinal cord and performed timelapse imaging of microglia migration. I found that microglia migrate toward the ATP uncaging site within 30 min (Fig. 5.3), consistent with ATP's known role as a chemoattractant. However, microglial competence to respond and migrate toward ATP does not identify ATP as the endogenous chemoattractant that recruits microglia to the myelinated axons in the spinal cord. Identification of the find-me cues will require loss-of-function experiments to eliminate signaling, or potentially loss-of-gradient experiments similar to those performed by Davalos et al. (2005) in which exogenous ATP analogues are applied to swamp the endogenous ATP gradient (Davalos et al., 2005), eliminating its potential as a guidance cue.

2. Do eat-me signals decorate sheaths for removal?

We found that microglia dynamically engage with sheaths in myelinated tracts and phagocytose a subset of nascent sheaths (Chapter III). This may imply selective expression of an eat-me cue, but such a cue could be oligodendrocyte-, axon-, or

microglia-derived, and it could be an eat-me or a don’t-eat-me cue, and may intersect with the expression of find-me cues described in the previous section.

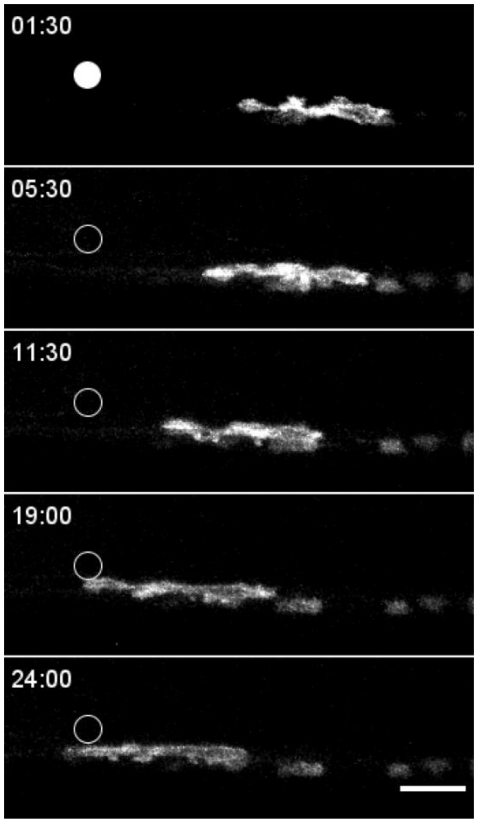

Figure 5.3. ATP uncaging. Ventral spinal cord microglia in a *Tg(mpeg1.1:mVenus-CAAX)* larva migrates toward 405 nm focal uncaging of NPE-caged ATP (immersed in 10 µm) at the circle (radius 2.5 µm). Time is in minutes and scale bar is 10 µm.

What eat-me cues specify myelin sheaths for phagocytosis? One possibility from the synapse elimination field is the classical branch of the complement cascade. Mice deficient for multiple components of the classical complement cascade, including the initiating factor C1q and the downstream component C3 had extra synapses (Stevens et al., 2007) and reduced synapse engulfment by microglia (Schafer et al., 2012), raising the possibility that complement may also tag a subset of myelin sheaths for elimination (Fig. 5.4). Consistent with this possibility, the outer lamellar myelin protein myelin oligodendrocyte glycoprotein (MOG) has been shown to directly bind the complement initiator C1q *in vitro* (Brunner et al., 1989), purified myelin phagocytosis by macrophages was increased with addition of serum complement (van der Laan et al., 1996), and multiple sclerosis lesions in human postmortem brain tissue were found to be immunoreactive for a cleavage product of C3 (Barnett et al., 2009). To test if C1q differentially localizes to myelin sheaths, I generated a fusion protein tagging one of the three chains that comprises C1q, C1qC, because it was the only chain that tolerated C-terminal addition of a FLAG tag without alteration in structure or function (Bally et al., 2013). I then drove expression of C1qC-eGFP in myelinating oligodendrocytes. I found that some sheaths exhibited localized C1qC-eGFP but others did not (Fig. 5.5), potentially indicating that C1q expressed by oligodendrocytes localizes to sheaths fated for removal. However, it is not known if oligodendrocytes express C1q or if in such a model the C1q is instead deposited by microglia, which highly express the genes encoding C1q chains in both mouse and zebrafish (Oosterhof et al., 2017; Zhang et al., 2014). Future experiments, such as enhancer-trapping, might be used to identify the cells that express C1q in the developing spinal cord. Alternatively, antibody labeling of

C1q would allow one to determine whether this tag labels a subset of sheaths without identifying the cellular source.

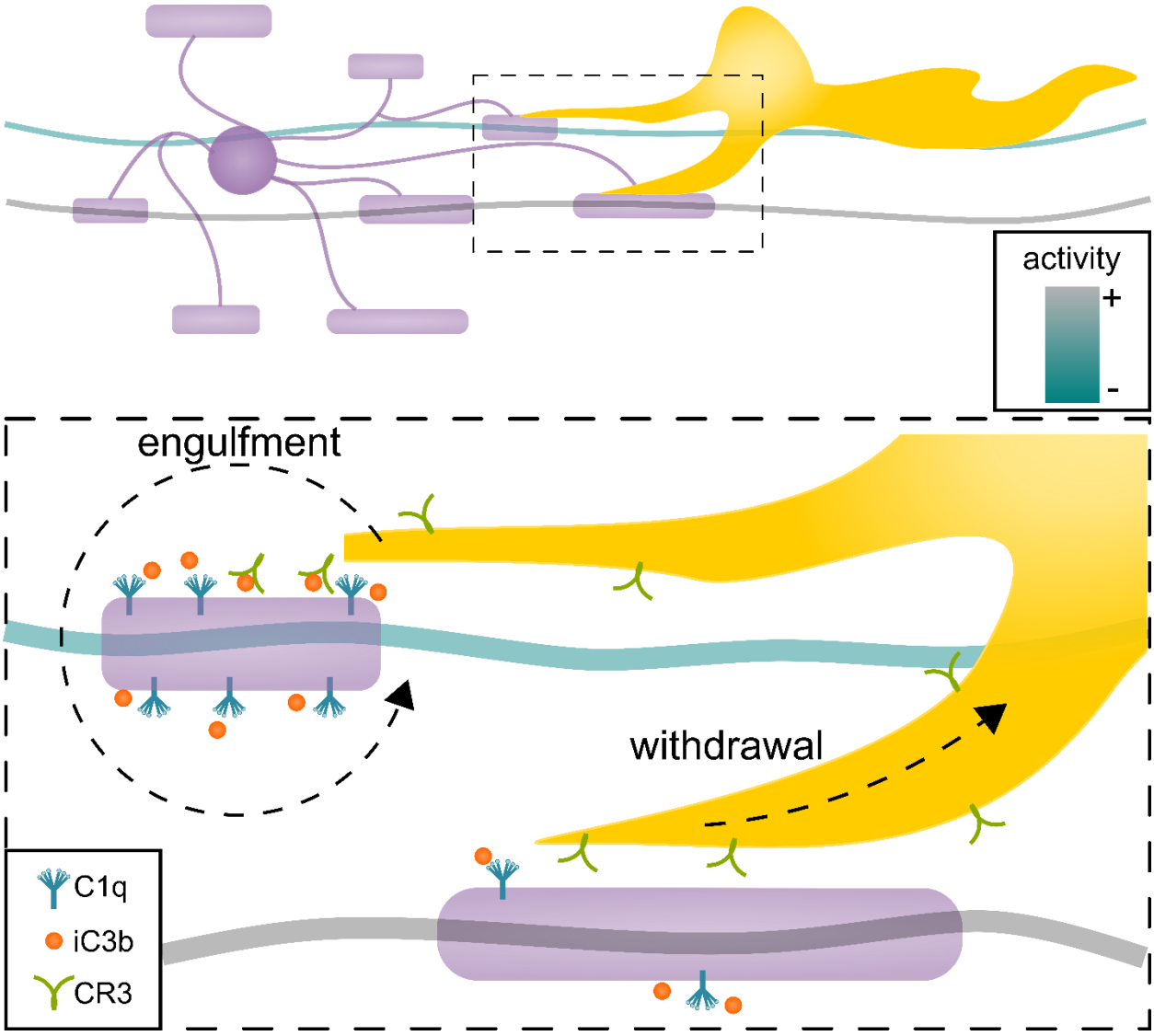

Figure 5.4. Hypothesized model of complement-neuronal activity interaction. The initiating molecule in the classical complement cascade, C1q, is deposited on myelin sheaths on inactive neurons that are destined for clearance by microglia. The downstream cleavage product iC3b is detected by C3 receptors (CR3) located on microglia.

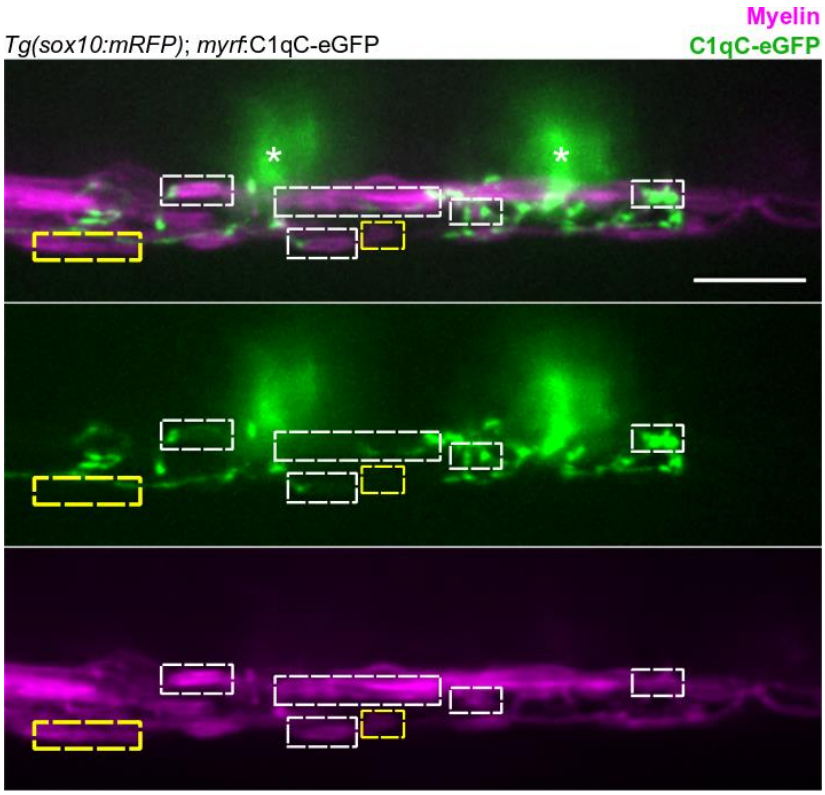

Figure 5.5. C1qC-eGFP localization in oligodendrocytes. Two oligodendrocytes (somas marked with asterisks) in the ventral spinal cord of a *Tg(sox10:mRFP)* larva mosaically expressing C1qC-eGFP. White boxes frame sheaths with localized C1qC-eGFP expression; yellow boxes indicate sheaths that do not. Scale bar, 10 µm.

Just as recent work indicates that microglial synapse engulfment is complement-independent in some brain regions (Gunner et al., 2019), studies of myelin phagocytosis have produced a number of signaling candidates that also appear to regulate myelin phagocytosis, including Fc-receptor gamma and scavenger receptor-AI/II (Rotshenker et al., 2008). Potentially, nascent myelin sheaths containing localized organelles and other material to support early lipid and protein synthesis might also harbor a don't-eat-me cue. In mammalian systems, oligodendrocytes express a don't-eat-me cue, CD47, which interacts with SIRPα located on microglia and macrophages (Gitik et al., 2011). This CD47-SIRPα interaction was recently implicated in downregulating synapse elimination in the developing visual system (Lehrman et al., 2018). Although neither CD47 nor its receptor SIRPα are expressed in zebrafish, other candidate don't-eat-me cues may fulfill a similar role to protect a subset of sheaths from elimination. Similar to microglial engulfment of nascent synapses, the cues that direct phagocytosis may also vary between brain regions (Gunner et al., 2019), depend on identifying receptors in regionally heterogeneous microglia (De Biase et al., 2017; Hammond et al., 2019; Li et al., 2019), or cues displayed by heterogeneous oligodendrocytes (Marisca et al., 2020; Marques et al., 2016, 2018). Identifying the cues that regulate myelin phagocytosis, and the possibility that those cues may overlap or be distinct from cues regulating synapse elimination, has the possibility to teach us a great deal about general principles of brain wiring during development.

REFERENCES

Alabi, A.A., and Tsien, R.W. (2012). Synaptic vesicle pools and dynamics. Cold Spring Harb. Perspect. Biol. *4*, a013680.

Allison, D.W., Chervin, A.S., Gelfand, V.I., and Craig, A.M. (2000). Postsynaptic scaffolds of excitatory and inhibitory synapses in hippocampal neurons: maintenance of core components independent of actin filaments and microtubules. J. Neurosci. *20*, 4545–4554.

Almeida, R., and Lyons, D. (2016). Oligodendrocyte Development in the Absence of Their Target Axons In Vivo. PLoS One *11*, e0164432.

Almeida, R.G., and Lyons, D.A. (2014). On the resemblance of synapse formation and CNS myelination. Neuroscience *276*, 98–108.

Almeida, R.G., Czopka, T., ffrench-Constant, C., and Lyons, D.A. (2011). Individual axons regulate the myelinating potential of single oligodendrocytes in vivo. Development.

Almeida, R.G., Pan, S., Cole, K.L.H., Williamson, J.M., Early, J.J., Czopka, T., Klingseisen, A., Chan, J.R., and Lyons, D.A. (2018). Myelination of Neuronal Cell Bodies when Myelin Supply Exceeds Axonal Demand. Curr. Biol. *28*, 1296-1305.e5.

Anitei, M. (2006). A role for Sec8 in oligodendrocyte morphological differentiation. J. Cell Sci. *119*, 807–818.

Auer, F., Vagionitis, S., and Czopka, T. (2018). Evidence for Myelin Sheath Remodeling in the CNS Revealed by In Vivo Imaging. Curr. Biol. *28*, 549-559.e3.

Bai, Q., Sun, M., Stolz, D.B., and Burton, E.A. (2011). Major isoform of zebrafish P0 is a 23.5 kDa myelin glycoprotein expressed in selected white matter tracts of the central nervous system. J. Comp. Neurol. *519*, 1580–1596.

Bally, I., Ancelet, S., Moriscot, C., Gonnet, F., Mantovani, A., Daniel, R., Schoehn, G., Arlaud, G.J., and Thielens, N.M. (2013). Expression of recombinant human complement C1q allows identification of the C1r/C1s-binding sites. Proc. Natl. Acad. Sci. U. S. A. *110*, 8650–8655.

Baraban, M., Koudelka, S., and Lyons, D.A. (2018). Ca2+ activity signatures of myelin sheath formation and growth in vivo. Nat. Neurosci. *21*, 19–23.

Barnett, M.H., Parratt, J.D.E., Cho, E.S., and Prineas, J.W. (2009). Immunoglobulins and complement in postmortem multiple sclerosis tissue. Ann. Neurol. *65*, 32–46.

Baror, R., Neumann, B., Segel, M., Chalut, K.J., Fancy, S.P.J., Schafer, D.P., and Franklin, R.J.M. (2019). Transforming growth factor-beta renders ageing microglia inhibitory to oligodendrocyte generation by CNS progenitors. Glia *67*, 1374–1384.

Barrera, K., Chu, P., Abramowitz, J., Steger, R., Ramos, R.L., and Brumberg, J.C. (2013). Organization of myelin in the mouse somatosensory barrel cortex and the effects of sensory deprivation. Dev. Neurobiol. *73*, 297–314.

Barres, B.A. (1991). Glial ion channels. Curr. Opin. Neurobiol. *1*, 354–359.

Barres, B.A., and Raff, M.C. (1993). Proliferation of oligodendrocyte precursor cells depends on electrical activity in axons. Nature *361*, 258–260.

Barres, B.A., Chun, L.L.Y.Y., and Corey, D.P. (1988). Ion channel expression by white

matter glia: I. Type 2 astrocytes and oligodendrocytes. Glia *1*, 10–30.

Barres, B.A., Koroshetz, W.J., Swartz, K.J., Chun, L.L.Y., and Corey, D.P. (1990). Ion channel expression by white matter glia: The O-2A glial progenitor cell. Neuron *4*, 507–524.

Battefeld, A., Popovic, M.A., de Vries, S.I., and Kole, M.H.P. (2019). High-Frequency Microdomain Ca2+ Transients and Waves during Early Myelin Internode Remodeling. Cell Rep. *26*, 182-191.e5.

Bennett, M.L., Bennett, F.C., Liddelow, S.A., Ajami, B., Zamanian, J.L., Fernhoff, N.B., Mulinyawe, S.B., Bohlen, C.J., Adil, A., Tucker, A., et al. (2016). New tools for studying microglia in the mouse and human CNS. Proc. Natl. Acad. Sci. *113*, E1738–E1746.

Bergles, D.E., and Richardson, W.D. (2016). Oligodendrocyte Development and Plasticity. Cold Spring Harb. Perspect. Biol. *8*, a020453.

Bergles, D.E., Roberts, J.D., Somogyi, P., and Jahr, C.E. (2000). Glutamatergic synapses on oligodendrocyte precursor cells in the hippocampus. Nature *405*, 187–191.

Bernardos, R.L., and Raymond, P.A. (2006). GFAP transgenic zebrafish. Gene Expr. Patterns *6*, 1007–1013.

De Biase, L.M., Kang, S.H., Baxi, E.G., Fukaya, M., Pucak, M.L., Mishina, M., Calabresi, P.A., and Bergles, D.E. (2011). NMDA receptor signaling in oligodendrocyte progenitors is not required for oligodendrogenesis and myelination. J. Neurosci. *31*, 12650–12662.

De Biase, L.M., Schuebel, K.E., Fusfeld, Z.H., Jair, K., Hawes, I.A., Cimbro, R., Zhang,

H.Y., Liu, Q.R., Shen, H., Xi, Z.X., et al. (2017). Local Cues Establish and Maintain Region-Specific Phenotypes of Basal Ganglia Microglia. Neuron *95*, 341-356.e6.

Biederer, T., Sara, Y., Mozhayeva, M., Atasoy, D., Liu, X., Kavalali, E.T., and Südhof, T.C. (2002). SynCAM, a synaptic adhesion molecule that drives synapse assembly. Science (80-.). *297*, 1525–1531.

Blinzinger, K., and Kreutzberg, G. (1968). Displacement of synaptic terminals from regenerating motoneurons by microglial cells. Zeitschrift Für Zellforsch. Und Mikroskopische Anat. *85*, 145–157.

Bliss, T.V.P., and Lømo, T. (1973). Long-lasting potentiation of synaptic transmission in the dentate area of the anaesthetized rabbit following stimulation of the perforant path. J. Physiol. *232*, 331–356.

Bolte, S., and Cordelières, F.P. (2006). A guided tour into subcellular colocalization analysis in light microscopy. J. Microsc. *224*, 213–232.

Boullerne, A.I. (2016). The history of myelin. Exp. Neurol. *283*, 431–445.

Brasko, C., Hawkins, V., De La Rocha, I.C., and Butt, A.M. (2017). Expression of Kir4.1 and Kir5.1 inwardly rectifying potassium channels in oligodendrocytes, the myelinating cells of the CNS. Brain Struct. Funct. *222*, 41–59.

Brose, N. (2009). Synaptogenic Proteins and Synaptic Organizers: “Many Hands Make Light Work.” Neuron *61*, 650–652.

Brown, G.C., and Neher, J.J. (2014). Microglial phagocytosis of live neurons. Nat. Rev. Neurosci. *15*, 209–216.

Brunner, C., Lassmann, H., Waehneldt, T. V, Matthieu, J.M., and Linington, C. (1989). Differential ultrastructural localization of myelin basic protein, myelin/oligodendroglial glycoprotein, and 2',3'-cyclic nucleotide 3'-phosphodiesterase in the CNS of adult rats. J. Neurochem. *52*, 296–304.

Buckley, C.E., Marguerie, A., Alderton, W.K., and Franklin, R.J.M. (2010). Temporal dynamics of myelination in the zebrafish spinal cord. Glia *58*, NA-NA.

Bunge, M.B., Bunge, R.P., and Ris, H. (1961). Ultrastructural study of remyelination in an experimental lesion in adult cat spinal cord. J. Biophys. Biochem. Cytol. *10*, 67–94.

Bunge, R.P., Bunge, M.B., and Ris, H. (1960). Electron microscopic study of demyelination in an experimentally induced lesion in adult cat spinal cord. J. Biophys. Biochem. Cytol. *7*, 685–696.

Burette, A., Collman, F., Micheva, K.D., Smith, S.J., and Weinberg, R.J. (2015). Knowing a synapse when you see one. Front. Neuroanat. *9*, 100.

Caley, D.W., and Maxwell, D.S. (1968). An electron microscopic study of the neuroglia during postnatal development of the rat cerebrum. J. Comp. Neurol. *133*, 45–69.

Camargo, N., Goudriaan, A., van Deijk, A.L.F., Otte, W.M., Brouwers, J.F., Lodder, H., Gutmann, D.H., Nave, K.A., Dijkhuizen, R.M., Mansvelder, H.D., et al. (2017). Oligodendroglial myelination requires astrocyte-derived lipids. PLoS Biol. *15*.

Chan, C.-F., Kuo, T.-W., Weng, J.-Y., Lin, Y.-C., Chen, T.-Y., Cheng, J.-K., and Lien, C.-C. (2013). Ba^{2+} - and bupivacaine-sensitive background K^{+} conductances mediate rapid EPSP attenuation in oligodendrocyte precursor cells. J. Physiol. *591*, 4843–4858.

Chen, S., Chiu, C.N., McArthur, K.L., Fetcho, J.R., and Prober, D.A. (2016). TRP channel mediated neuronal activation and ablation in freely behaving zebrafish. Nat. Methods *13*, 147–150.

Coelho, R.P., Saini, H.S., and Sato-Bigbee, C. (2010). Sphingosine-1-phosphate and oligodendrocytes: From cell development to the treatment of multiple sclerosis. Prostaglandins Other Lipid Mediat. *91*, 139–144.

Cohen, C.C.H., Popovic, M.A., Klooster, J., Weil, M.T., Möbius, W., Nave, K.A., and Kole, M.H.P. (2020). Saltatory Conduction along Myelinated Axons Involves a Periaxonal Nanocircuit. Cell *180*, 311-322.e15.

Core, R. (2015). Team. R A Lang. Environ. Stat. Comput.

Coull, J.A.M.M., Beggs, S., Boudreau, D., Boivin, D., Tsuda, M., Inoue, K., Gravel, C., Salter, M.W., and De Koninck, Y. (2005). BDNF from microglia causes the shift in neuronal anion gradient underlying neuropathic pain. Nature *438*, 1017–1021.

Cserép, C., Pósfai, B., Lénárt, N., Fekete, R., László, Z.I., Lele, Z., Orsolits, B., Molnár, G., Heindl, S., Schwarcz, A.D., et al. (2020). Microglia monitor and protect neuronal function through specialized somatic purinergic junctions (American Association for the Advancement of Science).

Darcy, K.J., Staras, K., Collinson, L.M., and Goda, Y. (2006). Constitutive sharing of recycling synaptic vesicles between presynaptic boutons. Nat. Neurosci. *9*, 315–321.

Davalos, D., Grutzendler, J., Yang, G., Kim, J. V., Zuo, Y., Jung, S., Littman, D.R., Dustin, M.L., and Gan, W.B. (2005). ATP mediates rapid microglial response to local

brain injury in vivo. Nat. Neurosci. *8*, 752–758.

Demerens, C., Stankoff, B., Logak, M., Angladet, P., Allinquantt, B., Couraud, F., Zalc, B., and Lubetzki, A.C. (1996). Induction of myelination in the central nervous system by electrical activity. Neurobiology *93*, 9887–9892.

Diaz Verdugo, C., Myren-Svelstad, S., Aydin, E., Van Hoeymissen, E., Deneubourg, C., Vanderhaeghe, S., Vancraeynest, J., Pelgrims, R., Cosacak, M.I., Muto, A., et al. (2019). Glia-neuron interactions underlie state transitions to generalized seizures. Nat. Commun. *10*, 1–13.

Djannatian, M., Timmler, S., Arends, M., Luckner, M., Weil, M.-T., Alexopoulos, I., Snaidero, N., Schmid, B., Misgeld, T., Möbius, W., et al. Two adhesive systems cooperatively regulate axon ensheathment and myelin growth in the CNS.

Doyle, S., Hansen, D.B., Vella, J., Bond, P., Harper, G., Zammit, C., Valentino, M., and Fern, R. (2018). Vesicular glutamate release from central axons contributes to myelin damage. Nat. Commun. *9*.

Dunn, K.W., Kamocka, M.M., and McDonald, J.H. (2011). A practical guide to evaluating colocalization in biological microscopy. AJP Cell Physiol. *300*, C723–C742.

Dupouey, P., Jacque, C., Bourre, J.M., Cesselin, F., Privat, A., and Baumann, N. (1979). Immunochemical studies of myelin basic protein in shiverer mouse devoid of major dense line of myelin. Neurosci. Lett. *12*, 113–118.

Dutta, D.J., Woo, D.H., Lee, P.R., Pajevic, S., Bukalo, O., Huffman, W.C., Wake, H., Basser, P.J., SheikhBahaei, S., Lazarevic, V., et al. (2018). Regulation of myelin

structure and conduction velocity by perinodal astrocytes. Proc. Natl. Acad. Sci. U. S. A. *115*, 11832–11837.

Eaton, R.C., Bombardieri, R.A., and Meyer, D.L. (1977). THE MAUTHNER-INITIATED STARTLE RESPONSE IN TELEOST FISH.

Eichhoff, G., Brawek, B., and Garaschuk, O. (2011). Microglial calcium signal acts as a rapid sensor of single neuron damage in vivo. Biochim. Biophys. Acta - Mol. Cell Res. *1813*, 1014–1024.

Elazar, N., Vainshtein, A., Golan, N., Vijayaragavan, B., Schaeren-Wiemers, N., Eshed-Eisenbach, Y., and Peles, E. (2018). Axoglial Adhesion by Cadm4 Regulates CNS Myelination. Neuron.

Elazar, N., Vainshtein, A., Rechav, K., Tsoory, M., Eshed-Eisenbach, Y., and Peles, E. (2019). Coordinated internodal and paranodal adhesion controls accurate myelination by oligodendrocytes. J. Cell Biol. *218*, 2887–2895.

Ellett, F., Pase, L., Hayman, J.W., Andrianopoulos, A., and Lieschke, G.J. (2011). mpeg1 promoter transgenes direct macrophage-lineage expression in zebrafish. Blood *117*, e49-56.

Elmore, M.R.P., Najafi, A.R., Koike, M.A., Dagher, N.N., Spangenberg, E.E., Rice, R.A., Kitazawa, M., Matusow, B., Nguyen, H., West, B.L., et al. (2014). Colony-Stimulating Factor 1 Receptor Signaling Is Necessary for Microglia Viability, Unmasking a Microglia Progenitor Cell in the Adult Brain. Neuron *82*, 380–397.

Emery, B., Agalliu, D., Cahoy, J.D., Watkins, T.A., Dugas, J.C., Mulinyawe, S.B.,

Ibrahim, A., Ligon, K.L., Rowitch, D.H., and Barres, B.A. (2009). Myelin Gene Regulatory Factor Is a Critical Transcriptional Regulator Required for CNS Myelination. Cell *138*, 172–185.

Erblich, B., Zhu, L., Etgen, A.M., Dobrenis, K., and Pollard, J.W. (2011). Absence of Colony Stimulation Factor-1 Receptor Results in Loss of Microglia, Disrupted Brain Development and Olfactory Deficits. PLoS One *6*, e26317.

Espitia Pinzon, N., van Mierlo, H., de Jonge, J.C., Brevé, J.J.P., Bol, J.G.J.M., Drukarch, B., van Dam, A.M., and Baron, W. (2019). Tissue transglutaminase promotes early differentiation of oligodendrocyte progenitor cells. Front. Cell. Neurosci. *13*, 281.

Etxeberria, A., Mangin, J.-M., Aguirre, A., and Gallo, V. (2010). Adult-born SVZ progenitors receive transient synapses during remyelination in corpus callosum. Nat. Neurosci. *13*, 287–289.

Etxeberria, A., Hokanson, K.C., Dao, D.Q., Mayoral, S.R., Mei, F., Redmond, S.A., Ullian, E.M., and Chan, J.R. (2016). Dynamic Modulation of Myelination in Response to Visual Stimuli Alters Optic Nerve Conduction Velocity. J. Neurosci. *36*, 6937–6948.

Eyo, U.B., Peng, J., Swiatkowski, P., Mukherjee, A., Bispo, A., and Wu, L.-J. (2014). Neuronal Hyperactivity Recruits Microglial Processes via Neuronal NMDA Receptors and Microglial P2Y12 Receptors after Status Epilepticus.

Fannon, J., Tarmier, W., and Fulton, D. (2015). Neuronal activity and AMPA-type glutamate receptor activation regulates the morphological development of oligodendrocyte precursor cells. Glia *63*, 1021–1035.

Ferrer, I., Bernet, E., Soriano, E., Del Rio, T., and Fonseca, M. (1990). Naturally occurring cell death in the cerebral cortex of the rat and removal of dead cells by transitory phagocytes. Neuroscience *39*, 451–458.

Fields, R.D. (2004). Volume transmission in activity-dependent regulation of myelinating glia. Neurochem. Int. *45*, 503–509.

Fogel, A.I., Stagi, M., Perez de Arce, K., and Biederer, T. (2011). Lateral assembly of the immunoglobulin protein SynCAM 1 controls its adhesive function and instructs synapse formation. EMBO J. *30*, 4728–4738.

Ford, M.C., Alexandrova, O., Cossell, L., Stange-Marten, A., Sinclair, J., Kopp-Scheinpflug, C., Pecka, M., Attwell, D., and Grothe, B. (2015). Tuning of Ranvier node and internode properties in myelinated axons to adjust action potential timing. Nat. Commun. *6*, 8073.

Fowler, D.K., Peters, J.H., Williams, C., and Washbourne, P. (2017). Redundant Postsynaptic Functions of SynCAMs 1–3 during Synapse Formation. Front. Mol. Neurosci. *10*, 24.

Frade, J.M., and Barde, Y.A. (1998). Microglia-derived nerve growth factor causes cell death in the developing retina. Neuron *20*, 35–41.

Frost, J.L., and Schafer, D.P. (2016). Microglia: Architects of the Developing Nervous System. Trends Cell Biol. *26*, 587–597.

Fulmer, C.G., Vondran, M.W., Stillman, A.A., Huang, Y., Hempstead, B.L., and Dreyfus, C.F. (2014). Astrocyte-derived BDNF supports myelin protein synthesis after cuprizone-

induced demyelination. J. Neurosci. *34*, 8186–8196.

Fünfschilling, U., Supplie, L.M., Mahad, D., Boretius, S., Saab, A.S., Edgar, J., Brinkmann, B.G., Kassmann, C.M., Tzvetanova, I.D., Möbius, W., et al. (2012). Glycolytic oligodendrocytes maintain myelin and long-term axonal integrity. Nature *485*.

Geirsdottir, L., David, E., Keren-Shaul, H., Weiner, A., Bohlen, S.C., Neuber, J., Balic, A., Giladi, A., Sheban, F., Dutertre, C.-A.A., et al. (2019). Cross-Species Single-Cell Analysis Reveals Divergence of the Primate Microglia Program. Cell *179*, 1609-1622.e16.

Geraghty, A.C., Gibson, E.M., Ghanem, R.A., Greene, J.J., Ocampo, A., Goldstein, A.K., Ni, L., Yang, T., Marton, R.M., Paşca, S.P., et al. (2019). Loss of Adaptive Myelination Contributes to Methotrexate Chemotherapy-Related Cognitive Impairment. Neuron 250-265.e8.

Gibson, E.M., Purger, D., Mount, C.W., Goldstein, A.K., Lin, G.L., Wood, L.S., Inema, I., Miller, S.E., Bieri, G., Zuchero, J.B., et al. (2014). Neuronal activity promotes oligodendrogenesis and adaptive myelination in the mammalian brain. Science (80-.). *344*.

Giera, S., Luo, R., Ying, Y., Ackerman, S.D., Jeong, S.J., Stoveken, H.M., Folts, C.J., Welsh, C.A., Tall, G.G., Stevens, B., et al. (2018). Microglial transglutaminase-2 drives myelination and myelin repair via GPR56/ADGRG1 in oligodendrocyte precursor cells. Elife *7*.

Ginhoux, F., Greter, M., Leboeuf, M., Nandi, S., See, P., Gokhan, S., Mehler, M.F., Conway, S.J., Ng, L.G., Stanley, E.R., et al. (2010). Fate mapping analysis reveals that

adult microglia derive from primitive macrophages. Science (80-.). *330*, 841–845.

Gitik, M., Liraz-Zaltsman, S., Oldenborg, P.A., Reichert, F., and Rotshenker, S. (2011). Myelin down-regulates myelin phagocytosis by microglia and macrophages through interactions between CD47 on myelin and SIRPα (signal regulatory protein-α) on phagocytes. J. Neuroinflammation *8*, 1–11.

Gollan, L., Salomon, D., Salzer, J.L., and Peles, E. (2003). Caspr regulates the processing of contactin and inhibits its binding to neurofascin. J. Cell Biol. *163*, 1213–1218.

Gomes, C., Ferreira, R., George, J., Sanches, R., Rodrigues, D.I., Gonçalves, N., and Cunha, R.A. (2013). Activation of microglial cells triggers a release of brain-derived neurotrophic factor (BDNF) inducing their proliferation in an adenosine A2A receptor-dependent manner: A2A receptor blockade prevents BDNF release and proliferation of microglia. J. Neuroinflammation *10*, 780.

Gould, E.A., Busquet, N., Shepherd, D., Dietz, R.M., Herson, P.S., De Souza, F.M.S., Li, A., George, N.M., Restrepo, D., and Macklin, W.B. (2018). Mild myelin disruption elicits early alteration in behavior and proliferation in the subventricular zone. Elife *7*.

Granseth, B., Odermatt, B., Royle, S.J., and Lagnado, L. (2006). Clathrin-Mediated Endocytosis Is the Dominant Mechanism of Vesicle Retrieval at Hippocampal Synapses. Neuron *51*, 773–786.

Grassivaro, F., Menon, R., Acquaviva, M., Ottoboni, L., Ruffini, F., Andrea Bergamaschi, X., Muzio, L., Farina, C., and Gianvito Martino, X. (2020). Convergence between microglia and peripheral macrophages phenotype during development and

neuroinflammation. J. Neurosci. *40*, 784–795.

Green, L.A., Nebiolo, J.C., and Smith, C.J. (2019). Microglia exit the CNS in spinal root avulsion. PLOS Biol. *17*, e3000159.

Gross, G.G., Junge, J.A., Mora, R.J., Kwon, H.-B., Olson, C.A., Takahashi, T.T., Liman, E.R., Ellis-Davies, G.C.R., McGee, A.W., Sabatini, B.L., et al. (2013). Recombinant probes for visualizing endogenous synaptic proteins in living neurons. Neuron *78*, 971–985.

Grunwald, D.J., and Eisen, J.S. (2002). Headwaters of the zebrafish - emergence of a new model vertebrate. Nat. Rev. Genet. *3*, 717–724.

Gunner, G., Cheadle, L., Johnson, K.M., Ayata, P., Badimon, A., Mondo, E., Nagy, M.A., Liu, L., Bemiller, S.M., Kim, K.W., et al. (2019). Sensory lesioning induces microglial synapse elimination via ADAM10 and fractalkine signaling. Nat. Neurosci. *22*, 1075–1088.

Gustafsson, N., Culley, S., Ashdown, G., Owen, D.M., Pereira, P.M., and Henriques, R. (2016). Fast live-cell conventional fluorophore nanoscopy with ImageJ through super-resolution radial fluctuations. Nat. Commun. *7*, 12471.

Haeussler, M., Schönig, K., Eckert, H., Eschstruth, A., Mianné, J., Renaud, J.-B., Schneider-Maunoury, S., Shkumatava, A., Teboul, L., Kent, J., et al. (2016). Evaluation of off-target and on-target scoring algorithms and integration into the guide RNA selection tool CRISPOR. Genome Biol. *17*, 148.

Hagemeyer, N., Hanft, K.-M.M., Akriditou, M.-A.A., Unger, N., Park, E.S., Stanley, E.R.,

Staszewski, O., Dimou, L., and Prinz, M. (2017). Microglia contribute to normal myelinogenesis and to oligodendrocyte progenitor maintenance during adulthood. Acta Neuropathol. *134*, 441–458.

Hale, M.E., Katz, H.R., Peek, M.Y., and Fremont, R.T. (2016). Neural circuits that drive startle behavior, with a focus on the Mauthner cells and spiral fiber neurons of fishes. J. Neurogenet. *30*, 89–100.

Hamilton, S.P., and Rome, L.H. (1994). Stimulation of in vitro myelin synthesis by microglia. Glia *11*, 326–335.

Hammond, T.R., Dufort, C., Dissing-Olesen, L., Giera, S., Young, A., Wysoker, A., Walker, A.J., Gergits, F., Segel, M., Nemesh, J., et al. (2019). Single-Cell RNA Sequencing of Microglia throughout the Mouse Lifespan and in the Injured Brain Reveals Complex Cell-State Changes. Immunity *50*, 253-271.e6.

Heap, L.A., Goh, C.C., Kassahn, K.S., and Scott, E.K. (2013). Cerebellar Output in Zebrafish: An Analysis of Spatial Patterns and Topography in Eurydendroid Cell Projections. Front. Neural Circuits *7*, 53.

Hecker, A., Schulze, W., Oster, J., Richter, D.O., and Schuster, S. (2020). Removing a single neuron in a vertebrate brain forever abolishes an essential behavior. Proc. Natl. Acad. Sci. U. S. A. *117*, 3254–3260.

Herbert, A.L., Fu, M.M., Drerup, C.M., Gray, R.S., Harty, B.L., Ackerman, S.D., O'Reilly-Pol, T., Johnson, S.L., Nechiporuk, A. V., Barres, B.A., et al. (2017). Dynein/dynactin is necessary for anterograde transport of Mbp mRNA in oligodendrocytes and for myelination in vivo. Proc. Natl. Acad. Sci. U. S. A. *114*, E9153–E9162.

Herbomel, P., Thisse, B., and Thisse, C. (2001). Zebrafish Early Macrophages Colonize Cephalic Mesenchyme and Developing Brain, Retina, and Epidermis through a M-CSF Receptor-Dependent Invasive Process. Dev. Biol. *238*, 274–288.

Higashijima, S.-I., Mandel, G., and Fetcho, J.R. (2004). Distribution of prospective glutamatergic, glycinergic, and GABAergic neurons in embryonic and larval zebrafish. J. Comp. Neurol. *480*, 1–18.

Hildebrand, D.G.C., Cicconet, M., Torres, R.M., Choi, W., Quan, T.M., Moon, J., Wetzel, A.W., Scott Champion, A., Graham, B.J., Randlett, O., et al. (2017). Whole-brain serial-section electron microscopy in larval zebrafish. Nature *545*, 345–349.

Hines, J.H., Ravanelli, A.M., Schwindt, R., Scott, E.K., and Appel, B. (2015). Neuronal activity biases axon selection for myelination in vivo. Nat. Neurosci. *18*, 683–689.

Hishikawa, T., Cheung, J.Y., Yelamarty, R. V, and Knutson, D.W. (1991). Calcium transients during Fc receptor-mediated and nonspecific phagocytosis by murine peritoneal macrophages. J. Cell Biol. *115*, 59–66.

Hodgkin, A.L., and Huxley, A.F. (1952). A quantitative description of membrane current and its application to conduction and excitation in nerve. J. Physiol. *117*, 500–544.

Holtschke, T., Löhler, J., Kanno, Y., Fehr, T., Giese, N., Rosenbauer, F., Lou, J., Knobeloch, K.P., Gabriele, L., Waring, J.F., et al. (1996). Immunodeficiency and chronic myelogenous leukemia-like syndrome in mice with a targeted mutation of the ICSBP gene. Cell *87*, 307–317.

Hong, S., Beja-Glasser, V.F., Nfonoyim, B.M., Frouin, A., Li, S., Ramakrishnan, S.,

Merry, K.M., Shi, Q., Rosenthal, A., Barres, B.A., et al. (2016). Complement and microglia mediate early synapse loss in Alzheimer mouse models. Science *352*, 712–716.

Howe, K., Clark, M.D., Torroja, C.F., Torrance, J., Muffato, M., Collins, J.E., Humphray, S., Mclaren, K., Matthews, L., Mclaren, S., et al. (2013). The zebrafish reference genome sequence. Nature *496*, 498–503.

Hrvatin, S., Hochbaum, D.R., Nagy, M.A., Cicconet, M., Robertson, K., Cheadle, L., Zilionis, R., Ratner, A., Borges-monroy, R., Klein, A.M., et al. (2017). Transcriptomic States in the Mouse Visual Cortex. Nat. Neurosci. *21*, 1–19.

Huff, T.B., Shi, Y., Sun, W., Wu, W., Shi, R., and Cheng, J.-X. (2011). Real-Time CARS Imaging Reveals a Calpain-Dependent Pathway for Paranodal Myelin Retraction during High-Frequency Stimulation. PLoS One *6*, e17176.

Hughes, A.N., and Appel, B. (2019). Oligodendrocytes express synaptic proteins that modulate myelin sheath formation. Nat. Commun. *10*, 4125.

Hughes, A.N., and Appel, B. (2020). Microglia phagocytose myelin sheaths to modify developmental myelination. Nat. Neurosci. 1–12.

Hughes, E.G., Orthmann-Murphy, J.L., Langseth, A.J., and Bergles, D.E. (2018). Myelin remodeling through experience-dependent oligodendrogenesis in the adult somatosensory cortex. *21*, 696–706.

Ibrahim, M.Z.M., Khreis, Y., and Koshayan, D.S. (1974). The histochemical identification of microglia. J. Neurol. Sci. *22*, 211–233.

Imagawa, K., de Andrés, M.C., Hashimoto, K., Itoi, E., Otero, M., Roach, H.I., Goldring, M.B., and Oreffo, R.O.C. (2014). Association of reduced type IX collagen gene expression in human osteoarthritic chondrocytes with epigenetic silencing by DNA hypermethylation. Arthritis Rheumatol. (Hoboken, N.J.) *66*, 3040–3051.

Ito, D., Imai, Y., Ohsawa, K., Nakajima, K., Fukuuchi, Y., and Kohsaka, S. (1998). Microglia-specific localisation of a novel calcium binding protein, Iba1. Mol. Brain Res. *57*, 1–9.

Jahn, O., Tenzer, S., and Werner, H.B. (2009). Myelin proteomics: Molecular anatomy of an insulating sheath. Mol. Neurobiol. *40*, 55–72.

Jahn, O., Siems, S.B., Kusch, K., Hesse, D., Jung, R.B., Liepold, T., Uecker, M., Sun, T., and Werner, H.B. (2020). The CNS Myelin Proteome: Deep Profile and Persistence After Post-mortem Delay. Front. Cell. Neurosci. *14*, 239.

Káradóttir, R., Cavelier, P., Bergersen, L.H., and Attwell, D. (2005). NMDA receptors are expressed in oligodendrocytes and activated in ischaemia. Nature *438*, 1162–1166.

Kassambara, A. (2017). ggpubr:“ggplot2” based publication ready plots. R Packag. Version 0.1 *6*.

Kettenmann, H., Hoppe, D., Gottmann, K., Banati, R., and Kreutzberg, G. (1990). Cultured microglial cells have a distinct pattern of membrane channels different from peritoneal macrophages. J. Neurosci. Res. *26*, 278–287.

Kim, S., Burette, A., Chung, H.S., Kwon, S.-K., Woo, J., Lee, H.W., Kim, K., Kim, H., Weinberg, R.J., and Kim, E. (2006). NGL family PSD-95-interacting adhesion molecules

regulate excitatory synapse formation.

Kimmel, C.B., Ballard, W.W., Kimmel, S.R., Ullmann, B., and Schilling, T.F. (1995). Stages of embryonic development of the zebrafish. Dev. Dyn. *203*, 253–310.

Kimura, Y., Hisano, Y., Kawahara, A., and Higashijima, S.I. (2014). Efficient generation of knock-in transgenic zebrafish carrying reporter/driver genes by CRISPR/Cas9-mediated genome engineering. Sci. Rep. *4*, 6545.

Kirby, B.B., Takada, N., Latimer, A.J., Shin, J., Carney, T.J., Kelsh, R.N., and Appel, B. (2006). In vivo time-lapse imaging shows dynamic oligodendrocyte progenitor behavior during zebrafish development. Nat. Neurosci. *9*, 1506–1511.

Klingseisen, A., Ristoiu, A.M., Kegel, L., Sherman, D.L., Rubio-Brotons, M., Almeida, R.G., Koudelka, S., Benito-Kwiecinski, S.K., Poole, R.J., Brophy, P.J., et al. (2019). Oligodendrocyte Neurofascin Independently Regulates Both Myelin Targeting and Sheath Growth in the CNS. Dev. Cell *51*, 730-744.e6.

Klugmann, M., Schwab, M.H., Pühlhofer, A., Schneider, A., Zimmermann, F., Griffiths, I.R., and Nave, K.A. (1997). Assembly of CNS myelin in the absence of proteolipid protein. Neuron *18*, 59–70.

Koudelka, S., Voas, M.G.G., Almeida, R.G.G., Baraban, M., Soetaert, J., Meyer, M.P.P., Talbot, W.S.S., and Lyons, D.A.A. (2016). Individual Neuronal Subtypes Exhibit Diversity in CNS Myelination Mediated by Synaptic Vesicle Release. Curr. Biol.

Kougioumtzidou, E., Shimizu, T., Hamilton, N.B., Tohyama, K., Sprengel, R., Monyer, H., Attwell, D., and Richardson, W.D. (2017). Signalling through AMPA receptors on

oligodendrocyte precursors promotes myelination by enhancing oligodendrocyte survival.

Krasnow, A.M., and Attwell, D. (2016). NMDA Receptors: Power Switches for Oligodendrocytes. Neuron *91*, 3–5.

Krasnow, A.M., Ford, M.C., Valdivia, L.E., Wilson, S.W., and Attwell, D. (2018). Regulation of developing myelin sheath elongation by oligodendrocyte calcium transients in vivo. Nat. Neurosci. *21*, 24–28.

Kucenas, S., Wang, W. Der, Knapik, E.W., and Appel, B. (2009). A selective glial barrier at motor axon exit points prevents oligodendrocyte migration from the spinal cord. J. Neurosci. *29*, 15187–15194.

Kukley, M., Nishiyama, A., and Dietrich, D. (2010). The Fate of Synaptic Input to NG2 Glial Cells: Neurons Specifically Downregulate Transmitter Release onto Differentiating Oligodendroglial Cells.

Kuwada, J.Y. (1986). Cell recognition by neuronal growth cones in a simple vertebrate embryo. Science (80-.). *233*, 740–746.

Kuwada, J.Y., Bernhardt, R.R., and Nguyen, N. (1990). Development of spinal neurons and tracts in the zebrafish embryo. J. Comp. Neurol. *302*, 617–628.

Kwan, K.M., Fujimoto, E., Grabher, C., Mangum, B.D., Hardy, M.E., Campbell, D.S., Parant, J.M., Yost, H.J., Kanki, J.P., and Chien, C. Bin (2007). The Tol2kit: A multisite gateway-based construction Kit for Tol2 transposon transgenesis constructs. Dev. Dyn. *236*, 3088–3099.

van der Laan, L.J., Ruuls, S.R., Weber, K.S., Lodder, I.J., Dopp, E.A., and Dijkstra, C.D. (1996). Macrophage phagocytosis of myelin in vitro determined by flow cytometry: phagocytosis is mediated by CR3 and induces production of tumor necrosis factor-alpha and nitric oxide. Artic. J. Neuroimmunol. *70*, 145–152.

Lampron, A., Larochelle, A., Laflamme, N., Préfontaine, P., Plante, M.M., Sánchez, M.G., Wee Yong, V., Stys, P.K., Tremblay, M.È., and Rivest, S. (2015). Inefficient clearance of myelin debris by microglia impairs remyelinating processes. J. Exp. Med. *212*, 481–495.

Langebeck-Jensen, K., Shahar, O.D., Schuman, E.M., Langer, J.D., and Ryu, S. (2019). Larval Zebrafish Proteome Regulation in Response to an Environmental Challenge. Proteomics *19*.

Larson, V.A., Mironova, Y., Vanderpool, K.G., Waisman, A., Rash, J.E., Agarwal, A., and Bergles, D.E. (2018). Oligodendrocytes control potassium accumulation in white matter and seizure susceptibility. Elife *7*.

Latefi, N.S., Pedraza, L., Schohl, A., Li, Z., and Ruthazer, E.S. (2009). N-cadherin prodomain cleavage regulates synapse formation in vivo. Dev. Neurobiol.

Lee, Y., Morrison, B.M., Li, Y., Lengacher, S., Farah, M.H., Hoffman, P.N., Liu, Y., Tsingalia, A., Jin, L., Zhang, P.W., et al. (2012). Oligodendroglia metabolically support axons and contribute to neurodegeneration. Nature *487*, 443–448.

Legland, D., Arganda-Carreras, I., and Andrey, P. (2016). MorphoLibJ: integrated library and plugins for mathematical morphology with ImageJ. Bioinformatics *32*, btw413.

Lehrman, E.K., Wilton, D.K., Litvina, E.Y., Welsh, C.A., Chang, S.T., Frouin, A., Walker, A.J., Heller, M.D., Umemori, H., Chen, C., et al. (2018). CD47 Protects Synapses from Excess Microglia-Mediated Pruning during Development.

Lewis, K.E., and Eisen, J.S. (2003). From cells to circuits: Development of the zebrafish spinal cord. Prog. Neurobiol.

Li, L., Jin, H., Xu, J., Shi, Y., and Wen, Z. (2011). Irf8 regulates macrophage versus neutrophil fate during zebrafish primitive myelopoiesis. Blood *117*, 1359–1369.

Li, Q., Cheng, Z., Zhou, L., Darmanis, S., Neff, N.F., Okamoto, J., Gulati, G., Bennett, M.L., Sun, L.O., Clarke, L.E., et al. (2019). Developmental Heterogeneity of Microglia and Brain Myeloid Cells Revealed by Deep Single-Cell RNA Sequencing. Neuron *101*, 207-223.e10.

Li, Y., Du, X., Liu, C., Wen, Z.-L., and Du, J. (2012). Reciprocal regulation between resting microglial dynamics and neuronal activity in vivo. Dev. Cell *23*, 1189–1202.

Lin, S., and Bergles, D.E. (2004). Synaptic signaling between GABAergic interneurons and oligodendrocyte precursor cells in the hippocampus. Nat. Neurosci. *7*, 24–32.

Lin, S., Huck, J.H.J., Roberts, J.D.B., Macklin, W.B., Somogyi, P., and Bergles, D.E. (2005). Climbing Fiber Innervation of NG2-Expressing Glia in the Mammalian Cerebellum. Neuron *46*, 773–785.

Linhoff, M.W., Laurén, J., Cassidy, R.M., Dobie, F.A., Takahashi, H., Nygaard, H.B., Airaksinen, M.S., Strittmatter, S.M., and Craig, A.M. (2009). An Unbiased Expression Screen for Synaptogenic Proteins Identifies the LRRTM Protein Family as Synaptic

Organizers. Neuron *61*, 734–749.

Lips, E.S., Cornelisse, L.N., Toonen, R.F., Min, J.L., Hultman, C.M., Holmans, P.A., O'Donovan, M.C., Purcell, S.M., Smit, A.B., Verhage, M., et al. (2012). Functional gene group analysis identifies synaptic gene groups as risk factor for schizophrenia. Mol. Psychiatry *17*, 996–1006.

Liu, P., Du, J., and He, C. (2013). Developmental pruning of early-stage myelin segments during CNS myelination in vivo. Cell Res. *23*, 962–964.

Liu, Q., Sinnen, B.L., Boxer, E.E., Schneider, M.W., Grybko, M.J., Buchta, W.C., Gibson, E.S., Wysoczynski, C.L., Ford, C.P., Gottschalk, A., et al. (2019a). A Photoactivatable Botulinum Neurotoxin for Inducible Control of Neurotransmission. Neuron *101*, 863-875.e6.

Liu, Y.U., Ying, Y., Li, Y., Eyo, U.B., Chen, T., Zheng, J., Umpierre, A.D., Zhu, J., Bosco, D.B., Dong, H., et al. (2019b). Neuronal network activity controls microglial process surveillance in awake mice via norepinephrine signaling. Nat. Neurosci. *22*, 1771–1781.

Longair, M.H., Baker, D.A., and Armstrong, J.D. (2011). Simple Neurite Tracer: open source software for reconstruction, visualization and analysis of neuronal processes. Bioinformatics *27*, 2453–2454.

Lu, D.C., Niu, T., and Alaynick, W.A. (2015). Molecular and cellular development of spinal cord locomotor circuitry. Front. Mol. Neurosci. *8*, 1–18.

Lundgaard, I., Luzhynskaya, A., Stockley, J.H., Wang, Z., Evans, K.A., Swire, M.,

Volbracht, K., Gautier, H.O.B., Franklin, R.J.M., ffrench-Constant, C., et al. (2013). Neuregulin and BDNF induce a switch to NMDA receptor-dependent myelination by oligodendrocytes. PLoS Biol. *11*, e1001743.

Lyons, D.A., and Talbot, W.S. (2015). Glial cell development and function in zebrafish. Cold Spring Harb. Perspect. Biol. *7*.

Mächler, P., Wyss, M.T., Elsayed, M., Stobart, J., Gutierrez, R., Von Faber-Castell, A., Kaelin, V., Zuend, M., San Martín, A., Romero-Gómez, I., et al. (2016). In Vivo Evidence for a Lactate Gradient from Astrocytes to Neurons. Cell Metab. *23*, 94–102.

Makinodan, M., Rosen, K.M., Ito, S., and Corfas, G. (2012). A critical period for social experience-dependent oligodendrocyte maturation and myelination. Science *337*, 1357–1360.

Mangin, J.M., and Gallo, V. (2011). The curious case of NG2 cells: Transient trend or game changer? ASN Neuro *3*, 37–49.

Marcus, R.C., and Easter, S.S. (1995). Expression of glial fibrillary acidic protein and its relation to tract formation in embryonic zebrafish (Danio rerio). J. Comp. Neurol. *359*, 365–381.

Marín-Teva, J.L., Dusart, I., Colin, C., Gervais, A., Van Rooijen, N., and Mallat, M. (2004). Microglia Promote the Death of Developing Purkinje Cells. Neuron *41*, 535–547.

Marisca, R., Hoche, T., Agirre, E., Hoodless, L.J., Barkey, W., Auer, F., Castelo-Branco, G., and Czopka, T. (2020). Functionally distinct subgroups of oligodendrocyte precursor cells integrate neural activity and execute myelin formation. Nat. Neurosci. *23*, 363–374.

Marques, S., Zeisel, A., Codeluppi, S., van Bruggen, D., Mendanha Falcão, A., Xiao, L., Li, H., Häring, M., Hochgerner, H., Romanov, R.A., et al. (2016). Oligodendrocyte heterogeneity in the mouse juvenile and adult central nervous system. Science *352*, 1326–1329.

Marques, S., van Bruggen, D., Vanichkina, D.P., Floriddia, E.M., Munguba, H., Väremo, L., Giacomello, S., Falcão, A.M., Meijer, M., Björklund, Å.K., et al. (2018). Transcriptional Convergence of Oligodendrocyte Lineage Progenitors during Development. Dev. Cell *46*, 504-517.e7.

Mathews, E.S., Mawdsley, D.J., Walker, M., Hines, J.H., Pozzoli, M., and Appel, B. (2014). Mutation of 3-hydroxy-3-methylglutaryl CoA synthase I reveals requirements for isoprenoid and cholesterol synthesis in oligodendrocyte migration arrest, axon wrapping, and myelin gene expression. J. Neurosci. *34*.

Mathias, J.R., Zhang, Z., Saxena, M.T., and Mumm, J.S. (2014). Enhanced cell-specific ablation in zebrafish using a triple mutant of Escherichia coli nitroreductase. Zebrafish *11*, 85–97.

Mauch, D.H., Nägier, K., Schumacher, S., Göritz, C., Müller, E.C., Otto, A., and Pfrieger, F.W. (2001). CNS synaptogenesis promoted by glia-derived cholesterol. Science (80-.). *294*, 1354–1357.

Maxwell, D.S., and Kruger, L. (1965). Small blood vessels and the origin of phagocytes in the rat cerebral cortex following heavy particle irradiation. Exp. Neurol. *12*, 33–54.

McKenzie, I.A., Ohayon, D., Li, H., De Faria, J.P., Emery, B., Tohyama, K., and Richardson, W.D. (2014). Motor skill learning requires active central myelination.

Science (80-.). *346*, 318–322.

McKinsey, G.L., Lizama, C.O., Keown-Lang, A.E., Niu, A., Santander, N., Larpthaveesarp, A., Chee, E., Gonzalez, F.F., and Arnold, T.D. (2020). A new genetic strategy for targeting microglia in development and disease. Elife *9*, 1–34.

McNamara, N.B., and Miron, V.E. (2020). Microglia in developing white matter and perinatal brain injury. Neurosci. Lett. *714*, 134539.

Mctigue, D.M., Horner, P.J., Stokes, B.T., and Gage, F.H. (1998). Neurotrophin-3 and Brain-Derived Neurotrophic Factor Induce Oligodendrocyte Proliferation and Myelination of Regenerating Axons in the Contused Adult Rat Spinal Cord.

Mensch, S., Baraban, M., Almeida, R., Czopka, T., Ausborn, J., El Manira, A., and Lyons, D.A. (2015). Synaptic vesicle release regulates myelin sheath number of individual oligodendrocytes in vivo. Nat. Neurosci. *18*, 628–630.

Meyer, N., Richter, N., Fan, Z., Siemonsmeier, G., Pivneva, T., Jordan, P., Steinhäuser, C., Semtner, M., Nolte, C., Kettenmann, H., et al. (2018). Oligodendrocytes in the Mouse Corpus Callosum Maintain Axonal Function by Delivery of Glucose. Cell Rep. *22*, 2383–2394.

Micu, I., Plemel, J.R., Lachance, C., Proft, J., Jansen, A.J., Cummins, K., van Minnen, J., and Stys, P.K. (2016). The molecular physiology of the axo-myelinic synapse. Exp. Neurol. *276*, 41–50.

Miron, V.E. (2017). Microglia-driven regulation of oligodendrocyte lineage cells, myelination, and remyelination. J. Leukoc. Biol. *101*, 1103–1108.

Missler, M., Südhof, T.C., and Biederer, T. (2012). Synaptic cell adhesion. Cold Spring Harb. Perspect. Biol. *4*, a005694.

Mitew, S., Gobius, I., Fenlon, L.R., McDougall, S.J., Hawkes, D., Xing, Y.L., Bujalka, H., Gundlach, A.L., Richards, L.J., Kilpatrick, T.J., et al. (2018). Pharmacogenetic stimulation of neuronal activity increases myelination in an axon-specific manner. Nat. Commun. *9*.

Moran, L.B., and Graeber, M.B. (2004). The facial nerve axotomy model. Brain Res. Rev. *44*, 154–178.

Mori, S., and Leblond, C.P. (1970). Electron microscopic identification of three classes of oligodendrocytes and a preliminary study of their proliferative activity in the corpus callosum of young rats. J. Comp. Neurol. *139*, 1–29.

Morsch, M., Radford, R., Lee, A., Don, E.K., Badrock, A.P., Hall, T.E., Cole, N.J., and Chung, R. (2015). In vivo characterization of microglial engulfment of dying neurons in the zebrafish spinal cord. Front. Cell. Neurosci. *9*, 321.

Mu, Y., Bennett, D. V., Rubinov, M., Narayan, S., Yang, C.T., Tanimoto, M., Mensh, B.D., Looger, L.L., and Ahrens, M.B. (2019). Glia Accumulate Evidence that Actions Are Futile and Suppress Unsuccessful Behavior. Cell *178*, 27-43.e19.

Murakami, S., Sakurai-Yageta, M., Maruyama, T., and Murakami, Y. (2014). Trans-homophilic interaction of CADM1 activates PI3K by forming a complex with MAGuK-family proteins MPP3 and Dlg. PLoS One *9*, e110062.

Muro, E., Ekin Atilla-Gokcumen, G., and Eggert, U.S. (2014). Lipids in cell biology: How

can we understand them better? Mol. Biol. Cell *25*, 1819–1823.

Nakajima, K., Tohyama, Y., Kohsaka, S., and Kurihara, T. (2002). Ceramide activates microglia to enhance the production/secretion of brain-derived neurotrophic factor (BDNF) without induction of deleterious factors in vitro (John Wiley & Sons, Ltd).

Nam, C.I., and Chen, L. (2005). Postsynaptic assembly induced by neurexin-neuroligin interaction and neurotransmitter. Proc. Natl. Acad. Sci. U. S. A. *102*, 6137–6142.

Nave, K.-A. (2010). Myelination and support of axonal integrity by glia. Nature *468*, 244–252.

Nave, K.-A., and Werner, H.B. (2014). Myelination of the Nervous System: Mechanisms and Functions. Annu. Rev. Cell Dev. Biol. *30*, 503–533.

Nawaz, S., Sánchez, P., Schmitt, S., Snaidero, N., Mitkovski, M., Velte, C., Brückner, B.R., Alexopoulos, I., Czopka, T., Jung, S.Y., et al. (2015). Actin Filament Turnover Drives Leading Edge Growth during Myelin Sheath Formation in the Central Nervous System. Dev. Cell *34*, 139–151.

Nayak, D., Roth, T.L., and McGavern, D.B. (2014). Microglia development and function. Annu. Rev. Immunol. *32*, 367–402.

Nelson, H.N., Treichel, A.J., Eggum, E.N., Martell, M.R., Kaiser, A.J., Trudel, A.G., Gronseth, J.R., Maas, S.T., Bergen, S., and Hines, J.H. (2019). Individual neuronal subtypes control initial myelin sheath growth and stabilization. BioRxiv 809996.

Neumann, H., Kotter, M.R., and Franklin, R.J.M. (2009). Debris clearance by microglia: an essential link between degeneration and regeneration. Brain *132*, 288–295.

Nevin, L.M., Robles, E., Baier, H., and Scott, E.K. (2010). Focusing on optic tectum circuitry through the lens of genetics. BMC Biol. *8*.

Niell, C.M., Meyer, M.P., and Smith, S.J. (2004). In vivo imaging of synapse formation on a growing dendritic arbor. Nat. Neurosci. *7*, 254–260.

Nimmerjahn, A., Kirchhoff, F., and Helmchen, F. (2005). Resting microglial cells are highly dynamic surveillants of brain parenchyma in vivo. Science *308*, 1314–1318.

Oosterhof, N., Holtman, I.R., Kuil, L.E., van der Linde, H.C., Boddeke, E.W.G.M., Eggen, B.J.L., and van Ham, T.J. (2017). Identification of a conserved and acute neurodegeneration-specific microglial transcriptome in the zebrafish. Glia *65*, 138–149.

Oosterhof, N., Chang, I.J., Karimiani, E.G., Kuil, L.E., Jensen, D.M., Daza, R., Young, E., Astle, L., van der Linde, H.C., Shivaram, G.M., et al. (2019). Homozygous Mutations in CSF1R Cause a Pediatric-Onset Leukoencephalopathy and Can Result in Congenital Absence of Microglia. Am. J. Hum. Genet. *104*, 936–947.

Paez, P.M., and Lyons, D.A. (2020). Calcium Signaling in the Oligodendrocyte Lineage: Regulators and Consequences. Annu. Rev. Neurosci. *43*, 163–186.

Pajevic, S., Basser, P.J., and Fields, R.D. (2014). Role of myelin plasticity in oscillations and synchrony of neuronal activity. Neuroscience *276*, 135–147.

Pan, S., Mayoral, S.R., Choi, H.S., Chan, J.R., and Kheirbek, M.A. (2020). Preservation of a remote fear memory requires new myelin formation. Nat. Neurosci. *23*, 487–499.

Paolicelli, R.C., Bolasco, G., Pagani, F., Maggi, L., Scianni, M., Panzanelli, P., Giustetto, M., Ferreira, T.A., Guiducci, E., Dumas, L., et al. (2011). Synaptic pruning by

microglia is necessary for normal brain development. Science *333*, 1456–1458.

Park, J. (2001). The Cell: A Molecular Approach, Second Edition. *74*.

Parkhurst, C.N., Yang, G., Ninan, I., Savas, J.N., Yates, J.R., Lafaille, J.J., Hempstead, B.L., Littman, D.R., and Gan, W.B. (2013). Microglia promote learning-dependent synapse formation through brain-derived neurotrophic factor. Cell *155*, 1596–1609.

Pascual, O., Casper, K.B., Kubera, C., Zhang, J., Revilla-Sanchez, R., Sul, J.-Y., Takano, H., Moss, S.J., McCarthy, K., and Haydon, P.G. (2005). Astrocytic purinergic signaling coordinates synaptic networks. Science *310*, 113–116.

Paterson, J.A., Privat, A., Ling, E.A., and Leblond, C.P. (1973). Investigation of glial cells in semithin sections. III. Transformation of subependymal cells into glial cells, as shown by radioautography after3H-thymidine injection into the lateral ventricle of the brain of young rats. J. Comp. Neurol. *149*, 83–102.

Pellissier, F., Gerber, A., Bauer, C., Ballivet, M., and Ossipow, V. (2007). The adhesion molecule Necl-3/SynCAM-2 localizes to myelinated axons, binds to oligodendrocytes and promotes cell adhesion. BMC Neurosci. *8*, 90.

Peng, J., Liu, Y., Umpierre, A.D., Xie, M., Tian, D.S., Richardson, J.R., and Wu, L.J. (2019). Microglial P2Y12 receptor regulates ventral hippocampal CA1 neuronal excitability and innate fear in mice. Mol. Brain *12*, 71.

Pennuto, M. (2003). Synaptophysin I Controls the Targeting of VAMP2/Synaptobrevin II to Synaptic Vesicles. Mol. Biol. Cell *14*, 4909–4919.

Pérez-Cerdá, F., Sánchez-Gómez, M.V., and Matute, C. (2015). Pío del Río Hortega

and the discovery of the oligodendrocytes. Front. Neuroanat. *9*, 92.

Pietri, T., Easley-Neal, C., Wilson, C., and Washbourne, P. (2008). Six cadm/SynCAM genes are expressed in the nervous system of developing zebrafish. Dev. Dyn. *237*, 233–246.

Poliak, S., Salomon, D., Elhanany, H., Sabanay, H., Kiernan, B., Pevny, L., Stewart, C.L., Xu, X., Chiu, S.-Y., Shrager, P., et al. (2003). Juxtaparanodal clustering of Shaker-like K channels in myelinated axons depends on Caspr2 and TAG-1. J. Cell Biol. *162*, 1149–1160.

Pozner, A., Xu, B., Palumbos, S., Gee, J.M., Tvrdik, P., and Capecchi, M.R. (2015). Intracellular calcium dynamics in cortical microglia responding to focal laser injury in the PC::G5-tdT reporter mouse. Front. Mol. Neurosci. *8*, 12.

Raff, M.C., Miller, R.H., and Noble, M. (1983). A glial progenitor cell that develops in vitro into an astrocyte or an oligodendrocyte depending on culture medium. Nature *303*, 390–396.

Ramón y Cajal, S. (1913). Contribución al conocimiento de la neuroglía del cerebro humano. Trab. Lab. Investig. En Biol. Univ. Madrid *18*.

Rasband, M.N., and Peles, E. (2016). The nodes of Ranvier: Molecular assembly and maintenance. Cold Spring Harb. Perspect. Biol. *8*, a020495.

Ravanelli, A.M., Kearns, C.A., Powers, R.K., Wang, Y., Hines, J.H., Donaldson, M.J., and Appel, B. (2018). Sequential specification of oligodendrocyte lineage cells by distinct levels of Hedgehog and Notch signaling. Dev. Biol. *444*, 93–106.

del Rio-Hortega, P. (1921). Estudios sobre la neurogia. La glia de escasas radiaciones (oligodendroglia).

del Rio-Hortega, P. (1928). Tercera aportacion al conocimiento morfologico e interpretacion funcional de la oligodendroglia.

Rotshenker, S., Reichert, F., Gitik, M., Haklai, R., Elad-Sfadia, G., and Kloog, Y. (2008). Galectin-3/MAC-2, ras and PI3K activate complement receptor-3 and scavenger receptor-AI/II mediated myelin phagocytosis in microglia. Glia *56*, 1607–1613.

Saab, A.S., Tzvetavona, I.D., Trevisiol, A., Baltan, S., Dibaj, P., Kusch, K., Möbius, W., Goetze, B., Jahn, H.M., Huang, W., et al. (2016). Oligodendroglial NMDA Receptors Regulate Glucose Import and Axonal Energy Metabolism. Neuron *91*, 119–132.

Saher, G., Brügger, B., Lappe-Siefke, C., Möbius, W., Tozawa, R.I., Wehr, M.C., Wieland, F., Ishibashi, S., and Nave, K.A. (2005). High cholesterol level is essential for myelin membrane growth. Nat. Neurosci. *8*, 468–475.

Sampaio-Baptista, C., Khrapitchev, A.A., Foxley, S., Schlagheck, T., Scholz, J., Jbabdi, S., DeLuca, G.C., Miller, K.L., Taylor, A., Thomas, N., et al. (2013). Motor skill learning induces changes in white matter microstructure and myelination. J Neurosci *33*, 19499–19503.

Sandau, U.S., Mungenast, A.E., Alderman, Z., Sardi, S.P., Fogel, A.I., Taylor, B., Parent, A.S., Biederer, T., Corfas, G., and Ojeda, S.R. (2011). SynCAM1, a synaptic adhesion molecule, is expressed in astrocytes and contributes to erbB4 receptor-mediated control of female sexual development. Endocrinology *152*, 2364–2376.

Satoh, J., Kino, Y., Asahina, N., Takitani, M., Miyoshi, J., Ishida, T., and Saito, Y. (2016). TMEM119 marks a subset of microglia in the human brain. Neuropathology *36*, 39–49.

Schafer, D.P., Lehrman, E.K., Kautzman, A.G., Koyama, R., Mardinly, A.R., Yamasaki, R., Ransohoff, R.M., Greenberg, M.E., Barres, B.A., and Stevens, B. (2012). Microglia Sculpt Postnatal Neural Circuits in an Activity and Complement-Dependent Manner. Neuron *74*, 691–705.

Scheiffele, P., Fan, J., Choih, J., Fetter, R., and Serafini, T. (2000). Neuroligin expressed in nonneuronal cells triggers presynaptic development in contacting axons. Cell *101*, 657–669.

Scheller, M., Foerster, J., Heyworth, C.M., Waring, J.F., Löhler, J., Gilmore, G.L., Shadduck, R.K., Dexter, T.M., and Horak, I. (1999). Altered Development and Cytokine Responses of Myeloid Progenitors in the Absence of Transcription Factor, Interferon Consensus Sequence Binding Protein. Blood *94*, 3764–3771.

Scholz, J., Klein, M.C., Behrens, T.E.J., and Johansen-Berg, H. (2009). Training induces changes in white-matter architecture. Nat. Neurosci. *12*, 1370–1371.

Sedel, F., Béchade, C., Vyas, S., and Triller, A. (2004). Macrophage-Derived Tumor Necrosis Factor α, an Early Developmental Signal for Motoneuron Death. J. Neurosci. *24*, 2236–2246.

Setzu, A., Lathia, J.D., Zhao, C., Wells, K., Rao, M.S., ffrench-Constant, C., and Franklin, R.J.M. (2006). Inflammation stimulates myelination by transplanted oligodendrocyte precursor cells. Glia *54*, 297–303.

Seyedsadr, M.S., Weinmann, O., Amorim, A., Ineichen, B. V., Egger, M., Mirnajafi-Zadeh, J., Becher, B., Javan, M., and Schwab, M.E. (2019). Inactivation of sphingosine-1-phosphate receptor 2 (S1PR2) decreases demyelination and enhances remyelination in animal models of multiple sclerosis. Neurobiol. Dis. *124*, 189–201.

Shen, G.Y., Chen, W.R., Midtgaard, J., Shepherd, G.M., and Hines, M.L. (1999). Computational analysis of action potential initiation in mitral cell soma and dendrites based on dual patch recordings. J. Neurophysiol. *82*, 3006–3020.

Shiau, C.E., Monk, K.R., Joo, W., and Talbot, W.S. (2013). An Anti-inflammatory NOD-like Receptor Is Required for Microglia Development. Cell Rep. *5*, 1342–1352.

Shiau, C.E., Kaufman, Z., Meireles, A.M., and Talbot, W.S. (2015). Differential Requirement for irf8 in Formation of Embryonic and Adult Macrophages in Zebrafish. PLoS One *10*, e0117513.

Shigemoto-Mogami, Y., Hoshikawa, K., Goldman, J.E., Sekino, Y., and Sato, K. (2014). Microglia enhance neurogenesis and oligodendrogenesis in the early postnatal subventricular zone. J. Neurosci. *34*, 2231–2243.

Sieger, D., Moritz, C., Ziegenhals, T., Prykhozhij, S., and Peri, F. (2012). Long-Range Ca2+ Waves Transmit Brain-Damage Signals to Microglia. Dev. Cell *22*, 1138–1148.

Sierra, A., de Castro, F., del Río-Hortega, J., Rafael Iglesias-Rozas, J., Garrosa, M., and Kettenmann, H. (2016). The “Big-Bang” for modern glial biology: Translation and comments on Pío del Río-Hortega 1919 series of papers on microglia. Glia *64*, 1801–1840.

Sierra, A., Paolicelli, R.C., and Kettenmann, H. (2019). Cien Años de Microglía: Milestones in a Century of Microglial Research. Trends Neurosci.

Smith, M.E., and Hoerner, M.T. (2000). Astrocytes modulate macrophage phagocytosis of myelin in vitro. J. Neuroimmunol. *102*, 154–162.

Snaidero, N., Möbius, W., Czopka, T., Hekking, L.H.P., Mathisen, C., Verkleij, D., Goebbels, S., Edgar, J., Merkler, D., Lyons, D.A., et al. (2014). Myelin Membrane Wrapping of CNS Axons by PI(3,4,5)P3-Dependent Polarized Growth at the Inner Tongue. Cell *156*, 277–290.

Somjen, G.G. (1975). Electrophysiology of Neuroglia. Annu. Rev. Physiol. *37*, 163–190.

Son, J.-H., Keefe, M.D., Stevenson, T.J., Barrios, J.P., Anjewierden, S., Newton, J.B., Douglass, A.D., and Bonkowsky, J.L. (2016). Transgenic FingRs for Live Mapping of Synaptic Dynamics in Genetically-Defined Neurons. Sci. Rep. *6*, 18734.

Spitzer, S.O., Sitnikov, S., Kamen, Y., Evans, K.A., Kronenberg-Versteeg, D., Dietmann, S., de Faria, O., Agathou, S., and Káradóttir, R.T. (2019). Oligodendrocyte Progenitor Cells Become Regionally Diverse and Heterogeneous with Age. Neuron *101*, 459-471.e5.

Steadman, P.E., Xia, F., Ahmed, M., Mocle, A.J., Penning, A.R.A., Geraghty, A.C., Steenland, H.W., Monje, M., Josselyn, S.A., and Frankland, P.W. (2020). Disruption of Oligodendrogenesis Impairs Memory Consolidation in Adult Mice. Neuron *105*, 150-164.e6.

Stevens, B., Allen, N.J., Vazquez, L.E., Howell, G.R., Christopherson, K.S., Nouri, N.,

Micheva, K.D., Mehalow, A.K., Huberman, A.D., Stafford, B., et al. (2007). The Classical Complement Cascade Mediates CNS Synapse Elimination. Cell *131*, 1164–1178.

Stowell, R.D., Sipe, G.O., Dawes, R.P., Batchelor, H.N., Lordy, K.A., Whitelaw, B.S., Stoessel, M.B., Bidlack, J.M., Brown, E., Sur, M., et al. (2019). Noradrenergic signaling in the wakeful state inhibits microglial surveillance and synaptic plasticity in the mouse visual cortex. Nat. Neurosci. *22*, 1782–1792.

Streisinger, G., Walker, C., Dower, N., Knauber, D., and Singer, F. (1981). Production of clones of homozygous diploid zebra fish (Brachydanio rerio). Nature *291*, 293–296.

Svahn, A.J., Graeber, M.B., Ellett, F., Lieschke, G.J., Rinkwitz, S., Bennett, M.R., and Becker, T.S. (2012). Development of Ramified Microglia from Early Macrophages in the Zebrafish Optic Tectum. Dev. Neurobiol *73*, 60–71.

Szalay, G., Martinecz, B., Lénárt, N., Környei, Z., Orsolits, B., Judák, L., Császár, E., Fekete, R., West, B.L., Katona, G., et al. (2016). Microglia protect against brain injury and their selective elimination dysregulates neuronal network activity after stroke. Nat. Commun. *7*, 1–13.

Tait, S., Gunn-Moore, F., Collinson, J.M., Huang, J., Lubetzki, C., Pedraza, L., Sherman, D.L., Colman, D.R., and Brophy, P.J. (2000). An Oligodendrocyte Cell Adhesion Molecule at the Site of Assembly of the Paranodal Axo-Glial Junction. J. Cell Biol. *150*, 657–666.

Thakurela, S., Garding, A., Jung, R.B., Müller, C., Goebbels, S., White, R., Werner, H.B., and Tiwari, V.K. (2016). The transcriptome of mouse central nervous system myelin. Sci. Rep. *6*, 25828.

Thompson, A.W., Vanwalleghem, G.C., Heap, L.A., and Scott, E.K. (2016). Functional profiles of visual-, auditory-, and water flow-responsive neurons in the Zebrafish Tectum. Curr. Biol. *26*, 743–754.

Tomizawa, K., Inoue, Y., and Nakayasu, H. (2000). A monoclonal antibody stains radial glia in the adult zebrafish (Danio rerio) CNS. J. Neurocytol. *29*, 119–128.

Traka, M., Goutebroze, L., Denisenko, N., Bessa, M., Nifli, A., Havaki, S., Iwakura, Y., Fukamauchi, F., Watanabe, K., Soliven, B., et al. (2003). Association of TAG-1 with Caspr2 is essential for the molecular organization of juxtaparanodal regions of myelinated fibers. J. Cell Biol. *162*, 1161–1172.

Tremblay, M.-È., Lowery, R.L., and Majewska, A.K. (2010). Microglial Interactions with Synapses Are Modulated by Visual Experience. PLoS Biol. *8*, e1000527.

Uranova, N.A., Vikhreva, O. V, Rachmanova, V.I., and Orlovskaya, D.D. (2011). Ultrastructural alterations of myelinated fibers and oligodendrocytes in the prefrontal cortex in schizophrenia: a postmortem morphometric study. Schizophr. Res. Treatment *2011*, 325789.

Utz, S.G., See, P., Becher, B., and Ginhoux, F. (2020). Early Fate Defines Microglia and Non-parenchymal Brain Macrophage Development. Cell *181*, 557-573.e18.

Vaughn, J.E. (1969). An electron microscopic analysis of gliogenesis in rat optic nerves. Zeitschrift Für Zellforsch. Und Mikroskopische Anat. *94*, 293–324.

Wake, H., Ortiz, F.C., Woo, D.H., Lee, P.R., Angulo, M.C., Fields, R.D., Bergles, D.E., Roberts, J.D., Somogyi, P., Jahr, C.E., et al. (2015). Nonsynaptic junctions on

myelinating glia promote preferential myelination of electrically active axons. Nat. Commun. *6*, 7844.

Walz, W., Iischner, ' S, Ohlemeyer, C., Banati, F., and Kettenmann', H. (1993). Extracellular ATP Activates a Cation Conductance and a K+ Conductance in Cultured Microglial Cells from Mouse Brain.

Wang, F., Ren, S.Y., Chen, J.F., Liu, K., Li, R.X., Li, Z.F., Hu, B., Niu, J.Q., Xiao, L., Chan, J.R., et al. (2020). Myelin degeneration and diminished myelin renewal contribute to age-related deficits in memory. Nat. Neurosci. *23*, 481–486.

Wang, P., Howard, M.D., Zhang, H., Chintagari, N.R., Bell, A., Jin, N., Mishra, A., and Liu, L. (2012). Characterization of VAMP-2 in the lung: implication in lung surfactant secretion. Cell Biol. Int. *36*, 785–791.

Wang, Y., DelRosso, N. V., Vaidyanathan, T. V., Cahill, M.K., Reitman, M.E., Pittolo, S., Mi, X., Yu, G., and Poskanzer, K.E. (2019). Accurate quantification of astrocyte and neurotransmitter fluorescence dynamics for single-cell and population-level physiology. Nat. Neurosci. *22*, 1936–1944.

Watson, W.E. (1974). Physiology of Neuroglia. Physiol. Rev. *54*.

Weinhard, L., Di Bartolomei, G., Bolasco, G., Machado, P., Schieber, N.L., Neniskyte, U., Exiga, M., Vadisiute, A., Raggioli, A., Schertel, A., et al. (2018). Microglia remodel synapses by presynaptic trogocytosis and spine head filopodia induction. Nat. Commun. *9*, 1–14.

Werkman, I.L., Kövilein, J., Jonge, J.C., Baron, W., de Jonge, J.C., and Baron, W.

(2020). Impairing committed cholesterol biosynthesis in white matter astrocytes, but not grey matter astrocytes, enhances in vitro myelination. J. Neurochem. jnc.15113.

White, T., Schmidt, M., and Karatekin, C. (2009). White matter 'potholes' in early-onset schizophrenia: A new approach to evaluate white matter microstructure using diffusion tensor imaging. Psychiatry Res. Neuroimaging *174*, 110–115.

Wickham, H. (2017). Tidyverse: Easily install and load'tidyverse'packages. R Packag. Version *1*.

Wilke, C.O. (2016). cowplot: streamlined plot theme and plot annotations for 'ggplot2.' CRAN Repos.

Wlodarczyk, A., Holtman, I.R., Krueger, M., Yogev, N., Bruttger, J., Khorooshi, R., Benmamar-Badel, A., Boer-Bergsma, J.J., Martin, N.A., Karram, K., et al. (2017). A novel microglial subset plays a key role in myelinogenesis in developing brain. EMBO J. *36*, 3292–3308.

Wolff, J.J., Gu, H., Gerig, G., Elison, J.T., Styner, M., Gouttard, S., Botteron, K.N., Dager, S.R., Dawson, G., Estes, A.M., et al. (2012). Differences in white matter fiber tract development present from 6 to 24 months in infants with autism. Am. J. Psychiatry *169*, 589–600.

Yeung, M.S.Y., Zdunek, S., Bergmann, O., Bernard, S., Salehpour, M., Alkass, K., Perl, S., Tisdale, J., Possnert, G., Brundin, L., et al. (2014). Dynamics of oligodendrocyte generation and myelination in the human brain. Cell *159*, 766–774.

York, E.M., Bernier, L.-P., and MacVicar, B.A. (2018). Microglial modulation of neuronal

activity in the healthy brain. Dev. Neurobiol. *78*, 593–603.

Zbili, M., and Debanne, D. (2020). Myelination Increases the Spatial Extent of Analog-Digital Modulation of Synaptic Transmission: A Modeling Study. Front. Cell. Neurosci. *14*, 40.

Zhang, Y., Chen, K., Sloan, S.A., Bennett, M.L., Scholze, A.R., O'Keeffe, S., Phatnani, H.P., Guarnieri, P., Caneda, C., Ruderisch, N., et al. (2014). An RNA-sequencing transcriptome and splicing database of glia, neurons, and vascular cells of the cerebral cortex. J. Neurosci. *34*, 11929–11947.

Ziskin, J.L., Nishiyama, A., Rubio, M., Fukaya, M., and Bergles, D.E. (2007). Vesicular release of glutamate from unmyelinated axons in white matter. Nat. Neurosci. *10*, 321–330.

Zottoli, S.J., Hordes, A.R., and Faber, D.S. (1987). Localization of optic tectal input to the ventral dendrite of the goldfish Mauthner cell. Brain Res. *401*, 113–121.

Zuchero, J.B., Fu, M. meng, Sloan, S.A., Ibrahim, A., Olson, A., Zaremba, A., Dugas, J.C., Wienbar, S., Caprariello, A. V., Kantor, C., et al. (2015). CNS Myelin Wrapping Is Driven by Actin Disassembly. Dev. Cell *34*, 152–167.

Zuend, M., Saab, A.S., Wyss, M.T., Ferrari, K.D., Hösli, L., Looser, Z.J., Stobart, J.L., Duran, J., Guinovart, J.J., Barros, L.F., et al. (2020). Arousal-induced cortical activity triggers lactate release from astrocytes. Nat. Metab. *2*, 179–191.

Appendix I: Supplementary Tables

Supplementary Table 2.1. Table of oligonucleotides.

Construct	Template	Primer	Sequence
pME-vamp2	cDNA	F-attB1	GGG GAC AAG TTT GTA CAA AAA AGC AGG CTA CC ATGTCTGCCCCAGCCGG
		R-attB2	GGG GAC CAC TTT GTA CAA GAA AGC TGG GTT GGTGCTGAAGTACACAATGATTATAA
pME-cadm1b (wt)	cDNA	F-attB1	GGG GAC AAG TTT GTA CAA AAA AGC AGG CTA CC ATGAAAAGTCTGAAGCAGGTGT
		R-attB2	GGG GAC CAC TTT GTA CAA GAA AGC TGG GTT AATGTAGTATTCCTTCTTGTCATC
Ig1-dnCadm1b frag1 (N-term to Ig1)	cDNA	F	ATGAAAAGTCTGAAGCAGGTGT
		R-BamHI	CGC GGATCC CACTGAGACATTATTTGTCACCAG
Ig1-dnCadm1b frag2 (post-Ig1 to C-term)	cDNA	F-BamHI	CGC GGATCC GTTCCACCAGGCAACCCAATC
		R	AATGTAGTATTCCTTCTTGTCATC
pME-Ig1-dnCadm1b	Ig1-dnCadm1b frag1+2 ligation	F-attB1	GGG GAC AAG TTT GTA CAA AAA AGC AGG CTA CC ATGAAAAGTCTGAAGCAGGTGT
		R-attB2	GGG GAC CAC TTT GTA CAA GAA AGC TGG GTT AATGTAGTATTCCTTCTTGTCATC
pME-PSD95.FingR-GFP-CCR5TC-KRAB(A)	Addgene 72638	F-attB1	GGG GAC AAG TTT GTA CAA AAA AGC AGG CTA CC ATGCTCGAAGTCAAGGAAGC
		R-attB2	GGG GAC CAC TTT GTA CAA GAA AGC TGG GTT AGCCATAGAAGCAAGATTAGAATAA
pME-sypb	cDNA	F-attB1	GGG GAC AAG TTT GTA CAA AAA AGC AGG CTA CC ATGGATGTTGCCAACCAGTTGGTCG
		R-attB2	GGG GAC CAC TTT GTA CAA GAA AGC TGG GTT CATCTCGTTGGAGAAGGACGTGGG
p3E-cadm1b	cDNA	F-attB2r	GGG GAC AGC TTT CTT GTA CAA AGT GG AA ATGGCGATCTCGGGACTCGG
		R-attB3	GGG GAC AAC TTT GTA TAA TAA AGT TG AATGTAGTATTCCTTCTTGTCATCCG
pME-nlgn1	SourceBioscience	F-attB1	GGG GAC AAG TTT GTA CAA AAA AGC AGG CTA CC ATGCCCTTCCAACAACCAAACC

delPDZ (-STTRV)	danio rerio nlgn1, cat# IMAGp998B1911381Q		
		R-attB2	GGG GAC CAC TTT GTA CAA GAA AGC TGG GTT GTGTGAATGAGGGTGTGGATGGG
pME-nlgn2b delPDZ (-STTRV)	SourceBioscience danio rerio nlgn2b, cat# IMAGp998J1117607Q	F-attB1	GGG GAC AAG TTT GTA CAA AAA AGC AGG CTA CC ATGTCATCGGTGGACGTGGC
		R-attB2	GGG GAC CAC TTT GTA CAA GAA AGC TGG GTT GTGCTGATGGGGCAGGGC
pME-lrrtm2 delICD,delPDZ	cDNA	F-attB1	GGG GAC AAG TTT GTA CAA AAA AGC AGG CTA CC ATGGGTTTCCATTCAAGGTGGC
		R-attB2	GGG GAC CAC TTT GTA CAA GAA AGC TGG GTT GTTCTGAATGGCCGAGCAATGG
pME-lrrtm2 (wt full length)	cDNA	F-attB1	GGG GAC AAG TTT GTA CAA AAA AGC AGG CTA CC ATGGGTTTCCATTCAAGGTGGC
		R-attB2	GGG GAC CAC TTT GTA CAA GAA AGC TGG GTT TACTTCACACTCTTTGTAAGGCAG
pME-lrrtm1 delICD,delPDZ	cDNA	F-attB1	GGG GAC AAG TTT GTA CAA AAA AGC AGG CTA CC ATGCTAATGGATTTCCTTCTAATTGG
		R-attB2	GGG GAC CAC TTT GTA CAA GAA AGC TGG GTT CTGGCTGGTGAAGCACTGC
pME-lrrtm1 (wt full length)	cDNA	F-attB1	GGG GAC AAG TTT GTA CAA AAA AGC AGG CTA CC ATGCTAATGGATTTCCTTCTAATTGG
		R-attB2	GGG GAC CAC TTT GTA CAA GAA AGC TGG GTT CACTTCGCACTCTCGAGATGC
pME-lrrc4ba delPDZ (-ETQI)	SourceBioscience danio rerio lrrc4ba, cat# IMAGp998H1711205Q	F-attB1	GGG GAC AAG TTT GTA CAA AAA AGC AGG CTA CC ATGCGCATCACCACGGTGACC
		R-attB2	GGG GAC CAC TTT GTA CAA GAA AGC TGG GTT TTGGACATTCTCCTTGGAGCCAC
pME-cadm1b delPDZ (-KEYYI)	cDNA	F-attB1	GGG GAC AAG TTT GTA CAA AAA AGC AGG CTA CC ATGAAAAGTCTGAAGCAGGTGT

		R-attB2	GGG GAC CAC TTT GTA CAA GAA AGC TGG GTT CTTGTCATCCGAATTGTTGTGTCCG
pME-GCaMP6s-CAAX	p3E-2A-GCaMP6s-CAAX	F-attB1	GGG GAC AAG TTT GTA CAA AAA AGC AGG CTA CC ATGGGTTCTCATCATCATCATC
		R-attB2	GGG GAC CAC TTT GTA CAA GAA AGC TGG GTT TCAGGAGAGCACACACTT
XbaI-CAAX-PstI (to make p3E-2A-GCaMP6s-CAAX)	n/a, annealed oligos	F ultramer	CTAGAAAGCTGAACCCTCCTGATGAGAGTGGCCCCGGCT GCATGAGCTGCAAGTGTGTGCTCTCCTGACTGCA
PstI-CAAX-XbaI (to make p3E-2A-GCaMP6s-CAAX)	n/a, annealed oligos	R ultramer	GTCAGGAGAGCACACACTTGCAGCTCATGCAGCCGGGGC CACTCTCATCAGGAGGGTTCAGCTTT
EcoRI-GCaMP6s-XbaI (to make p3E-2A-GCaMP6s-CAAX)	Addgene #40753	F-EcoRI	CCGGAATTCAATGGGTTCTCATCATCATCATC
		R-XbaI	TGCTCTAGACTTCGCTGTCATCATTTGTACA
pME-sypHy	Addgene #24478	F-attB1	GGG GAC AAG TTT GTA CAA AAA AGC AGG CTA CC ATGGACGTGGTGAATCAGCTGG
		R-attB2	GGG GAC CAC TTT GTA CAA GAA AGC TGG GTT CATCTGATTGGAGAAGGAGGTGGG
p3E-mScarlet	Addgene #85042	F-attB2r	GGG GAC AGC TTT CTT GTA CAA AGT GG AA ATGGTGAGCAAGGGCGAGGC
		R-attB3	GGG GAC AAC TTT GTA TAA TAA AGT TG CTTGTACAGCTCGTCCATGCCG
p3E-cadm2a	cDNA	F-attB2r	GGG GAC AGC TTT CTT GTA CAA AGT GG AA ATGATGGTGAAGCAGCATATGC
		R-attb3	GGG GAC AAC TTT GTA TAA TAA AGT TG CTAAATGAAATACTCTTTCTTCTCT
p3E-2A-BoNT/B	pQL86-eGFP-BoNT/B (yeast codon optimized)	F-EcoRI	CCG GAATTC A ATGCCTGTCACCATAAACAACTT
		R-Xba1	TGC TCTAGA CTATTTGACGGATTTGCACATTTG
p3E-2A-dnVamp2	cDNA	F-EcoRI	CCG GAATTC A ATGTCTGCCCCAGCCGGAG

(residues 1-89)			
		R-XbaI	TGC TCTAGA CATCTTGGCATTCTTCCACCAGTA
pME-caska	cDNA	F-attB1	GGG GAC AAG TTT GTA CAA AAA AGC AGG CTA CC ATGGCCGACGACGACGTG
		R-attB2	GGG GAC CAC TTT GTA CAA GAA AGC TGG GTT GTAGACCCAGGACACCGGAAC
pDR274-5'cadm1b (to make gRNA synthesis template)	n/a, annealed oligos	F	TAGGATCCAACATGCGCTAGAGAC
		R	AAACGTCTCTAGCGCATGTTGGAT
pDR274-5'dlg4b (to make gRNA synthesis template)	n/a, annealed oligos	F	TAGGTTCCAGGCTAATCACCTGG
		R	AAACCCAGGTGATTAGCCTGGAA

Supplementary Table 3.1. Summary of Ca^{2+} events detected by AQuA in microglia at 4 dpf.

Parameter	Area (μm^2)	Max dF/F	Duration (s) (50% to 50%)	Event distance from soma (µm)	Event frequency (events / s)
Mean +/- SD n = 645 events (31 microglia/31 fish)	8.81 +/- 15.98	0.079 +/- 0.03	76.87 +/- 74.57	18.70 +/- 16.99	0.053 +/- 0.034

Supplementary Table 3.2. Fiji macros to detect sheath disappearance.

Purpose	Use with	Language	
Select first and last frames; last frame subtract first frame	A single channel time-series image to detect overall changes between first and last frames (anything present in first, but gone by last, will appear void)	Python (Jython)	from ij import IJ, ImagePlus from ij.plugin import Duplicator from ij.plugin import ImageCalculator imp = IJ.getImage(); nframes=imp.getNFrames() imp2 = Duplicator().run(imp, 1, 1) imp3 = Duplicator().run(imp, nframes, nframes) imp2.setTitle("first") imp3.setTitle("last") imp2.show() imp3.show() imp4 = ImageCalculator().run("subtract create 32 bit", imp3, imp2) imp4.setTitle("lastSUBfirst") imp4.show()

Duplicate myelin channel (2); bleach correct (prepare for XOR scheme)	A sum-projected 2-channel time-series (myelin channel is 2 in our acquisitions; change as necessary)	ImageJ Macro	run("Correct 3D drift", "channel=2 multi_time_scale sub_pixel only=0 lowest=1 highest=1");
			run("Duplicate...", "duplicate channels=2");
			run("16-bit");
			run("Bleach Correction", "correction=[Exponential Fit]")

Perform consecutive XOR operation to detect change over time	The output of previous step (bleach corrected myelin time-series)	ImageJ Macro	setPasteMode("xor");
			run("Set Slice...", "slice="+nSlices);
			run("Select All");
			for(i=1; i<nSlices; i++) {
			run("Previous Slice [<]");
			run("Copy");
			run("Next Slice [>]");
			run("Paste");
			run("Previous Slice [<]");
			}

Supplementary Table 3.3. AQuA parameters used for event detection in microglia.

AQuA steps	Values
Signal: intensity threshold	2.5
Signal: smoothing	0.5
Signal: minimum size	8 px
Voxel: temporal cut	2.5
Voxel: growing z	1.5
Event: rising time uncertainty	3
Event: slowest delay in propagation	2
Event: propagation smoothness	1.0
Clean: Z-score threshold	6
Merging, reconstruction, delay Tau	Ignore all

Appendix II: Retracting sheaths and words[8]

My mentor, Bruce Appel, emphasizes the importance of communicating science clearly and precisely. Consequently, I have watched my peers and myself deliver ever-improving talks, posters, and manuscripts during our time in the lab. I think that many people in science appreciate that clear communication is essential for others to be able to interpret findings and effectively build upon what has been done. A corollary lesson that I wasn't expecting to learn from our latest project, published recently in *Nature Neuroscience* (Hughes and Appel, 2020), is how imprecise language can muddle and confound understanding, obstructing progress.

Our lab studies oligodendrocyte lineage cells using zebrafish as a model system. In the central nervous system, oligodendrocytes wrap neuronal axons with myelin, a lipid-rich membrane that increases conduction velocity. Zebrafish are both genetically and optically accessible, allowing us to image cellular interactions during myelination in live larvae. A live-imaging experiment can catch oligodendrocytes extending numerous, arborizing processes that search for and begin to wrap axons with myelin membrane. Some of these nascent wraps continue to grow and mature, whereas other wraps appear to be eliminated. How are myelin sheaths eliminated?

Many structures that also are studied by live-imaging, like neuronal neurites, undergo similar deformations during development. Neurons elaborate and occasionally withdraw neurites, and this latter process is termed "retraction". Oligodendrocytes generate processes that branch similarly to neurites. Like neurites, these processes

[8] Adapted from a blog piece invited and published by The Node, July 17, 2020, accessible at: thenode.biologists.com/retracting-sheaths-and-words/highlights

withdraw, and these events have been described as “retraction”. But oligodendrocyte processes also do something very different than neurites: upon contacting a target axon, an oligodendrocyte process can deposit a reservoir of myelin lipids that spreads like a liquid droplet as the process begins wrapping the axon (Nawaz et al., 2015). Can fluid myelin sheaths, like the simple processes that gave rise to them, also be withdrawn? Live confocal microscopy doesn’t show us sheaths unraveling or processes reeled in by the cell body. Instead, sheaths merely reduce in size and disappear. By using the word “retraction” to describe all oligodendrocyte process disappearances, an untested mechanism was invoked to account for all myelin sheath elimination.

If myelin sheaths aren’t retracted, what alternative mechanisms could remove sheaths? Many structures in the developing nervous system, including synapses, neuronal precursors, and neurons, are overproduced and can be pruned by microglia, the resident immune cell type of the CNS. We had previously found a number of similarities between the formation of myelin sheaths and neuronal postsynapses (Hughes and Appel, 2019), raising the possibility that these structures might also be eliminated similarly.

Admittedly, I spent a lot of time thinking about microglia before they constituted a reasonable suspect in sheath elimination. Early in grad school, I had read a paper that found that microglia regularly survey the zebrafish spinal cord and quickly swoop in to clear laser-ablated neurons (Morsch et al., 2015) and I was really curious to see if these cells interact with oligodendrocytes during normal development. Something I particularly like about working with zebrafish is how easy it is to casually pursue these types of side-curiosities. I lost no time to generating the construct to label microglia, because I did it in

parallel with other cloning I needed to do; I injected the construct to generate a microglia reporter transgenic line after I had performed my priority injections for experiments that week. A few months later, I had a microglia reporter line and was ready to find out if microglia and oligodendrocytes interact during myelination.

The first time I timelapse imaged microglia interacting with myelin, to my surprise and delight I found microglia engulfing nascent myelin sheaths. I presented a video at lab meeting and was encouraged by the enthusiasm and questions raised by my labmates. How many microglia are there and how many sheaths are they eating? Do oligodendrocytes die when their sheaths are eaten? What regulates sheath phagocytosis? These tractable questions started to crystallize the phenomenon into a project.

At this stage, our recognition that myelin sheath development shares numerous similarities with synapse development was pivotal. Work by Dorothy Schafer, Beth Stevens, and Marie-Ève Tremblay had previously shown that microglia contact and phagocytose synapses in a neuronal activity-regulated manner (Schafer et al., 2012; Tremblay et al., 2010). Inspired by this work, the hypothesis and predictions that would form the foundation of the project emerged by analogy. Like synapses, do microglia phagocytose myelin in an activity-regulated manner? Will preventing pruning cause extra myelin to persist? With a path laid out, experiments moved swiftly. We found that microglia do survey and phagocytose myelin sheaths, and neuronal activity spurs microglia to trade-off between interacting with neuronal somas and phagocytosing myelin from myelinated axons. We further found that this program is robust enough that blocking it (via microglial ablation) caused excessive and ectopic myelin to develop.

We wrote up and submitted a much shorter version of our paper, concurrent with deposition to the preprint server *BioRxiv*, in summer 2019. In review, it became clear that microglia-mediated myelin pruning was incompatible with our field's understanding that sheaths are solely eliminated by retraction. At first, I saw this as a purely semantic problem: myelin sheaths disappear, and the word "retract" has been used to describe this observation but oversteps into a mechanism that hasn't been tested. I was resistant to confronting retraction but was persuaded by a reviewer's argument that it would be informative to know what fraction of sheath elimination is contributed by microglia. Figuring out how to quantify sheath loss in an unbiased way took longer than any other experiment in the paper and pushed my image analysis forward in new ways. These data were the very last addition to the paper, but they appear inconspicuously in the middle of Figure 2! Ultimately, we found that sheaths are both phagocytosed by microglia and disappear independently of microglial contact, with phagocytosis accounting for the majority of sheath loss. This latter, microglia-independent category of lost sheaths might be called "retraction", as we do in the paper.

I still have some reservations about "retraction". Prior to labeling microglia, we accepted that sheaths were solely eliminated by retraction: When oligodendrocytes were the only cell type visible, it was easy to grant cell autonomy to all visible changes and to forget that other cell types are lurking in the dark. Similarly, it's possible that additional unlabeled cell types might engulf the microglia-independent subset of disappearing sheaths.